Unclassified **NEA/CSNI/R(2011)5**

Organisation de Coopération et de Développement Économiques
Organisation for Economic Co-operation and Development

12-May-2011

English text only

NUCLEAR ENERGY AGENCY
COMMITTEE ON THE SAFETY OF NUCLEAR INSTALLATIONS

Report of the OECD/NEA-Vattenfall T-Junction Benchmark exercise

JT03301661

NEA/CSNI/R(2011)5
Unclassified

English text only

ORGANISATION FOR ECONOMIC CO-OPERATION AND DEVELOPMENT

The OECD is a unique forum where the governments of 34 democracies work together to address the economic, social and environmental challenges of globalisation. The OECD is also at the forefront of efforts to understand and to help governments respond to new developments and concerns, such as corporate governance, the information economy and the challenges of an ageing population. The Organisation provides a setting where governments can compare policy experiences, seek answers to common problems, identify good practice and work to co-ordinate domestic and international policies.

The OECD member countries are: Australia, Austria, Belgium, Canada, Chile, the Czech Republic, Denmark, Estonia, Finland, France, Germany, Greece, Hungary, Iceland, Ireland, Israel, Italy, Japan, Korea, Luxembourg, Mexico, the Netherlands, New Zealand, Norway, Poland, Portugal, the Slovak Republic, Slovenia, Spain, Sweden, Switzerland, Turkey, the United Kingdom and the United States. The European Commission takes part in the work of the OECD.

OECD Publishing disseminates widely the results of the Organisation's statistics gathering and research on economic, social and environmental issues, as well as the conventions, guidelines and standards agreed by its members.

NUCLEAR ENERGY AGENCY

The OECD Nuclear Energy Agency (NEA) was established on 1st February 1958 under the name of the OEEC European Nuclear Energy Agency. It received its present designation on 20th April 1972, when Japan became its first non-European full member. NEA membership today consists of 29 OECD member countries: Australia, Austria, Belgium, Canada, the Czech Republic, Denmark, Finland, France, Germany, Greece, Hungary, Iceland, Ireland, Italy, Japan, Korea, Luxembourg, Mexico, the Netherlands, Norway, Poland, Portugal, the Slovak Republic, Spain, Sweden, Switzerland, Turkey, the United Kingdom and the United States. The European Commission also takes part in the work of the Agency.

The mission of the NEA is:

- to assist its member countries in maintaining and further developing, through international co-operation, the scientific, technological and legal bases required for a safe, environmentally friendly and economical use of nuclear energy for peaceful purposes, as well as
- to provide authoritative assessments and to forge common understandings on key issues, as input to government decisions on nuclear energy policy and to broader OECD policy analyses in areas such as energy and sustainable development.

Specific areas of competence of the NEA include safety and regulation of nuclear activities, radioactive waste management, radiological protection, nuclear science, economic and technical analyses of the nuclear fuel cycle, nuclear law and liability, and public information.

The NEA Data Bank provides nuclear data and computer program services for participating countries. In these and related tasks, the NEA works in close collaboration with the International Atomic Energy Agency in Vienna, with which it has a Co-operation Agreement, as well as with other international organisations in the nuclear field.

Corrigenda to OECD publications may be found online at: *www.oecd.org/publishing/corrigenda*.

COMMITTEE ON THE SAFETY OF NUCLEAR INSTALLATIONS

The Committee on the Safety of Nuclear Installations (CSNI) shall be responsible for the activities of the Agency that support maintaining and advancing the scientific and technical knowledge base of the safety of nuclear installations, with the aim of implementing the NEA Strategic Plan for 2011-2016 and the Joint CSNI/CNRA Strategic Plan and Mandates for 2011-2016 in its field of competence.

The Committee shall constitute a forum for the exchange of technical information and for collaboration between organisations, which can contribute, from their respective backgrounds in research, development and engineering, to its activities. It shall have regard to the exchange of information between member countries and safety R&D programmes of various sizes in order to keep all member countries involved in and abreast of developments in technical safety matters.

The Committee shall review the state of knowledge on important topics of nuclear safety science and techniques and of safety assessments, and ensure that operating experience is appropriately accounted for in its activities. It shall initiate and conduct programmes identified by these reviews and assessments in order to overcome discrepancies, develop improvements and reach consensus on technical issues of common interest. It shall promote the co-ordination of work in different member countries that serve to maintain and enhance competence in nuclear safety matters, including the establishment of joint undertakings, and shall assist in the feedback of the results to participating organisations. The Committee shall ensure that valuable end-products of the technical reviews and analyses are produced and available to members in a timely manner.

The Committee shall focus primarily on the safety aspects of existing power reactors, other nuclear installations and the construction of new power reactors; it shall also consider the safety implications of scientific and technical developments of future reactor designs.

The Committee shall organise its own activities. Furthermore, it shall examine any other matters referred to it by the Steering Committee. It may sponsor specialist meetings and technical working groups to further its objectives. In implementing its programme the Committee shall establish co-operative mechanisms with the Committee on Nuclear Regulatory Activities in order to work with that Committee on matters of common interest, avoiding unnecessary duplications.

The Committee shall also co-operate with the Committee on Radiation Protection and Public Health, the Radioactive Waste Management Committee, the Committee for Technical and Economic Studies on Nuclear Energy Development and the Fuel Cycle and the Nuclear Science Committee on matters of common interest.

AUTHORS

B. L. Smith, Paul Scherrer Institute, Switzerland

J. H. Mahaffy, Wheelsmith Farm, United States

K. Angele, Vattenfall Research and Development, Sweden

J. Westin, Vattenfall Research and Development, Sweden

TABLE OF CONTENTS

EXECUTIVE SUMMARY

The OECD/NEA-Vattenfall T-Junction Benchmark was initiated to test the ability of state-of-the-art Computational Fluid Dynamics (CFD) codes to predict the important parameters affecting high-cycle thermal fatigue in mixing tees. Interest in the subject first arose in the context of Liquid Metal Fast Breeder Reactors (LMFBRs) in the early 1980s, but then received renewed impetus following the incident at the Civaux-1 plant in France in 1998 in which both circumferential and longitudinal cracks appeared near a T-junction in the Residual Heat Removal (RHR) system.

T-junction mixing experiments have been conducted at a number of facilities in France, Germany, Sweden, Japan and Switzerland, but previously unreleased test data became available from tests carried out in November 2008 at the Älvkarleby laboratory of Vattenfall Research and Development in Sweden. These became the basis of the blind CFD benchmarking exercise described in this document. The test rig is made from Plexiglas® and consists of two main pipe sections, each of length 1070 mm and 140 mm internal diameter, mounted horizontally upstream and downstream of the junction, and a branch pipe of length 470 mm and 100 mm internal diameter mounted vertically above. The T-junction itself is constructed from a solid block of Plexiglas® through which circular channels of matching diameters to the pipes had been drilled. Each of the pipe sections is surrounded by square water boxes to provide undisturbed optical paths for the camera and laser used for measuring velocities. Cold water at room temperature is fed from a high-level reservoir to the main pipe via a long horizontal inlet pipe, and hot water ($\Delta T=17K$) is pumped to the branch line via a shorter inlet section. At a number of stations downstream of the T-junction, thermocouples are placed around the perimeter of the pipe cross-section 1mm from the pipe wall.

Participants in the benchmark exercise were given the (steady) volumetric flowrates in the two inlet pipes, together with precise details of the mean and root-mean-square (rms) velocity profiles at cross-sections about three diameters upstream of the centre of the T-junction. The cold and hot temperatures in the two inlet pipes were also given. In return, numerical data were requested at various measuring stations downstream of the junction for later comparison against the test data once these had been released, thus creating the conditions of a blind benchmark exercise.

An organizing committee was set up early in 2009, which included the expert from Vattenfall R&D who had carried out the experiment in the previous November. Detailed specifications were drawn up ahead of a formal announcement of the benchmark exercise and an invitation to attend a kick-off meeting held on May 20, 2009 at the NEA headquarters in Paris. The announcement was sent out to about 750 interested parties. Of these, 65 formally registered interest in the exercise and consequently received the detailed specifications, which also included instructions for standard formatting of the requested data files to facilitate easy processing of the numerical data. A deadline of April 30, 2010 was imposed for participants to present their data files to the organizers. The deadline had to be strictly adhered to, since release of the data would follow at an *Open Meeting* on May 12, 2010. Participants were warned that if they did present their blind predictions by the deadline, they would not later be able to withdraw them once the test data had been released.

In total, 29 participants submitted results by the deadline and these have therefore been included in the synthesis. The majority used commercial CFD software (eight used FLUENT, seven used ANSYS-CFX and four used STAR-CCM+), two used the open-source software OpenFOAM, while the rest used codes developed in-house. The number of control volumes used varied from 0.28M to 70.5M, though most were in the range 1-5M. The majority (19) chose some variant of Large Eddy Simulation (LES) for turbulence modelling, while others (3) chose Detached Eddy Simulation (DES) and the remainder some form of Reynolds-Averaged Navier Stokes (RANS) model. The time step for advancing the solution ranged from 0.06 ms to 1.0 ms with the average of 0.6 ms. The time for collecting data was set at a minimum of 5 s in the specifications, and 12 participants used this value. One calculation was taken to 28 s, with the average close to 10 s.

Detailed conclusions on benchmark results are not possible without a detailed review of nodalisations. However, at least two features stand out immediately for the velocity-based comparisons. For the same selection of turbulence model, total number of discrete volumes is generally a good indicator of quality. This suggests that most participants were careful in their selection of mesh within the constraints of available computer resources. Also, for roughly the same number of volumes, the SAS-SST[#] model appears to be significantly under-performing LES with the Dynamic Smagorinsky or WALE (Wall-Adapting Local Eddy-Viscosity) subgrid scale model. Other results show that SST is performing well, so problems with quality of results are probably due to SAS.

The factors considered to contribute to the risk of high-cycle thermal fatigue in structures are (i) the amplitude of the thermal fluctuations, (ii) a dominant frequency in the low Hz range, (iii) the number of cycles, and (iv) the material properties. The T-junction benchmark exercise was specifically aimed at establishing whether state-of-the-art CFD software can capture the first two of these parameters. It is a challenging task. To prevent numerical diffusion from smoothing the temperature fluctuations, fine-mesh resolution and high-order numerical differencing schemes are needed. These requirements come at high computational cost. The RANS turbulence models are robust and efficient, and are still considered to be the industrial standard for CFD computations. However, they involve a collective averaging over all the scales of turbulence, and mask many of the characteristics associated with them. It is difficult to see how a RANS-based model would be capable of identifying the frequency of a dominant, low-frequency turbulent fluctuation, which is why most participants to this benchmark put their trust in LES modelling approaches. With LES, the large scales of turbulence are computed explicitly, and only the smaller scales, i.e. those contributing to the turbulent diffusion process, are modelled.

To obtain overall impressions, the submissions were ranked according to three separate metrics, based on velocity data, temperature data and Fourier transform (of velocities) data. In all categories, the LES approaches collectively gave the best comparisons. Worst collectively were those based on the SAS-SST turbulence modelling approach, which appears to be unsuited for this kind of problem, significantly under-performing LES, independently of the sub-grid scale (SGS) model adopted for the latter. Other results show that a Detached Eddy Simulation (DES), with SST in the near-wall region, might be an approach worth pursuing further (only one submission using this model). Concerning the RANS approaches, SST-kω in particular was seen to be performing quite well, though it should noted that the number of control volumes used (11 M) far exceeded those of the other RANS simulations.

There is a wealth of data coming from this benchmarking activity, both experimental and numerical, all available for analysis. It is hoped that the participants will explore the possibilities in connection with their own simulations. Overall, the T-junction benchmark has been very successful. The participation was very high, given that the calculations were extremely demanding in terms of CPU time. The exercise

[#] SAS (Scale-Adapted Simulation); SST (Shear Stress Transport)

complements the activities in other areas in understanding the origins of thermal fatigue in this geometry, and being able to quantify them. Useful information has been obtained in this exercise even from numerical analysts using the same code. Some post-benchmark activity is recommended to examine areas that were not available here, such as the influence of near-wall modelling and the optimal degree of mesh refinement needed for efficient turn round in terms of CPU time.

Overall, LES has performed very well in this benchmark in regard to reproducing mean and fluctuating velocity profiles across the (outlet) pipe, and temperature profiles along the pipe. However, the ability of LES to identify peaks in the velocity spectra still indicates a user effect, which could not be clarified within the framework of this benchmark exercise. In any case, LES will remain computationally too expensive for most industrial-scale flows for some years yet.

1. MOTIVATION AND BACKGROUND

An *Exploratory Meeting of Experts to Define an Action Plan on the Application of Computational Fluid Dynamics (CFD) Codes to Nuclear Reactor Safety (NRS) Problems* took place in Aix-en-Provence, France on 15-16 May, 2002 [1]. It was a meeting jointly sponsored by the IAEA* and the OECD/NEA‡ and resulted in the formulation of an action plan recommending the creation of three Writing Groups, overseen by the OECD/NEA, and with mandates to perform the following tasks:

- WG1 Provide a set of guidelines for the application of CFD to NRS problems;
- WG2 Evaluate the existing CFD assessment bases, identify any gaps, and initiate activities aimed at broadening the assessment database;
- WG3 Summarise the extensions needed to CFD codes for application to two-phase NRS problems.

Work began early in 2003. Teams of experts were assigned to each of the groups, representing the following OECD member countries: the Czech Republic, France, Germany, Italy, Japan, S. Korea, the Netherlands, Norway, Sweden, Switzerland and the USA. Preliminary reports were submitted to the WGAMA# group in September 2004, which scoped the work needed to be carried out to fulfil the respective mandates, and which also made recommendations on how to achieve the defined objectives. In January 2005, all three groups were re-formed to carry out their respective tasks. The work was concluded in December 2007 and CSNI reports were eventually issued by each group describing the work undertaken [2,3,4].

The WG2 Writing Group provided evidence to show that CFD is a tried-and-tested technology, and that the main industrial-level CFD vendors were themselves taking active steps to quality-assure their software products by testing their codes against standard test data, and through active participation in international benchmarking exercises. However, in a situation of low growth in the nuclear power industry, the primary driving forces for the development of CFD technology remain in non-nuclear areas, such as in the aerospace, automotive, marine, turbo-machinery, chemical and process industries, and to a lesser extent the environmental and biomedical industries. In the power-generation arena, the principal applications are again non-nuclear: combustion dynamics for fossil-fuel burning and gas turbines, vanes for wind turbines, etc.

Accepting the commission to not only report on the existing assessment databases for the application of CFD to nuclear reactor safety issues, but to also take steps to broaden and extend the databases, three new initiatives were instigated:

1. To organise a new series of international workshops to provide a forum for experimenters and numerical analysts to exchange information;

---

* *International Atomic Energy Agency*

‡ *Organisation for Economic Cooperation and Development, Nuclear Energy Agency*

OECD/NEA Working Group on the Analysis and Management of Accidents

2. To encourage nuclear departments at universities and research organisations to release test data by initiating international numerical benchmark exercises; and
3. To establish a Wiki-type web portal to give online access to the information collated by the groups, as documented in their final reports, and, via user input, to provide a means for updating and extending the information they contained.

1.1 The CFD4NRS Workshop Series

The first of the international workshops took place in Garching, Germany in 2006 [5], and was organised directly by the WG2 group, which was still sitting at this time. Selected papers from the workshop were subsequently published in a special issue of Nuclear Engineering and Design [6]. Further workshops in the series, as well as the benchmarking and webpage initiatives, were accomplished via a smaller *Special CFD Group* formed later by WGAMA. This group consisted of the chairmen of the three Writing Groups together with the NEA secretariat.

The second workshop in the series, XCFD4NRS, took place in Grenoble, France in September 2008, and concentrated more on multi-phase aspects, the focus of the WG3 Writing Group [7]. Again, a special issue of Nuclear Engineering and Design has been dedicated to this workshop [8]. The third workshop, CFD4NRS-3, will take place in Washington DC in September 2010, and plans are in place for a fourth workshop to take place in Daejeon, Korea in 2012.

1.2 Construction of the CFD for NRS Wiki Pages

The three CSNI documents, like any state-of-the-art reports, are only up-to-date at the time of writing, and, given the rapidly expanding use of CFD as a refined analysis tool in nuclear technology, the information they contain will soon become outdated. To preserve their usefulness and topicality, improvements and extensions to the documents are foreseen. It was decided that the most efficient vehicle for regular updating would be to create a Wiki-type web portal. Consequently, in a pilot study, a dedicated webpage has been created on the NEA website using Wikimedia software [9]. The WG1 and WG2 documents in the forms they appear in the respective archival documents [2,3] have now been uploaded to provide on-line access to the material making up the archival documents. The webpages for the WG3 document [4] are under construction.

All the main chapters are active links to the subject material, and are subdivided if necessary. Active links are installed at all levels to enable the user to navigate quickly to other parts of the respective documents. All webpage addresses, for example to the commercial CFD sites, are also active, and it is planned to install a similar facility for the journal references too, which will be useful for registered subscribers with electronic access to the material. However, the most useful feature of the web portal will be the opportunity to modify, correct, update and extend the information contained there, the Wiki concept being the vehicle for this. The aim is to have a static site, with unrestricted access. Readers will not be able to directly edit or change the information there, but can communicate their suggestions to the website editors. In parallel, a beta version of the webpages will be maintained for installing updates prior to transfer to the static site. At present, access to the beta version is restricted to the three former chairmen of the Writing Groups, who have editing responsibility for the website versions of their respective documents, together with the NEA webmaster. It will be the editor's responsibility to review all new submissions, and implement them into the open-access version of the site, following approval from the CSNI. This responsibility is now being extended to a full *CFD Task Group* under the auspices of WGAMA, since the burden of work is expected to become excessive.

1.3 Benchmark Exercise on Thermal Fatigue

During a meeting of the three Writing Group chairmen convened in Grenoble in September 2008 at the conclusion of the 2nd of the workshops, XCFD4NRS [7], discussions were held concerning candidate experiments around which to organise an international CFD benchmark exercise; both single-phase and two-phase options were considered. It was generally acknowledged that it would be desirable to have the opportunity of performing a *blind* benchmark, and this would entail finding a completed experiment for which the data had not yet been released, or encouraging a new experiment (most likely in an existing facility) to be undertaken especially for this exercise. The group took on the responsibility of finding a suitable experiment, for providing the organisational basis for launching the benchmark exercise (though not on the scale of an International Standard Problem, ISP), and for the synthesis of the results. An early opportunity came in the area of thermal fatigue associated with flow mixing in a T-junction.

In T-junctions, where hot and cold streams join and mix (though often not completely), significant temperature fluctuations can be created near the walls. The wall temperature fluctuations can cause cyclical thermal stresses which may induce fatigue cracking. Thermal striping and the related fatigue problem were initially studied in the context of Liquid-Metal Fast Breeder Reactors (LMFBRs) in the 1980's, where it was considered to be a significant problem due to the high thermal conductivity of the liquid-metal coolant (sodium). Areas of concern included the upper core structure and the plenum region above the core, where mixing of hot and cold streams took place at the exits to the fuel and control rod channels. Thermal fatigue phenomena were also observed in the secondary loop of the French Phénix prototype LMFBR and in a T-junction of the full-scale Superphénix reactor. The IAEA organised benchmark studies to analyse these events, and subsequently issued a document on the subject [10].

The issue of thermal striping has since shifted to Light Water Reactors (LWRs), for which several incidents of high-cycle fatigue had been observed, mainly in T-junctions, such as the failure event at Civaux-1 in France in 1998 [11,12]. These incidents usually occurred in piping circuits of diameters 5 cm to 20 cm, the most susceptible parts subject to thermal fatigue being due to mixing in T-junctions of the Residual Heat Removal (RHR) system in both Boiling Water Reactors (BWRs) and Pressurised Water Reactors (PWRs). The incident has also raised thermal fatigue to being of serious safety concern and an important aspect in regard to ageing and life-management of LWRs.

High-cycle phenomena cannot be monitored and/or detected by standard thermocouple instrumentation, due to limitations in the sensor response time. Consequently, reliable prediction of thermal fatigue loads is an important part of managing the risk. The coolant temperature oscillations are due to turbulent thermal-mixing effects, with most risk of wall thermal fatigue being reported to be at frequencies up to several Hz [13]. Significantly higher frequencies than these appear not to be of concern, as they are strongly attenuated by the thermal inertia of the pipe wall. Recent research activity in the area includes the joint US-Japanese programme [14,15,16], the programme by EDF [17], the experiments and benchmarks undertaken by Vattenfall [18,19] and the comprehensive European 5th Framework Programme THERFAT [20], each addressing the different issues involved: namely, thermal-hydraulic analysis, material stress/fatigue analysis, crack initiation and propagation assessment. In addition, in a recent PIRT[%] study [21], the issue of thermal fatigue came moderately high on the list of priority single-phase NRS issues identified by the WG2 group [3], and there appeared to be a good degree of conformity of interest internationally.

Tests on thermal mixing in a T-junctions are being carried out in France, Germany, Japan, Sweden and Switzerland. In particular, very careful experiments have been performed since 2006 at the Älvkarleby Laboratory of Vattenfall Research and Development in Sweden, with the primary aim of providing high-quality validation data for CFD calculations for a variety of main/branch flowrate ratios. Following

[%] *Phenomena Identification and Ranking Table*

negotiations with Vattenfall staff, it was agreed to perform a special mixing test in the series, and keep the data secret to provide the basis for a blind benchmark exercise.

2. ORGANISATIONAL PROCEDURES

2.1 CSNI Approval

The offer of experimental data by Vattenfall R&D came at a very opportune moment: just before the annual WGAMA meeting in September 2008, and only days after the XCFD4NRS Workshop, where the idea of an international blind benchmarking activity had first been conceived. A CAPS[†] was prepared, and delivered to WGAMA for approval. The points put forward to support the proposal were:

- This was the third of the mandate items proposed by the WGAMA Special CFD Group in 2007, and the other two items – the organisation of the CFD4NRS workshops and the setting up of a web-based portal for information relating to the use of CFD in NRS – were already approved and ongoing.

- High-resolution CFD-grade velocity and temperature data would be available from the dedicated T-junction experiment performed at Vattenfall R&D.

- The Special CFD Group would undertake the synthesis of the numerical results, including the comparison with measured data, and report its findings at the next scheduled Workshop, CFD4NRS-3, to be held in September 2010.

- The exercise would complement ongoing national programmes studying thermal fatigue in T-junctions, and European initiatives such as THERFAT (5th FWP) and NULIFE (Network of Excellence).

- Failures of structures at nuclear power plants due to thermal fatigue had been reported at Genkai (Japan), Tihange (Belgium), Farley (USA), PFR (UK), Forsmark (Sweden), Tsuruga (Japan), Loviisa (Finland) and Civaux (France). Interest in thermal fatigue is international.

- In the PIRT study recently carried out by the Special CFD Group [21], thermal fatigue was identified as a topic of medium-to-high generic interest, with a good degree of conformity around the world, and several papers on the subject had been presented at the recent XCFD4NRS workshop. The issue is topical.

- Several organisations from Canada, the Czech Republic, Finland, France, Germany, Hungary, Italy, Japan, Korea, the Netherlands, Slovenia, Spain, Sweden, Switzerland and the USA expressed an interest, in principle. The EC is also interested in this CFD benchmark.

After some discussion, the CAPS was approved, and finally endorsed by the CSNI in December 2008. Work began on organising the benchmark activity early in 2009.

[†] *CSNI Activity Proposal Sheet*

2.2 The Work of the Benchmark Organising Committee

The organising committee was formed from members of the WGAMA Special CFD Group, together with the Vattenfall R&D staff member who carried out the T-junction experiment in November 2008. Table 1 lists the members of the committee, their affiliations, and their principal functions within the scope of the benchmark exercise.

Table 1: Members of the OECD/NEA–Vattenfall T-Junction Benchmark

Brian L. Smith	PSI, Switzerland	Chairman
Kristian Angele	Vattenfall R&D, Sweden	Performed T-junction experiment
John H. Mahaffy	PSU (Emeritus), USA	Will undertake the synthesis of results
Ghani Zigh	US NRC, USA	Responsible for organising CFD4NRS-3 workshop
Dominique Bestion	CEA, France	Expert, and special advisor on workshop organisation
Jong-Chul Jo	OECD/NEA, France	Secretariat

A date was fixed for a kick-off meeting of the benchmark exercise (20 May, 2009), and the secretariat made the arrangements for this to take place at the NEA Headquarters in Paris. An announcement was prepared (reproduced in Annex 1) and sent out to about 750 individuals on March 6, 2009 with an invitation to (i) attend the kick-off meeting, and/or (ii) register as a participant in the benchmarking exercise. In total, 65 registrations were made from organisations in 22 countries. Table 2 lists the countries specifically, and the number of registrations per country. All registered participants subsequently received the official benchmark specifications. The kick-off meeting was attended by 28 delegates, with apologies from a further 8 who had originally intended to come, but then could not for various reasons. The minutes of the meeting are documented [22].

Table 2: Registrations to the OECD/NEA–Vattenfall T-Junction Benchmark

Belgium	1	Germany	4	Netherlands	1	Sweden	6
Canada	2	Greece	1	Nigeria	1	Switzerland	7
Czech Republic	1	Hungary	2	Russia	4	Turkey	1
Egypt	1	Italy	3	Slovakia	1	USA	6
Finland	3	Japan	6	South Africa	1		
France	8	S. Korea	2	Spain	3		

To set the scene, Stéphane Chapuliot from AREVA, who had been responsible for the analysis of the Civaux-1 thermal fatigue incident [23], and led the NULIFE RA4-2 pilot project on thermal fatigue, gave

an invited talk. He explained that the cracks, both circumferential and longitudinal, appeared after only 1500 hours operation. In particular, he emphasised that the study showed that low-frequency turbulent oscillations could be damped (stable flow) or amplified by bends in the pipework. The main questions remaining are exact characterisation of the load amplitude and spectra transmitted from the fluid to the structure, identification of the most affected areas, and knowledge of the effect of the flow configuration (i.e. flowrate ratio). He stressed the importance of the OECD benchmark in assessing the capability of CFD to predict the flow characteristics, and in complementing a possible future NULIFE benchmark, which would address the near-wall heat transfer issue.

The final timetable for the benchmark activity is given in Table 3. A draft version of the benchmark specifications was circulated to all registered participants on June 30, 2009 with an invitation for feedback concerning errors, clarity, ambiguity and possible misunderstandings. A few scattered comments were received regarding exact dimensions, the influence of sealing rings connecting the Plexiglas pipes of the test section to the plastic inlet and outlet tubes, the temperature profiles at inlet (flat) and the dimensions of the water boxes used for the LDA measurements (not needed for the simulation). All questions were answered appropriately by email, but otherwise it was clear that the specifications had been compiled in a clear and unambiguous manner. With very few changes, the final and official version of the benchmark specifications could be circulated on July 15, 2009. The finalised benchmark specifications are reproduced in Annex 2. The timing gave participants 9½ months to complete their calculations and submit their results by the deadline date of April 30, 2010.

Table 3: Timetable for the OECD/NEA–Vattenfall T-Junction Benchmark

May 20, 2009	Kick-Off Meeting
June 10, 2009	Distribution of draft version of the Benchmark Specifications
June 30, 2009	Deadline for comment/queries from participants concerning the Benchmark Specifications
July 15, 2009	Distribution of final version of the Benchmark Specifications
April 30, 2010	Deadline for receipt of simulation results
May 12, 2010	Open Benchmark Meeting (first release of test data)
Sept. 14, 2010	Presentation of Results and Synthesis at CFD4NRS-3 Workshop

The deadline for submission had to be rigidly enforced because of the date of the Open Benchmark Meeting on May 12, 2010, at which time the test date would be released, this date having been chosen to combine with other already scheduled WGAMA CFD committee meetings. Reminders that the deadline for submission was approaching were sent to all registered participants on April 1 and April 22, 2010. Participants were also reminded that following the April 30 deadline they would not be permitted to exchange or withdraw their numerical results, which would then become part of the benchmark synthesis.

Arrangements were made on a Penn State University (PSU) website for automatic uploading of participants' data files. Instructions were sent out in February 2010 on how the procedure worked. Having created a password-protected account on the site, received email confirmation from John Mahaffy that their account was active, participants could then upload their results files directly to the benchmark drop box. No other participant would have access to these files. The owner could exchange the files for updated ones at any time up to the deadline date, but then no further access was permitted.

In total, 29 submissions were received. All were included in the subsequent analysis carried out by John Mahaffy, and the synthesis presented at the CFD4NRS-3 Workshop in Washington DC in September 2010. In addition, a special Poster Session was organised at the workshop where participants could display their results, and any subsequent post-test simulations they had performed could also be shown. This invitation was extended to those who were unable to meet the deadline for the blind benchmark exercise, these posters being marked accordingly.

The Open Benchmark Meeting was attended by 22 participants in the benchmark exercise, the Organising Committee (minus J. H. Mahaffy), and the NEA Secretariat. B. L. Smith (PSI) made a presentation giving a summary and status of the benchmark activity, G. Zigh (US NRC) described the preparations being made for the first time at the CFD4NRS-3 workshop in regards to the benchmark, and K. Angele (Vattenfall) presented the measured data from the test downstream of the junction. On behalf of J. H. Mahaffy, a first synthesis of the benchmark results was presented by B. L. Smith. All participants at the meeting received paper copies of all presentations. It was explained that the downstream temperature and velocity data would be made available on the PSU Angel website within a few days, and all those registered members of the website would then have access to the data files. These are in the form of text files and Excel spreadsheets for both transient and averaged data.

An open discussion session then followed, in which participants could ask questions, air views, and make suggestions for improvement in the organisation of the benchmark. Clearly, interest in the benchmark activity had remained high, and a suggestion was made of whether an open forum could be set up on the last afternoon of the CFD4NRS-3 workshop where delegates could exchange experiences. (A special room was so allocated.)

Most of the comments made were minor, and did not affect the submitted results.

- It was noted that all the boundary conditions needed to be defined carefully. In particular, better defined inlet conditions are needed when the flow is not fully developed. Also, it was assumed that the inlet streams were at uniform and constant temperature, though no profiles were measured.

- The need for careful spectral analysis was emphasised, since any low frequency peaks could be important from the point of view of any subsequent thermal fatigue analysis. (In fact, there is a small peak at about 4 Hz in the temperature spectrum at $x/D_2 = 4$ for this test.)

- Some thought that the minimum run time of 5s was too short for results to be considered converged, though accepted that some participants would have lacked adequate computing power if a longer time had been specified.

- The organisers defended the position that no recommendations had been given in the specifications regarding the “best” models (particularly turbulence models) to use. The choice of models was deliberately made part of the exercise, since this is how the situation would be for an authentic safety submission.

- After checking first with his management, K. Angele confirmed it was permissible to cite the experimental data directly (i.e. without normalisation), as long as Vattenfall R&D, as owner of the data, were properly acknowledged.

- There was a suggestion that the spectral data of u′ (the fluctuating component of the axial velocity) would be more revealing than the power spectrum.

- F. Moretti (UPisa) proposed that the benchmark results could be presented in a special issue of the online journal Science and Technology of Nuclear Installations. He cautioned that 10 papers at the minimum would be needed for such a publication. The suggestion was later confirmed by Professor D'Auria, Editor-in-Chief of the journal, who stated that a publication charge of Euro 500 would apply for each paper. This offer will be followed up in due course.

- There was a suggestion that a state-of-the art report on the subject would be attractive, this being standard procedure in the aerospace industry. The Organising Committee will consider this.

- B. L. Smith reiterated that it was not the intention of the OECD/NEA to sponsor any follow-up of the benchmark exercise in terms of post-test calculations. M. Scheuerer suggested that the German CFD Network might consider doing this. D. Pointer (ANL) offered to synthesise any new calculations if J. Mahaffy were not available.

- The two comments were made that (i) gaining access to valuable experimental data was an incentive to participate in this benchmark exercise, and (ii) the benchmark activity provided participants a good opportunity to know the state-of-the art of CFD codes.

3. EXPERIMENTAL FACILITY

3.1 General Layout

A full description of the experimental rig is included as part of the official Benchmark Specifications, reproduced in Annex 1. However, for completeness, the most salient points are given here also.

The model of the T-junction is manufactured in Plexiglas® and consists of a horizontal pipe with inner diameter (D_2) 140 mm for the cold water flow (Q_2), and a vertically oriented pipe with inner diameter (D_1) 100 mm for the hot water flow (Q_1). The hot water pipe is attached to the upper side of the horizontal cold water pipe. The junction itself is constructed from a solid Plexiglas® block into which the main and branch pipes fit. The edge at the intersection between the pipes is only slightly smoothed. The radius of curvature was not measured, but it is certainly smaller than 0.2 mm. For the given flow conditions, a mesh resolution of this scale would correspond (on the water side) to y+ ~ 3.25. Hence, it is conceivable that simulations for which the viscous boundary layer was fully resolved could take the finite curvature of the edges into account. However, no stipulation was made on this point in the benchmark specifications.

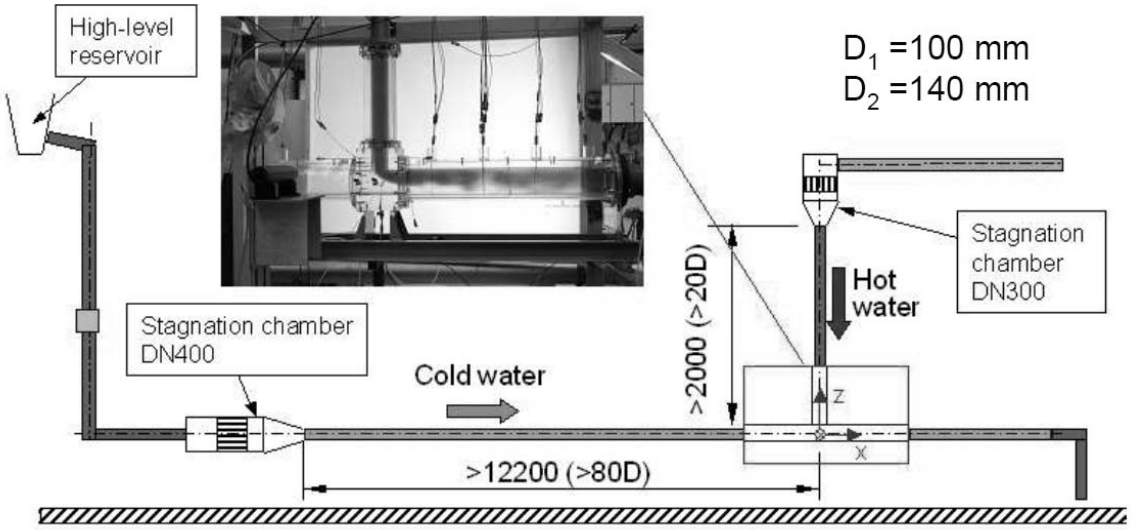

Figure 1. Side view of Vattenfall test rig

The test rig is illustrated in Fig. 1. The cold water pipe is supplied from a high-level reservoir equipped with a long horizontal weir to keep a constant water level independent of the flow rate through the model. The flowrate is measured using an electro-magnetic flow meter (blue square in Fig. 1). A stagnation chamber with diameter 400 mm is mounted at the beginning of the horizontal pipe, and contains two perforated plates, a tube bundle (inner diameter of the tubes is 10 mm and the length is 150 mm), a third

perforated plate, and finally a contraction with area ratio 8.2:1. The purpose of the stagnation chamber is to provide a high flow quality without large-scale turbulence or secondary flows. The stagnation chamber is connected to a 10 m long pipe section made from ABS plastic, which is followed by the Plexiglas® section extending 1260 mm upstream of the T-junction. The total upstream length of the pipe with constant diameter (D_2 = 140 mm) is then more than 80 hydraulic diameters, thus ensuring fully developed flow conditions at the entrance to the junction for all flowrates used during the test series.

The hot water is taken from a 80 m^3 reservoir, and a pump is used to feed the test section. The rotational speed of pump is automatically controlled to keep a constant flow rate through the flow meter (not shown in Fig. 1). The stagnation chamber (diameter 300 mm) is similar to that on the cold-water leg except that the water supply is from the side via a flow distributor. The stagnation chamber is connected to a steel pipe with inner diameter 100 mm, thus giving an area contraction ratio of 9:1. The total distance with constant diameter (D_1 = 100 mm) upstream of the T-junction is approximately 20 hydraulic diameters for the hot water pipe. Fully developed pipe flow conditions cannot be achieved in this case, but the flow quality is expected to be good due to the presence of the stagnation chamber.

3.2 Instrumentation, Data Acquisition and Measurement Uncertainties

3.2.1 Velocity measurements using LDV

Velocity profiles were measured with a two-component Laser Doppler Velocimetry (LDV) system in each inlet pipe, as well as in cross-sections located 2.6 and 6.6 diameters downstream of the T-junction (see Fig. 2). It was found to be difficult to perform laser measurements with a temperature difference between the hot and cold water due to the change in the index of refraction, which deflected the laser beams in the mixing region. Measurements were originally carried out both with a temperature difference of 15°C and at isothermal conditions at the cross-sections in the hot inlet pipe and downstream of the T-junction at x/D = 2.6 [24] in order to check that the flow at isothermal conditions was similar to the case with a temperature difference. The small changes in density due to the temperature difference should have a negligible effect on the flow, both in the inlet pipe and in the mixing region downstream of the T-junction.

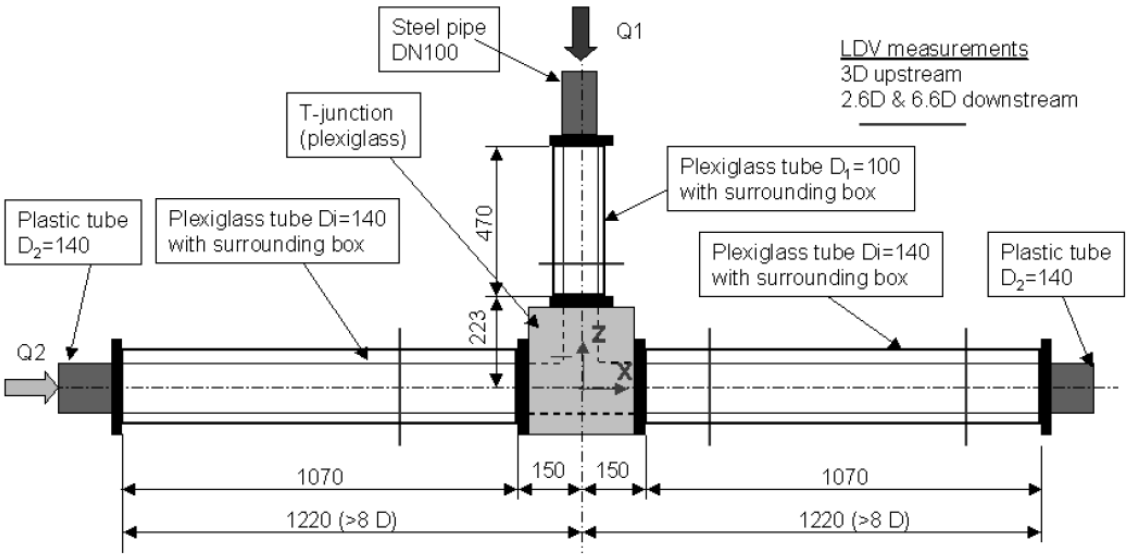

Figure 2. T-junction test section showing LDV measurement stations

The inlet mean velocity and turbulence profiles in the horizontal pipe are in good agreement with experimental data for fully developed pipe flow at similar Reynolds numbers [25]. However, the length of the hot water inlet pipe is too short to obtain fully developed flow conditions.

The uncertainty in the LDV-data is divided into random and systematic errors. The total random uncertainty, normalized with the bulk velocity, is within 2-3% for the streamwise mean velocity and 3-4% for its root-mean-square (rms) value. Systematic errors mainly derive from positioning errors for the LDV-system. The global uncertainty in the LDV-measurements is estimated to be between 6-8% for the different quantities. The discrepancy between the flowrate calculated on the basis of the integrated LDV data and that measured by the flow meter was approximately 5% according to Westin et al. [24].

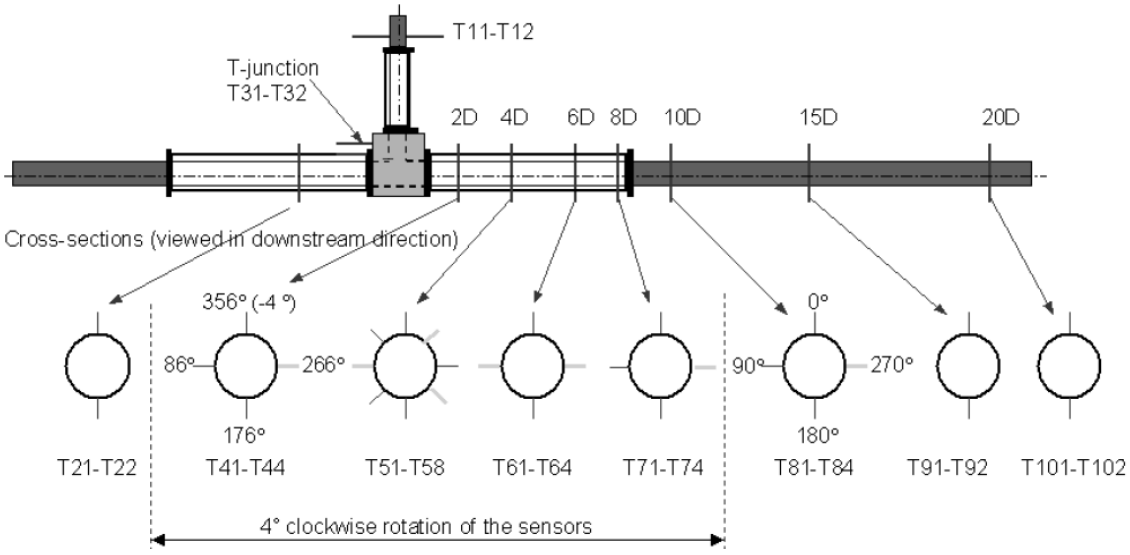

Figure 3. Cross-sections where thermocouple measurement are taken

3.2.2 Temperature measurements using thermocouples

The temperature fluctuations were recorded using thermocouples (TCs) located 1 mm from the wall at seven positions downstream of the T-junction. The positions of the TCs from the first experiments in 2006 are indicated in Fig. 3. The TCs in the experiments from 2008 are the same with the exception that the 4º-misalignment for x/D = 2-8 has been corrected and the extra TCs at 4D have been removed.

The mean temperature, the temperature fluctuations and the temperature fluctuation spectra were computed from the data collected. A typical response time for the TCs is 13 ms. This is measured by inserting the thermocouple into a hot water bath, and defining the response time as the rise time from $0.1\Delta T$ to $0.9\Delta T$, where $\Delta T = T_{hot} - T_{cold}$, the temperature difference between the inlet flows.

The uncertainty in the mean temperature measurements with thermocouples is estimated to be within ±0.5°C [24], which gives a constant uncertainty of 0.03 in terms of the normalised temperature T^* defined by

$$T^* = \left(T - T_{cold}\right) / \Delta T \qquad (1)$$

The statistical uncertainties in T_{rms} are typically less than 3%, except for a few locations near the lower wall where the signal is highly intermittent. However, an additional uncertainty of 5% has been added to account for possible systematic errors. The total uncertainty in the temperature fluctuations is then estimated to be 8% of the measured value, except near the lower wall, where an uncertainty of 13% has been assumed.

3.2.3 Velocity measurements using PIV

In the new tests carried out in 2008, Particle Imaging Velocimetry (PIV) was also used to measure the downstream velocities at stations x/D_2 = 1.6, 2.6, 3.6 and 4.6 (see Fig. 2 for the origin and orientation of the coordinate system). All PIV measurements were carried out under isothermal conditions to avoid laser distortion, as explained above for the LDV measurements. The PIV system consists of a LaVision GmbH's DaVis 7.1.1.0 with a double-pulsed Litron Nano L 50-100 Nd:YAG laser as a light source. The laser is mounted on a traverse system so that the laser sheet can be positioned accurately (with an uncertainty of less than 0.5 mm) along the pipe, downstream the T-junction. A LaVision FlowMaster Pro Plus HS camera, i.e. a 1280 x 1024 pixel CMOS camera with 10-bit dynamic range, was used along with a Nikkor 50 mm f/1.8D lens as a recording device.

The tracer particles used were AkzoNobel's Expancel 551 WU 20 hollow thermoplastic spheres with a diameters ranging from 2 μm to 30 μm, and a density of 1.2×10^{-3} kg/m^3. The typical particle image diameter is 2-3 pixels, and the ratio between the maximum light intensity at the centre of the particles and the background is more than 40. For each streamwise position, a background image (an average of 100 images) is subtracted from each frame prior to correlating. Despite the fact that the particle image diameter is clearly above the recommended value of 2 pixels, a slight tendency towards peak-locking could be observed in the probability density functions (PDF's) of the pixel displacements. The maximum errors introduced in the mean and rms-values are less than 1% when the ratio of the discretisation velocity (which is set by the PIV set-up parameters) to the rms (given by the flow) is smaller than 2. This is fulfilled for the major part of the flow field for the benchmark test. Furthermore, no oscillatory behaviour was seen in the statistics, this being a typical symptom of severe peak-locking. Provided that the sub-pixel interpolation is working properly the resolution is as high as 0.1 pixels, which corresponds to about 0.02 m/s with the current time delay.

For best spatial resolution across the pipe, the camera was aligned so that the short side of the CCD-sensor was parallel to the pipe. This results in an image size of 143 x 114 mm in the vertical and downstream directions respectively. A pixel in the image plane corresponds to 111.7 μm in physical space. The uncertainty in the calibration of the image size, and thereby the velocities, is small (less than 0.5 mm, corresponding to 0.36 % of the image size).

For the PIV evaluation, a normalised cross-correlation function with four multi-passes was used. In the two initial passes, an Interrogation Area (IA) with 128 x 128 pixels and an overlap of 25% was used. For the two final passes, the size was reduced to 64 x 64 pixels (which corresponds to a spatial resolution of 7 mm x 7 mm) with 50% overlap.

The 64 x 64 IA typically contains more than 10 clearly distinguishable particle images, which follows the recommendations of Keane and Adrian [26].

The time delay between each pair of PIV image recordings was chosen so that the maximum velocity in the measurement roughly corresponded to a particle displacement of 5 to 6 pixels. This time is varying around 500 μs throughout the different measurements.

For each position, two separate recordings are made: at 60 Hz and 4 Hz, with 1424 image pairs in each set. The dominant large-scale turbulent structures are captured using 60 Hz, while the 4 Hz recordings are used to calculate turbulent statistics based on independent samples.

A Peak Value Ratio (PVR), i.e. the ratio between the highest and the second highest peak in the correlation plane, of 1.3 was used as a validation criterion. Furthermore, the following restrictions on the allowable velocity range in the streamwise direction were applied: -0.6 m/s $< u <$ 2 m/s. The range was changed slightly depending on the flow ratio. For the cross-stream velocity component, the allowed range was ± 1 m/s for all cases. After the final pass, the results were post-processed using the same validation criteria. On average, 116 vectors were rejected in every PIV vector plot containing 32 x 40 vectors, giving a Valid Detection Rate (VDR) of about 90%. However, the VDR is not uniform throughout the vector field: there are more rejected vectors close to the walls, where reflections of the light sheet by the walls are present and the velocities are much smaller. The validation procedure does not detect all spurious vectors, and this contaminates the calculated statistics. On the other hand, stronger validation might remove some vectors that are correct, leading to a bias in the data. The undetected spurious vectors are random, and do not affect the mean velocities, but lead to visible noise in the rms-profiles.

By comparing the calculated statistical moment based on n and n+1 samples, the statistical errors in the PIV-data were shown to be below 1% for both the mean and rms-values.

As a sensitivity check, the data at one position was evaluated with two different software packages (based on different algorithms), and with slightly different settings displaying differences of 1.7% (on average) in the mean velocity and up to 4% locally.

If the different estimations for the relative errors are conservatively added as independent errors this leads to a total relative error of the order of 5 % in the mean velocity. In addition to that the absolute error for the uncertainty in the sub-pixel interpolation (corresponding to about 0.02 m/s) must be added. The errors in the rms-values are roughly doubled due to error propagation.

The above uncertainty holds primarily in the bulk of the flow and for the streamwise component for which the time delay is optimized.

Closer to the walls the uncertainty increases and is also harder to estimate. For example the errors in the rms-values can locally be larger, since the rms-velocities become very small (as they approach zero) peak-locking errors become important. Close to the walls the velocity gradients across the IA also usually become larger, which introduces an error that leads to a low-velocity bias. Reflexions from the wall that are not removed by the background subtraction can also lead to errors in terms of a low-velocity bias.

There are also some positions in the centre of the flow field where reflections have not been removed by the background subtraction, and the rms-values here are locally overestimated (seen as a local peak in the rms-profile).

In addition to the PIV uncertainty, the bulk velocity used for the normalisation of the PIV velocity profiles is based on two independent measurements of the flowrate using electro-magnetic flow meters with an accuracy of about 1 % (which corresponds to about 0.01 m/s). The differences between the readings from them and day-to-day variations in the measured flowrates are within the uncertainty.

3.3 Upstream Measurements (Boundary Conditions)

Full details of the measurements made upstream, which became the boundary conditions for the CFD simulations, are contained in the Official Benchmark Specifications (Annex 2). Only highlights are given here for orientation purposes.

The working fluid in this test is de-ionized tap water between 19°C and 36°C. It is considered that the physical properties are adequately described by the 1967 ASME Steam Tables, with additional information on the thermal expansion coefficient from the book of Incropera and DeWitt [27].

The volumetric flow rates used in the benchmark test are given in Table 4, together with the locations where the velocity distributions over the pipe cross-sections were measured (the left and upper red lines in Fig. 2). The temperatures for the cold and hot inlets are also given at these cross-sections. The temperatures of the inflowing streams were assumed to be uniform at the measuring locations, and only one thermocouple was placed there. The reading taken is that given in the 2nd column of Table 4.

Table 4: Inlet temperatures and flow rates

Inlet/designation	**Temperature (°C)**	**Pipe diameter (mm)**	**Measuring location (mm)#**	**Volumetric flow rate (litres/s)**
Main/InCo	19	140 (D_2)	-420 (-3D_2)	9.0
Branch/InHo	36	100 (D_1)	-310 (-3.1D_1)	6.0

See Fig. 2 for the origin and orientation of the coordinate system

The inlet velocity profiles at the upstream stations (Table 4) are those taken from an earlier test [24] in which the volumetric flow ratio between the main and branch streams was 2 rather than the 1.5 for the present test. The flowrate in the hot inlet was kept the same as before (6 l/s), whereas the one in the cold inlet was 9.0 l/s instead of 12.0 l/s used previously. Since the velocity profile is fully developed in the cold inlet, the results presented below just need scaling to fit the present flowrate. This exercise was left to the participants.

In the earlier test, the velocity measurements were taken at the upstream locations using a two-component LDA system, which gave one component of velocity in the main flow direction (i.e. parallel to the axis of the pipe) and one component transverse to this. The coordinate systems adopted in the measuring planes of the two upstream pipes are shown in Fig. 4. Velocity profiles and turbulence statistics are available in the two perpendicular directions (ycl and zcl) defined in Fig. 4 for both the main (InCo) and branch (InHo) pipes.

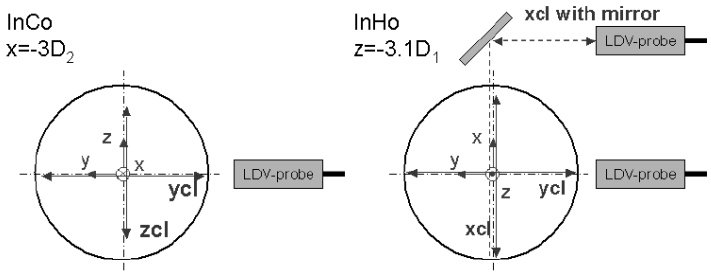

Figure 4: Overview of the upstream LDV measurement orientations

For the main pipe, the measuring plane is -3D_2 upstream of the centre of the T-junction. Mean and rms-profiles for the streamwise velocity component are drawn in the left column of Fig. 5 and for the cross-stream components in the right column. Note that the streamwise mean velocity component (U) is scaled with the bulk velocity; U_{bulk}, while the other velocity components are scaled with the mean centreline velocity, U_{cl}, where $U_{cl} = 1.17 \times U_{bulk}$. The two cross-stream profiles zcl and ycl for the streamwise component are in good agreement, which is to be expected given that the flow should be axisymmetric. Likewise for the cross-stream components. The definitions of the quantities are:

$$U = \bar{u} = \frac{1}{n}\sum_{i=1}^{n} u_i \quad U_{rms} = \left(\overline{(u-\bar{u})^2}\right)^{1/2} \qquad (2)$$

The profiles, and the associated Reynolds stresses, have been compared against other experimental data for a very similar Reynolds number [25], and all indications are that the profile is indeed fully developed, as expected.

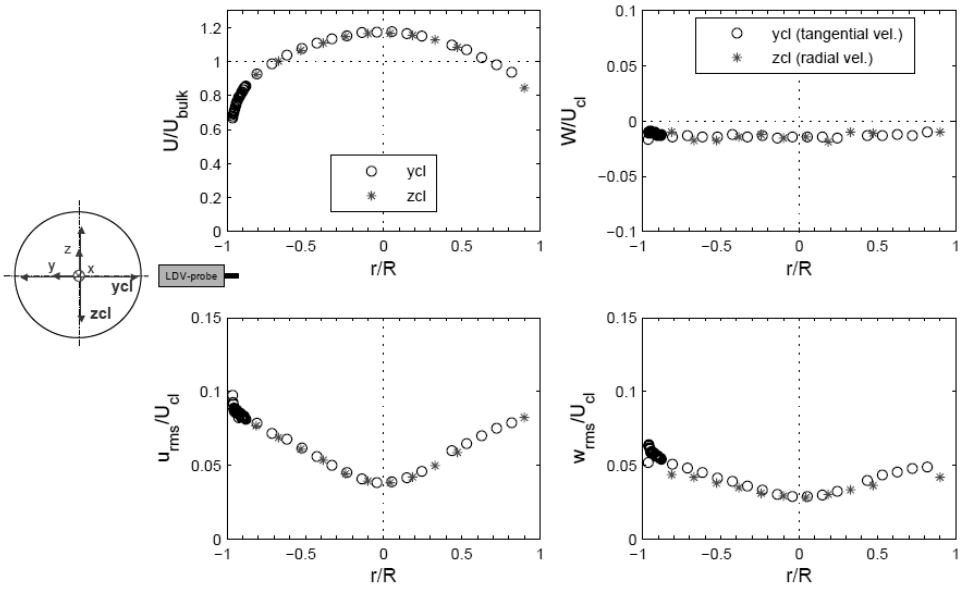

Figure 5: Velocity measurements in the cold inlet pipe at x = -3D_2, measured along zcl and ycl. The left column shows data for the axial velocity component (u), and the right column shows corresponding data for the transverse components.

As mentioned earlier, the inlet velocity profiles had been measured earlier [24] for a main/branch flow ratio of 2. For the benchmark test, the flowrate in the hot inlet has been kept the same, so the same velocity profiles can be applied for the present case too, with flow ratio of 1.5.

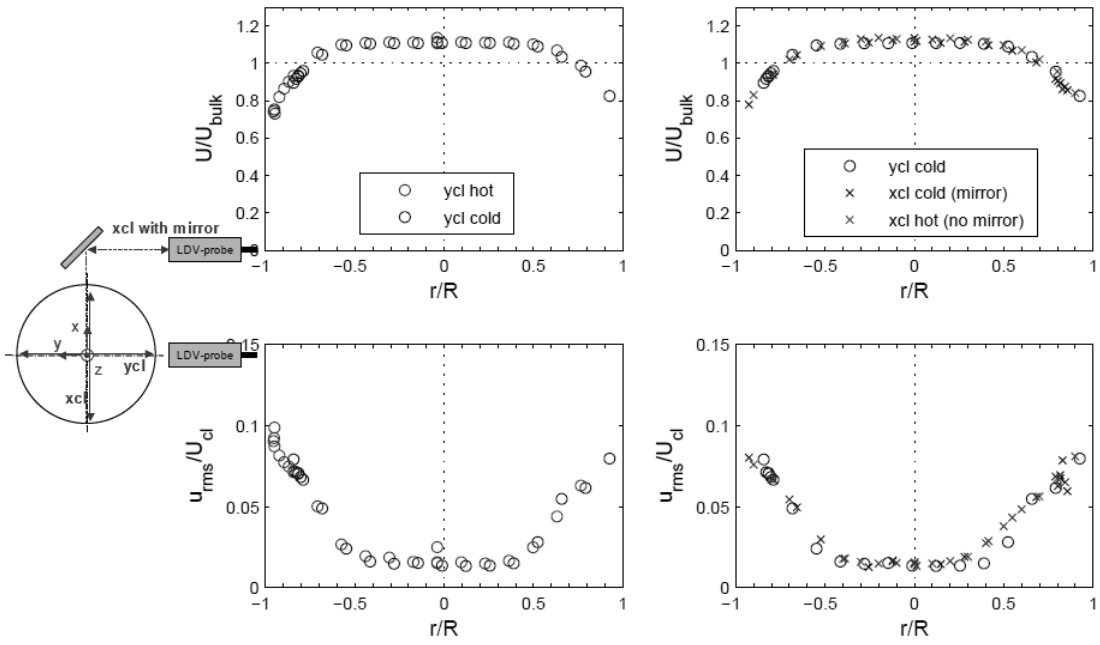

Figure 6: Streamwise (axial) velocity component for the hot inlet at z = -3.1D_1: left column, ycl with hot and cold water; right column, ycl with cold water, xcl with hot and cold water.

Figure 6 shows the axial velocity data for the hot water inlet pipe, measured at a cross-section -3.1D_1 upstream of the centre of the tee. Recalling that this inlet pipe is considerably shorter than the cold inlet pipe (only 20 hydraulic diameters compared with 80 for the cold inlet), fully developed turbulent pipe flow cannot be expected. Indeed, all profiles indicate a flow with developing boundary layers on the pipe wall, while the central region of the pipe shows characteristics similar to a mainly undisturbed free stream. The centreline velocity is $U_{cl} = 1.11 \times U_{bulk} \approx 0.86$ m/s.

As mentioned already, it was preferred to perform these measurements under isothermal conditions, since the changes in the refractive index of the water due the temperature difference $\Delta T \approx$ 15 K caused distortion of the laser beams in the mixing region. However, a check was made that the flow at isothermal conditions would be similar to that with hot and cold streams, as used for the temperature measurements with thermocouples. Both sets of data are included in Fig. 6 and show good correspondence.

Figure 7 gives the measured profiles of the velocity components in the xcl and ycl directions (see inset to Fig. 6 for coordinate orientation) at the same upstream cross-section (z = -3.1D_1). Information on Reynolds stresses (not shown in Fig. 7) was also provided.

For convenience, all data were also made available to the benchmark participants in tabular form.

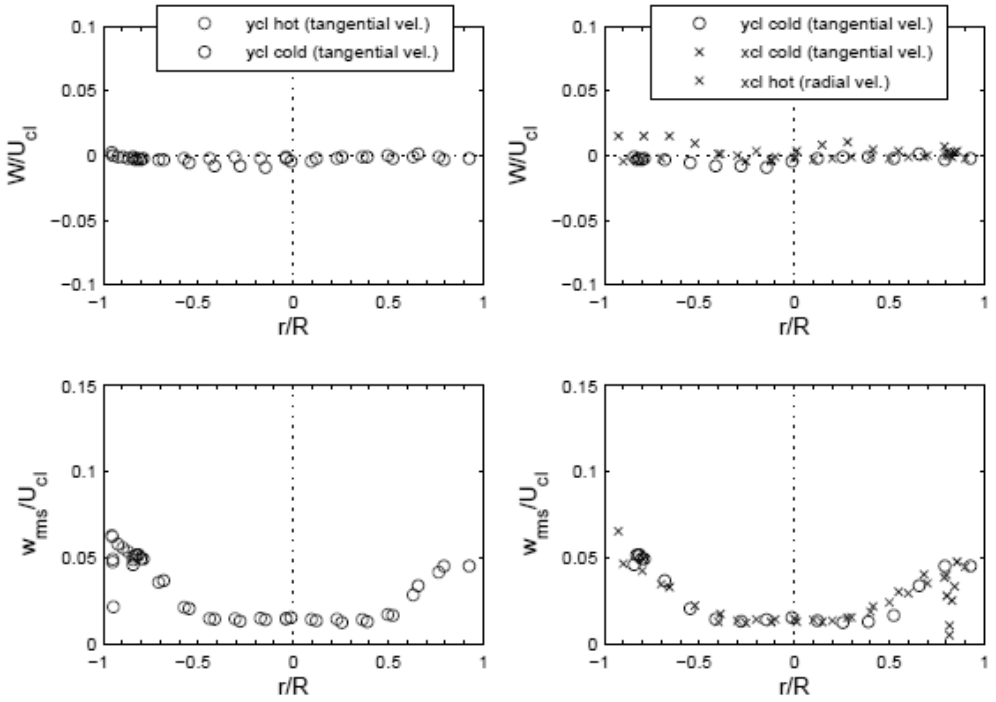

Figure 7: Scaled transverse (radial/tangential) velocity components for the hot inlet, measured at z = -3.1D_1: left column, ycl with hot and cold water; right column, ycl with cold water, and xcl with hot and cold water.

3.4 Downstream Measurements

All data presented in this report are the property of Vattenfall Research and Development AB and have been used with their permission.

3.4.1 Temperatures

With reference to Fig. 3, the inside diameter of the main pipe is 140 mm (D_2). Thermocouples of 0.13 mm diameter (frequency response 30 Hz) were placed approximately 1 mm (with an estimated uncertainty of about a couple of hundred microns, primarily in the positive direction) from the inner pipe wall at $x = 2D_2$, $4D_2$, $6D_2$, $8D_2$, $10D_2$, $15D_2$ and $20D_2$. Taking 0° to be the top of the main pipe ($y = 0$, $z = 70$ mm), thermocouple locations around the circumference of the pipe are given in Table 5. Angles in the Table increase in a counter-clockwise direction if the viewing perspective is from the tee junction (coordinate origin) towards the thermocouples (i.e. looking in the positive x-direction). Time-averaged temperatures and temperature fluctuations are available for all thermocouple locations. Data were collected over a period of 300 s.

Table 5. Thermocouple Locations

Location on x axis	**Angular Positions (Degrees)**
2 D_2	0, 90, 180, 270
4 D_2	0, 90, 180, 270
6 D_2	0, 90, 180, 270
8 D_2	0, 90, 180, 270

10 D_2	0, 90, 180, 270
15 D_2	0, 180
20 D_2	0, 180

Always important to the issue of thermal fatigue is the presence of low-frequency peaks in the temperature fluctuations. Figure 8 shows the temperature spectrum at $x/D_2 = 4$, 90° (see Fig. 3 for coordinate system orientation) for a flowrate ratio of 2 which was used in an earlier experiment. There is a definite peak close to 4 Hz. Similar peaks were noted in other tests in the series [20], for which the flowrate ratios were $Q_2/Q_1 = 1$ and 4. The peak shifted from 3 to 4 to 6 Hz as the flowrate ratio was changed from 1 to 2 to 4. In the present case, with a flowrate ratio $Q_2/Q_1 = 1.5$, the peak is at a frequency between 3 and 4 (see later). It will be a challenge for the CFD simulations to reproduce this peak.

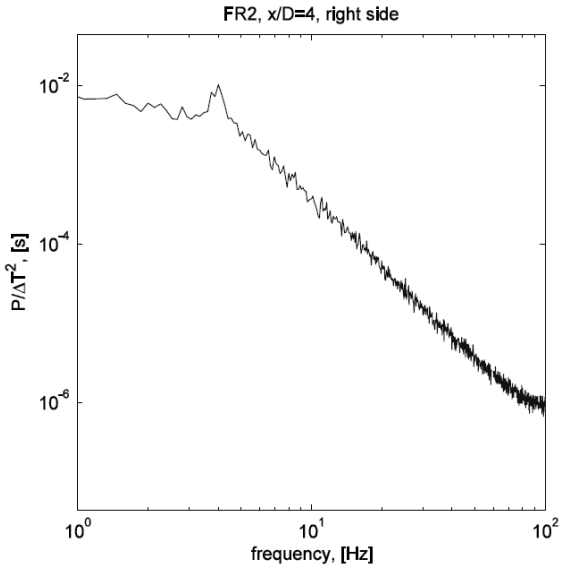

Figure 8: Sample temperature spectrum at $x/D_2 = 4$, 90° for a previous test case with a flowrate ratio of 2. The peak is at 4 Hz.

3.4.2 Velocities

Velocities were measured using PIV at $x = 1.6D_2$, $2.6D_2$, $3.6D_2$, and $4.6D_2$ along two lines perpendicular to the flow: horizontal (-70 mm < y < 70 mm, $z = 0$), and vertical (-70 mm < z < 70 mm, $y = 0$). Mean flow, RMS fluctuations and Reynolds stresses were computed at all four downstream locations. The number of values provided for each velocity component on each line varied somewhat with the streamwise position, but was roughly 35.

Time-dependent PIV information is also available at the same four downstream locations from measurements with a frequency of 60 Hz, sampled for 12 seconds in two separate sets. The time duration was limited by the storage capacity for the digital images. All velocity components were given on the pipe centreline. The x and z components (u and w) were provided at $y = 0$, $z = \pm 35$ mm, and the x and y components (u and v) provided at $z = 0$, $y = \pm 35$ mm.

Detailed discussion of the experimental findings is not given here, since the data are to be used for comparison against numerical predictions in Section 5 of this document, and will appear in that context. Readers interested in the purely experimental techniques employed in obtaining the test data in analogous experiments are referred to the specialist papers on the subject [18,20,24].

4. COMPUTATIONS

4.1 Participants

As stated earlier, following the kick-off meeting, there were 69 official registrations made to the NEA secretariat. All subsequently received the Benchmark Specifications. Of these, 29 submitted results before the deadline. The first 2 submissions were received in January 2010, and the last just a few hours before the deadline of Midnight GMT on April 30, 2010. Table 6 lists the names and affiliations of the participants in the order their submissions were received. Also listed are the codes used to perform the simulations.

Table 6. List of Participants, Affiliations and Codes Used

Participants	**Label**	**Organization**	**Code**
S. Kuhn	S1	PSI	FLUENT
C. Boyd, K. Armstrong, D. Eastman	S2	USNRC	FLUENT 12
T. Hoehne	S3	FZD	CFX5 v12
T. Farkas, I. Farkas	S4	AEKI	FLUENT 6.3.26
R.J.A Howard, J.-M. Ndombo	S5	EDF	Saturne
A. Frisani , Y.A. Hassan	S6	Texas A&M	STAR-CCM+/3.06.006
M. Scheuerer, J. Weiss	S7	GRS	CFX
S.T. Jayaraju, E. Komen, E. Baglietto	S8	NRG	STAR-CCM+/3.06.006
T. Morii	S9	JNES	Advance/FrontFlow/red (ver.4.0)
H. Ayhan, C. Kocar, C.N. Sokmen	S10	Hacettepe Uni. (Turkey)	FLUENT 12
J.-L. Muñoz-Cobo, S Chiva, M. Ali	S11	UPV (Valencia)	CFX
J. Szymanski, B. McLaughlin	S12	CNSC/AMEC-NSS	MODTURC_CLAS-IST
N.P.Petropoulos, K.G. Aivalis	S13	Nat. Tech. Uni. Athens	CFX v12
V. Goloviznin, A. Karabasov, M. Zaitsev	S14	NSI	CABARET
G. Pochet	S15	Tractebel Engineering	CFX
T. Rämä	S16	FNS, Finland	FLUENT 12
N. Forsberg, H. Bergersen, H. Lindqvist	S17	Forsmarks Kraftgrupp AB	OpenFOAM 1.6
D.G. Kang, K.W. Seul, Y.H. Ryu	S18	KINS	CFX
H. Lindqvist, H. Tinoco N. Forsberg	S19	Forsmark Kraftgrupp AB	FLUENT 12.1
P. Veber, L. Andersson	S20	Onsala Ingenjörsbyrå AB	FLUENT
P. Fischer, A. Obabko, A. Caceres, T. Tautges	S21	Argonne National Laboratory	Nek5000 (Spectral Element)

Participants	Label	Organization	Code
V. Petrov	S22	PSI	STAR-CCM+
M. Romero, J. Gillis, B. Belley	S23	Structural Integrity Associates	CFX
T. Brockmann	S24	Aalto University CFD group	OpenFOAM 1.6
M. Labois, D. Caviezel, D. Lakehal	S25	ASCOMP GmbH	TransAT
D. Kloeren	S26	IKE, University of Stuttgart	FLUENT 12.1
W. D. Pointer, E. Merzari	S27	Argonne National Laboratory	STAR-CCM+ v5.02.009
J. Kim	S28	KAERI	Internal KAERI CFD code
L.Mengali, F.Moretti, F.D'Auria	S29	GRNSPG/UNIPI	CFX

4.2 Codes and Models

Table 7 provides information on selection of turbulence model, total number of control volumes, run duration and time-step size for each contributor listed in Table 6. Regardless of time-step size, transient results were only to be reported every millisecond. Subgrid turbulence models are as reported by the contributors. No attempt has been made to standardise nomenclature where different phrases are used to describe the same code option.

Table 7. List of Participants, Affiliations and Codes Used

Participants	Turbulence	Total number of control volumes (millions)	Duration (s)	Time step (s)
S. Kuhn	LES	4.5	5	1.00E-003
C. Boyd	LES, Dynamic Smagorinki	34	20	1.00E-003
T. Hoehne	LES, WALE	0.97	20	1.00E-003
T. Farkas	LES, Dynamic Smagorinki	5.8	15	1.00E-003
R.J.A. Howard	LES, Dynamic Smagorinki	6.2	5	1.50E-004
A. Frisani	LES, WALE	9.3	10	1.00E-003
M. Scheuerer	SAS-SST	5	13	1.00E-003
S.T. Jayaraju	LES, WALE SGS	13.2	28	5.00E-004
T. Morii	LES, Smagorinsky	4.1	5	1.00E-004
H. Ayhan	LES, Smagorinsky-Lilly	0.92	14	2.50E-004
J-L Muñoz-Cobo	LES, WALE	3.4	6.9	1.00E-003
J. Szymanski	k-epsilon/RNG	0.89	-	0.00E+000
N.P. Petropoulos	SAS-SST	1.1	5	1.00E-003
V. Goloviznin	ILES	1.8	5	1.00E-003
G. Pochet	SAS-SST	2.3	5	1.00E-003
T. Rämä	LES, WALE	7.7	5.5	1.00E-003

Participants	Turbulence	Total number of control volumes (millions)	Duration (s)	Time step (s)
N. Forsberg	LES, 1eqn. Dynamic eddy	0.28	20	2.40E-004
D.G.Kang	DES-SST	2.4	13	1.00E-003
H. Lindqvist	SST-kω*	11	10	1.00E-003
P. Veber	LES, Dynamic Smagorinsky	70.5	23	2.00E-004
P. Fischer	LES, spectral damping	(62K)#	5.9	5.99E-005
V. Petrov	LES	4.4	6.2	5.00E-004
M. Romero	LES, WALE	1.9	5.2	5.00E-004
T. Brockmann	LES, Dynamic Smagorinsky	8	5	2.50E-004
M. Labois	LES, WALE	2.5	5.5	9.58E-005
D. Kloeren	LES, Dynamic Kinetic Energy SGS Model	7.2	18	1.00E-003
W. D. Pointer	V2F	0.62	5	1.00E-003
J. Kim	LES (Dynamic Vreman)	3.7	6	2.60E-004
L. Mengali	SAS-SST	1.0	10	1.000E-003

* Slightly modified version of the standard model in which the turbulent viscosity is scaled by a factor 0.38

4.3 Data Requested

Prior to the period of reported data, it was each participant's responsibility to run the simulation for a long enough time interval for time-averaged velocities to become steady. Past simulations of this facility have accomplished this in 2-4 seconds [20,24], though it was stipulated that these times served as a guide only. After this initial period, all transient data were to be reported at every 0.001 seconds (a number of participants ignored this stipulation) for at least the last 5 seconds of the transient calculation, and for no more than 20 seconds (to keep the sizes of the results files manageable – though two submissions of 23 and 28 seconds exceeded this limit). If time-step sizes other than the 0.001s required for the analysis were used in the calculation, contributors were requested to report their method for data conversion.

To characterise the velocity field, all three resolved components of the velocity vector at each measuring position were requested, and the turbulent kinetic energy (k_{SGS}) from the subgrid turbulence model (if available). The number of points along each line segment had to be no less than 20 and no more than 50 for each measuring plane.

This is a spectral element code with Lagrangian interpolants of degree 7.

5. SYNTHESIS OF RESULTS

5.1 Introduction

Because of the relatively large number of benchmark submissions, an extremely large number of possible comparisons with data and between submissions are possible. As a result, data reduction and plotting were all accomplished using a Python script [28] to control the total level of effort. In the end, most of the man-hours expended on this synthesis dealt with initial problems with the submissions, and trying to make sense of the plots produced by the script. This is a lesson for future benchmarks, for which it is recommended that the script be sent in advance to all participants so they can separately verify the accuracy of the formatting of their data files prior to submitting them.

The range of observations made during the synthesis was restricted by two factors. The work was a part-time, unpaid effort by a single individual, and within the context of CFD the amount of information available for analysis was relatively small. Anyone wanting a more detailed picture of the benchmark than presented here should also read the detailed description of experimental results and papers produced by benchmark participants.

5.2 Available Data

As a consequence of the sparsity of the PIV data, standard visualisation techniques could not be applied to characterise the flow oscillations resulting from the branch-line injection. However, Fourier analysis of the transient thermocouple and PIV data provides useful information for comparison with transient CFD results. Fourier spectra from both data and CFD tend to be noisy, so all results presented in this paper have been smoothed with a running average from five results before to five results after the actual result at a given time.

For other experiments in the same facility with flow ratios (cold inlet volumetric flow divided by hot inlet volumetric flow) of 1 and 2, Odemark et. al. report peaks in the temperature transforms at 3 Hz and 4 Hz, respectively. The flow ratio for this benchmark is 1.5 and discrete Fourier transforms of thermocouple data at x =2 D, 270º, x = 4D, 90º and 270º show a distinct peak at approximately 3.5 Hz (e.g. Fig. 9). Weaker peaks are visible in transforms of transient data from thermocouples at x = 2D, 90º and x = 6D, 270º. No other thermocouple data showed this peak.

Since the velocity field determines the temperature distribution, peaks are expected – and found – in transforms of some of the PIV data. Strong peaks are seen around 3.5 Hz at all four downstream locations for U (x component) at z = 0 and y = ±35mm, and for V (y component) on the centreline (see Figs. 10, 11). Strong peaks are also seen for V at 3.6 and 4.6 hydraulic diameters downstream of the junction at z = 0 and y = ±35mm. Weak peaks appear to be present for U on the centreline at all four x locations, and at y = 0, z = ±35mm for x = 3.6D and 4.6D.

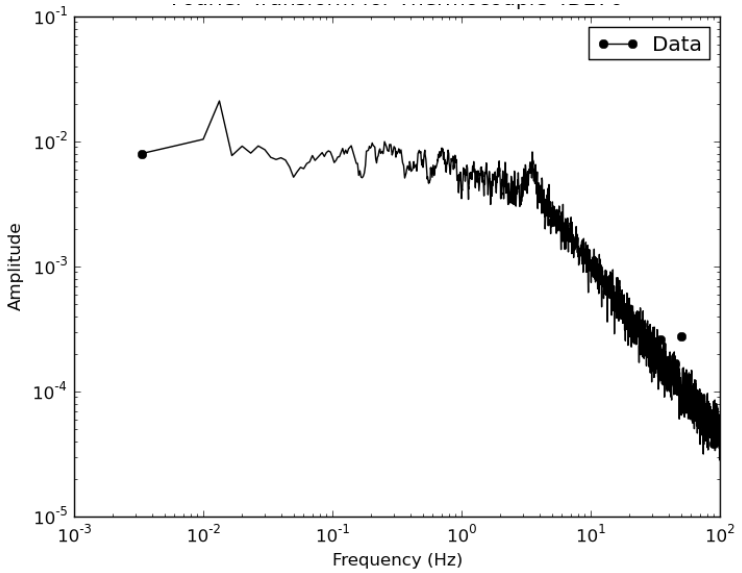

Figure 9. Thermocouple Spectrum at x = 2D, 270º

There is some indication of organized oscillations in the range of 4-6 Hz, and below 1 Hz. However, short duration of the PIV samples and the weak and infrequent occurrence of peaks above 4 Hz do not justify any conclusions at this time.

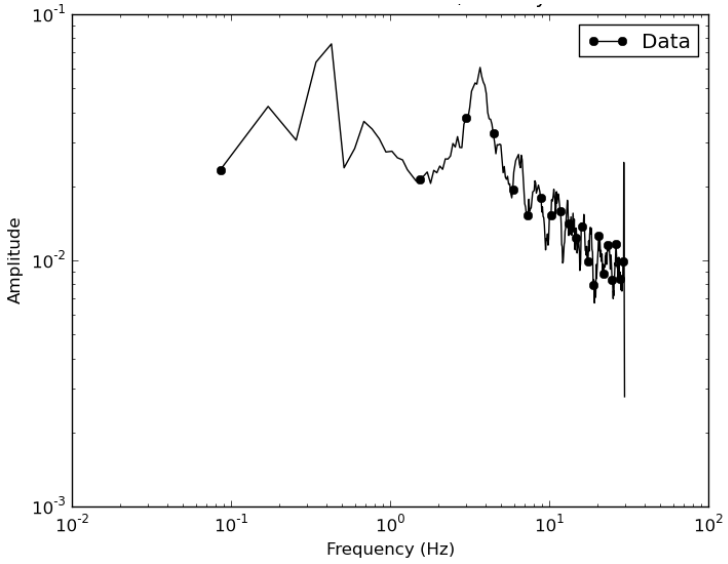

Figure 10. Velocity x-component Spectrum at x = 1.6D, y = -35mm, z = 0

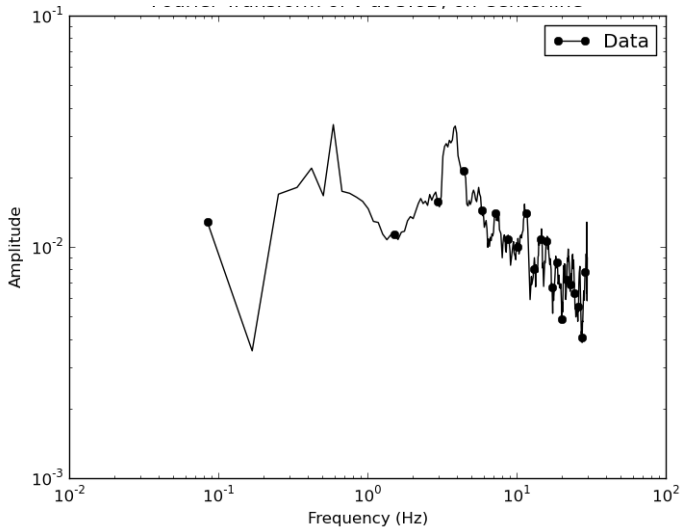

Figure 11. Velocity y-component Spectrum at x = 3.6D, y = 0, z = 0

5.3 Simple Metric for Comparison

Given the relatively large number of submissions, and the even larger number of possible comparisons between experiment and calculation, a good starting point was needed for the synthesis of results. A very simple metric was chosen to quickly compare the relative quality of the CFD calculations. For any given curve (e.g. x component of velocity along a vertical line through the pipe centre) the metric is defined as:

$$M = \frac{1}{N} \sum_{i=1,N} \left| C_i - D_i \right|$$

where N is the total number of CFD results in the curve, C_i is the i^{th} result from the CFD calculation and D_i is the measured value at the same location. In cases where reported CFD and experimental results are not co-located, a simple linear interpolation is applied to the experimental data to obtain an estimated value at the exact location of the CFD result.

These metrics were generated for all benchmark submissions using all comparisons of time averaged velocity components, RMS-velocity fluctuations, time averaged temperatures, and RMS temperature fluctuations. No attempt was made to compare time-dependent results in this way.

Ranking of submissions was performed separately for the velocity and temperature comparisons. For each application of the metric, the 29 submissions were assigned a rank from 1 (lowest metric value) to 29 (highest metric value). After all comparisons were completed, ranks associated with velocities were summed to provide one summary score and those associated with temperature were summed for a second summary score. The ranking of the time-averaged y-component of velocity was not included in the final score. In theory, because of the vertical symmetry plane in the experiment, this time-average should be zero. However, in practice, small non-zero values can be expected, and Fig. 12 suggests that small, unreported asymmetries in the experiment result in non-zero values.

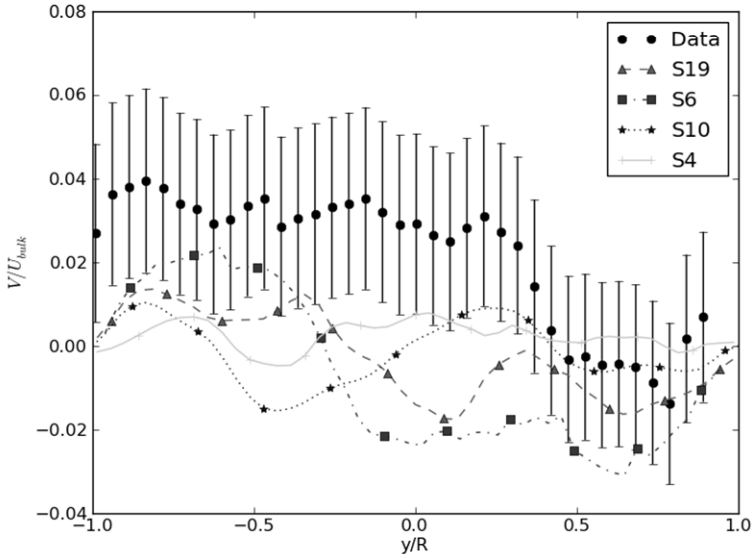

Figure 12. Time-averaged y-component of velocity at x = 2.6D

The final ranking for velocity-based comparisons is shown in Table 8 and that based on temperature comparisons is shown in Table 9. One submission is not included due to problems in locations of reported results discovered too late to be corrected. Another is not included in Table 8 due to a similar problem restricted to reporting of velocities. A lower score is a better result, but it should be noted that the ranking method was just intended as a rough way to extract useful information from the results. Better metrics are available, and with some study, better ways of weighting the metrics between data sets could be constructed.

Table 8. Submissions Ranked by Comparisons to PIV Data

Submission	**Velocity Score**	**Code**	**Turbulence**	**Volumes**
S20	75	FLUENT	LES, Dyn. Smagorinsky	70.5M
S2	166	Fluent 12	LES, Dyn. Smagorinsky	34M
S8	178	STAR-CCM+/3.06.006	LES-Wale SGS	13.2 M
S4	184	Fluent 6.3.26	LES, Dyn. Smagorinsky	5.8M
S24	212	OpenFOAM 1.6	LES, Dyn. Smagorinsky	8 M
S21	247	Nek5000	LES, spectral damping	21M
S16	270	Fluent 12	LES-WALE	7.7M
S3	311	CFX5 v12	LES, WALE	0.97M
S11	312	CFX	LES-Wale	3.4M
S19	322	FLUENT 12.1	SST-kω	11M
S18	349	CFX	DES-SST	2.4M
S14	358	CABARET	ILES	1.8M
S17	374	OpenFOAM 1.6	LES, 1eqn. Dyn. eddy	0.28M
S9	375	Advance/FrontFlow/red v4	LES-Smagorinsky	4.1 M
S22	404	STAR-CCM+	LES	4.4 M
S6	408	STAR-CCM+/3.06.006	LES-Wale	9.3 M
S26	432	FLUENT v12.1	LES - Dynamic KE SGS	7.2 M
S27	446	STAR-CCM+	V^2F	0.62 M
S23	458	CFX	LES-WALE	1.9 M
S10	477	Fluent 12	LES-Smagorinsky-Lilly	0.92M
S25	585	TransAT	LES-WALE	2.5 M
S1	589	Fluent	LES	4.5M

Submission	Velocity Score	Code	Turbulence	Volumes
S7	603	CFX	SAS-SST	5.0 M
S15	605	CFX	SAS-SST	2.3M
S13	706	CFX 12.0	SAS-SST	1.1M
S12	712	MODTURC_CLAS	k-epsilon/RNG	0.89M
S29	719	CFX	SAS-SST	1.0M

Detailed conclusions are not possible without a detailed review of nodalisations. However, at least two features stand out immediately for the velocity-based comparisons. For the same selection of turbulence model, total number of discrete volumes is generally a good indicator of quality of comparison. This suggests that most participants were reasonably careful in their selection of mesh within the constraints of available computer resources. Also, for roughly the same number of volumes, the SAS-SST appears to be significantly under-performing in comparison to LES with Dynamic Smagorinsky or WALE. Other results show that SST is performing well, so problems with quality of results are probably due to the SAS model. This issue is explored in more detail below.

Table 9. Submissions Ranked by Comparison to Thermocouple Data

Submission	TC Score	Code	Turbulence	Volumes
S21	36	Nek5000	LES, spectral damping	21M
S16	45	Fluent 12	LES-WALE	7.7M
S8	48	STAR-CCM+/3.06.006	LES-Wale SGS	13.2 M
S4	57	Fluent 6.3.26	LES, Dyn. Smagorinsky	5.8M
S22	72	Star-CCM+	LES	4.4 M
S23	78	CFX	LES-WALE	1.9 M
S5	81	Saturne	LES, Dyn. Smagorinsky	6.2M
S2	82	FLUENT 12.1	LES, Dyn. Smagorinsky	34M
S20	82	FLUENT	LES, Dyn. Smagorinsky	70.5M
S19	83	FLUENT 12.1	SST-kω	11M
S14	88	CABARET	ILES	1.8M
S25	88	TransAT	LES-WALE	2.5 M
S18	93	CFX	DES-SST	2.4M
S10	105	Fluent 12	LES-Smagorinsky-Lilly	0.92M
S26	105	FLUENT v12.1	LES - Dynamic KE SGSl	7.2 M
S6	110	STAR-CCM+/3.06.006	LES-Wale	9.3 M
S17	121	OpenFOAM 1.6	LES, 1eqn. Dyn. eddy	0.28M
S7	124	CFX	SAS-SST	5.0 M
S11	138	CFX	LES-Wale	3.4M
S1	139	Fluent	LES	4.5M
S24	151	OpenFOAM 1.6	LES, Dyn. Smagorinsky	8 M
S9	164	Advance/FrontFlow/red v4	LES-Smagorinsky	4.1 M
S15	164	CFX	SAS-SST	2.3M
S13	186	CFX 12.0	SAS-SST	1.1M
S27	186	Star-CCM+	V^2F	0.62 M
S29	197	CFX	SAS-SST	1.0M
S3	201	CFX5 v12	LES, WALE	0.97M
S12	224	MODTURC_CLAS-IST	k-epsilon/RNG	0.89M

A metric based on root-mean-square error produced ranking and scores very close to those above based upon the magnitude of the mean error. Submissions S3 and S11 swap positions in Table 8, and submissions

S19 and S20 swap positions in Table 9. In both instances, the scores only differed by one, so there are no significant changes.

5.4 Performance Based on Time-Averaged and RMS-velocity Component Data

In Figures 13-16 the submissions with the top four results rated by velocity (see Table 8) are compared. Quality judgments depend on the particular goals of the analysis. For many purposes, acceptable results for the averaged quantities can be obtained with far less than the 70 million volumes used in the LES analysis of submission S20.

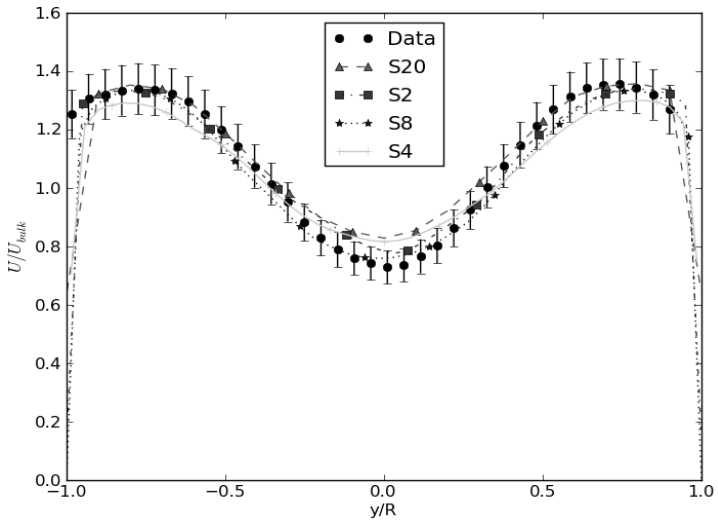

Figure 13. Time Averaged U at x = 1.6D, z = 0

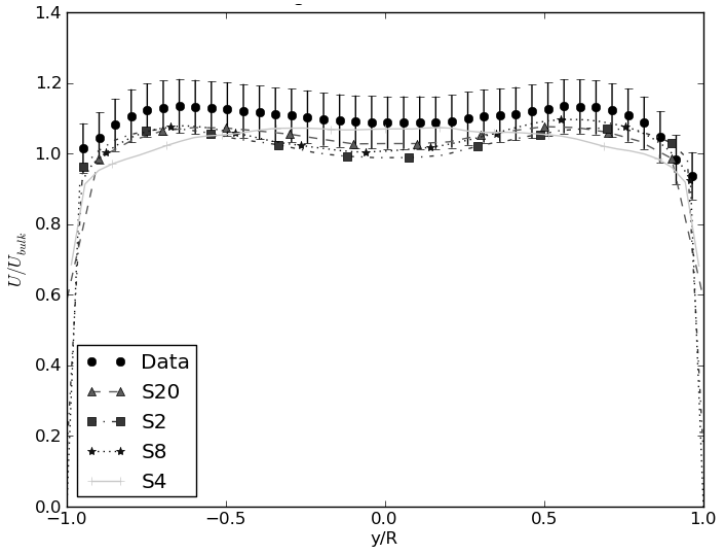

Figure 14. Time Averaged U at x = 4.6D, z = 0

Note that the submission with the smallest number of volumes (S4, 5.8M volumes) fails to capture the shape of the time-averaged U profile at x = 4.6D, z = 0 (Fig. 14). Results from the other three LES calculations retain two small, off-centre maxima, while S4 has a maximum at or near the pipe centreline.

It was already noted in connection with Fig. 12 that results for time-averaged V were expected to be poor, due to the symmetry about the y = 0 plane. Figure 17 shows that results for time-averaged W velocity component are not as close to each other as those seen for the time-averaged axial component U (Figs. 9, 10). However, the basic shape of the curve is reproduced by all four calculations.

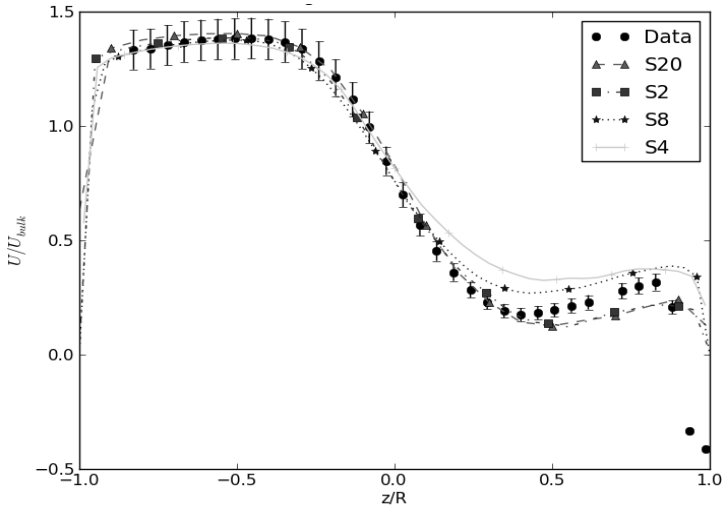

Figure 15. Time Averaged U at x = 1.6D, y = 0

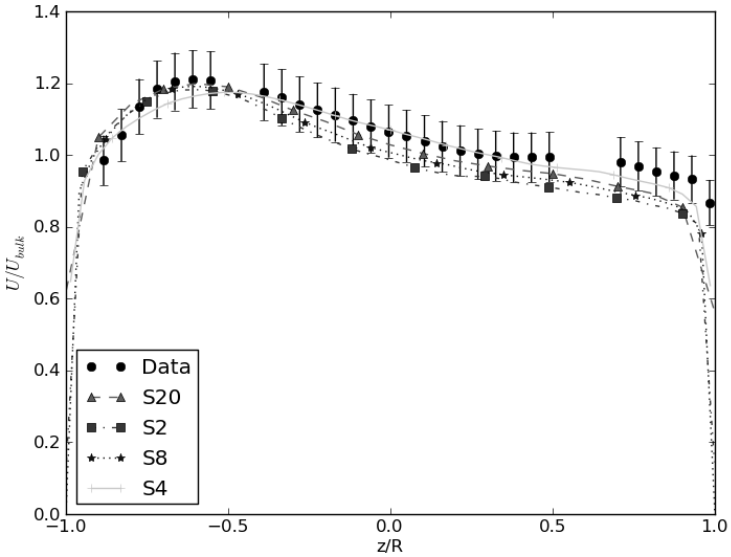

Figure 16. Time Averaged U for x = 4.6D, y = 0

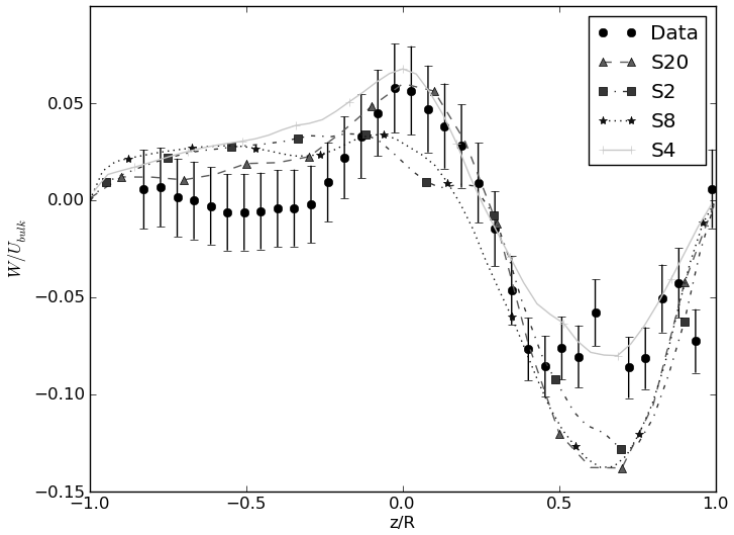

Figure 17. Time Averaged W for x = 1.6D, y=0

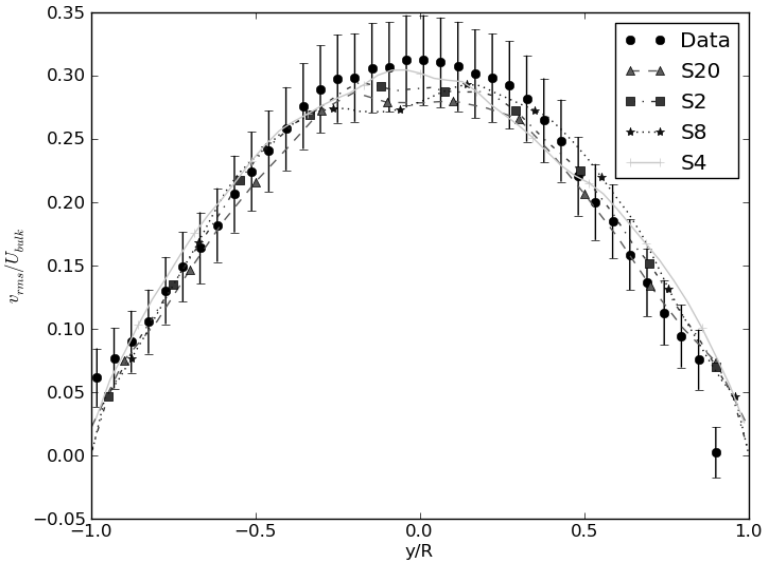

Figure 18. Time averaged RMS v for x = 1.6D, z = 0

The quality of results for the RMS value of v in Fig. 18 should be viewed in comparison with those for time-averaged V in Fig. 12. Notwithstanding the fact that the absolute value of V is small due to symmetry, and that the measurement uncertainty is large, calculated mean values are all closer to the theoretical value of zero for all mesh resolutions, while the measured values have a definite positive tendency, perhaps due to a slight bias in the experimental set-up. However, the RMS-profile (Fig. 18) is predicted within experimental error.

The next six Figures compare results from the best of the LES calculations using a dynamic Smagorinsky model to those from the best of the Scale-Adaptive Simulation approach with the Shear Stress Transport model (SAS-SST), along with those from use of a Detached Eddy Simulation (DES) model with SST, and a Very Large-Eddy Simulation (VLES) with an SST-kω turbulence model. They correspond to Figures 13-18 for the LES runs.

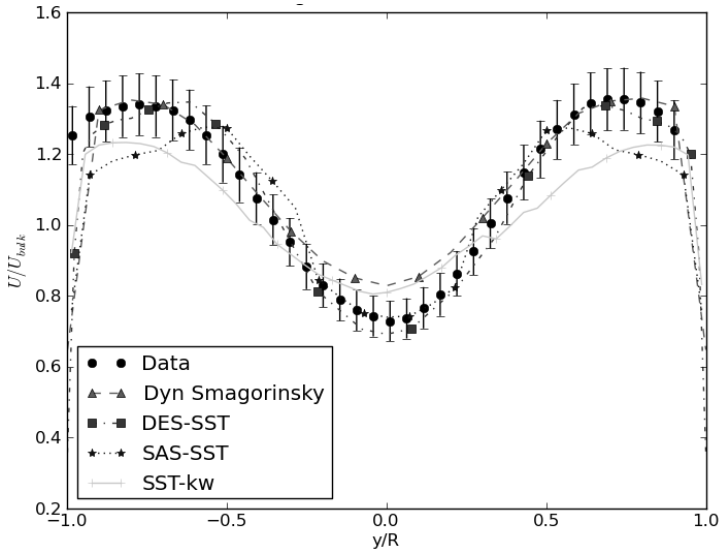

Figure 19. Comparison of Time Averaged U at x = 1.6D, z = 0

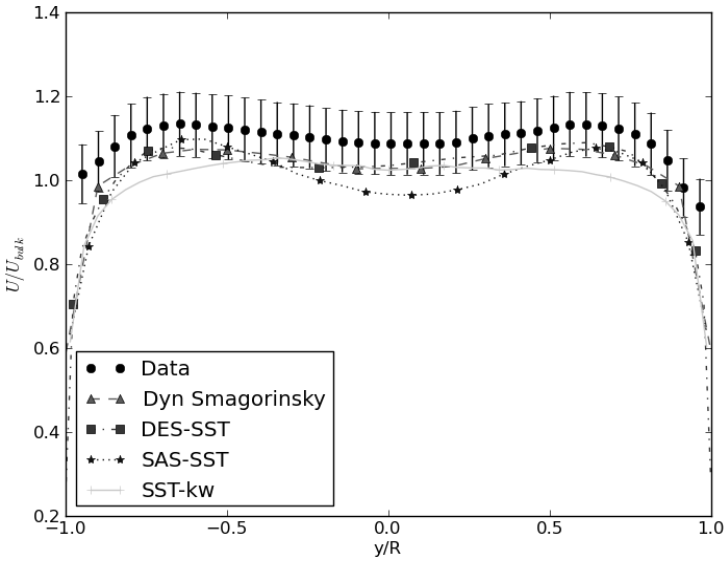

Figure 20. Comparison of Time Averaged U at x = 4.6D, z = 0

For Figure 19, the SAS-SST results have maxima that are significantly closer to the centreline than seen in the experiment or the other CFD results. The absolute values at the maxima are also underpredicted. For the SST-kω model, the difference between magnitudes at the maxima and the central minimum is significantly smaller than that measured and the numerical predictions. The DES-SST does exceptionally well given the relatively small number of computational volumes (2.4M). For Figure 20 (x=4.6D, z=0), the SST-kω analysis has not captured the double maximum, and SAS-SST has too large a difference between the values at the maxima and that at the central minimum.

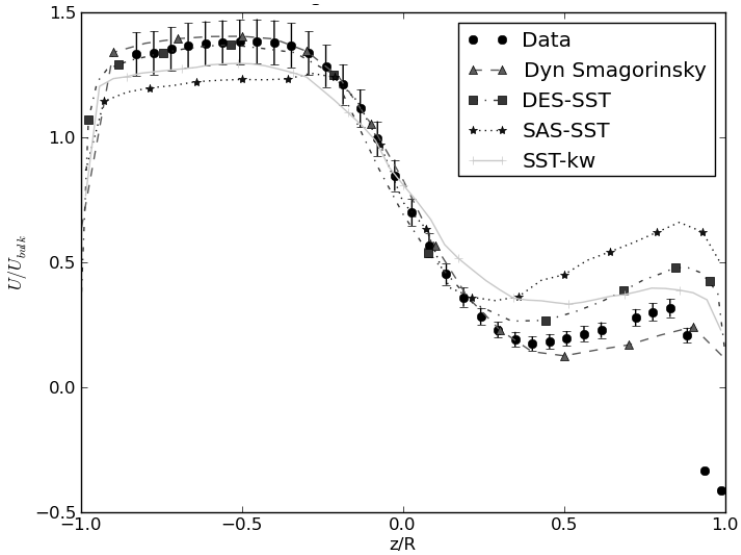

Figure 21. Comparison of Time Averaged U at x = 1.6D, y = 0

SAS-SST also shows distortions in time-averaged U profiles in the z (vertical) direction. Values are lower than they should be below the centreline, and significantly higher than they should be above the centreline at x = 1.6D (Fig. 21). At x = 4.6D, the SAS-SST predictions are not far out of line with measured data, but the shape of the curve is significantly different, exhibiting a central minimum (Fig. 22). Other model predictions are good.

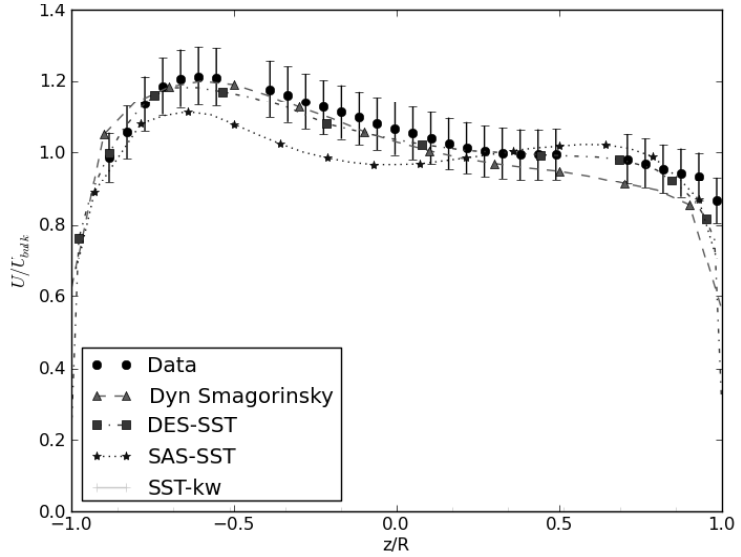

Figure 22. Comparison of Time Averaged U at x = 4.6D, y = 0

The time-averaged W (vertical) velocity profile at x = 1.6D, y = 0 are displayed in Fig. 23. The measured data indicate an undisturbed main flow in the lower section of the pipe, and evidence of a mixing region above this, with a distinct maximum (positive) and minimum (negative) for this velocity component. The LES and (surprisingly) the SST-kω simulations have captured this behaviour very well. For the DES-SST model, the extent of the mixing region is correct, but upward flow is not predicted, and the magnitude of the downward flow is overpredicted. Worst comparisons have been obtained using the SAS-SST model,

for which the undisturbed region of the flow is too shallow, there is no upward flow predicted and the downward flow is too strong.

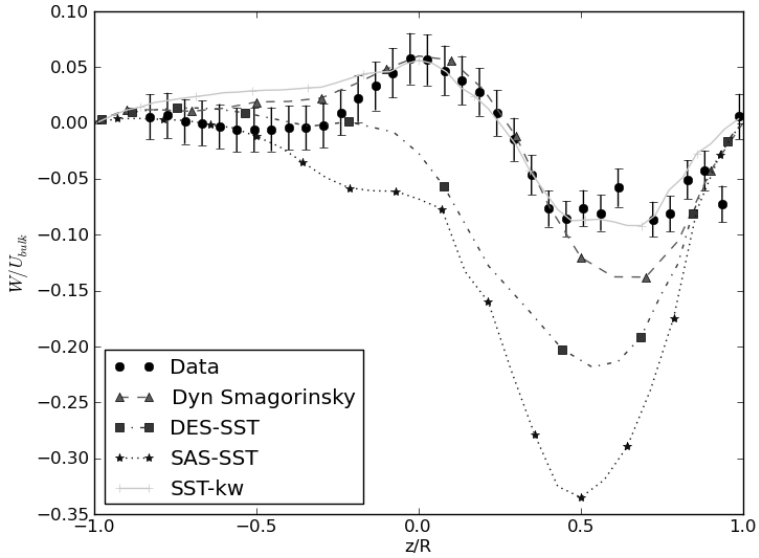

Figure 23. Comparison of Time Averaged W at x = 1.6D, y = 0

The SAS-SST model also seriously underpredicts the time-averaged RMS-profile for the horizontal velocity component v at x = 1.6D (Fig. 24), while the other models produce results in very good agreement with measured data.

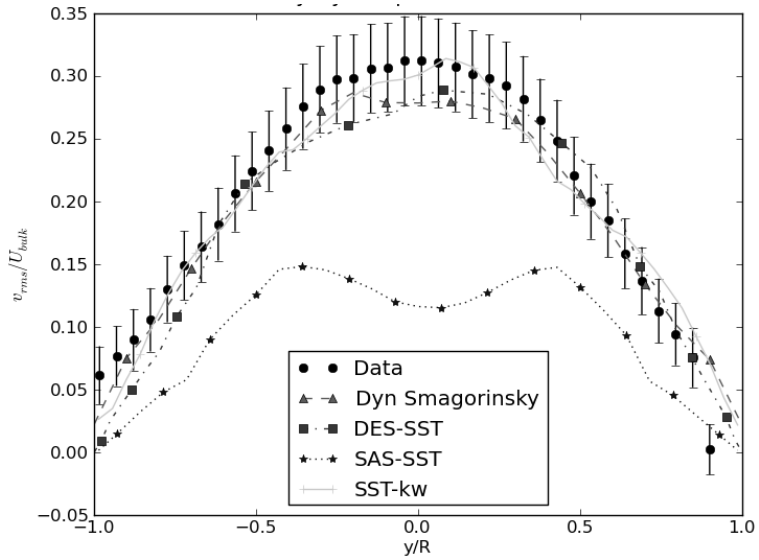

Figure 24. Comparison of RMS Fluctuations v for x = 1.6D, z = 0

The problems with the use of CFX and the SAS-SST turbulence model for this particular flow pattern suggest a need for better guidelines for utilisation of the model. Given the results for DES-SST with CFX, the guidelines might simply recommend use of the DES rather than the SAS option for some range of flow conditions. However, specific conclusions will require careful consideration of input details for submissions S7 and S18 not available in the documentation requested for this benchmark exercise.

5.5 Performance Based on Time Averaged and RMS Temperature Data

Some significant shifts occur in the ranking between Table 8 (based on velocity comparisons) and Table 9 (based on temperature comparisons). However, much of that reflects the very similar behaviour in results for the flow field over a wide range of submissions. Figures 25-28 show that predictions of the time-averaged component of velocity along the pipe are very close for the runs that are of the highest rank on velocity predictions (S20 and S2) and those with the highest rank on temperature predictions (S16 and S21).

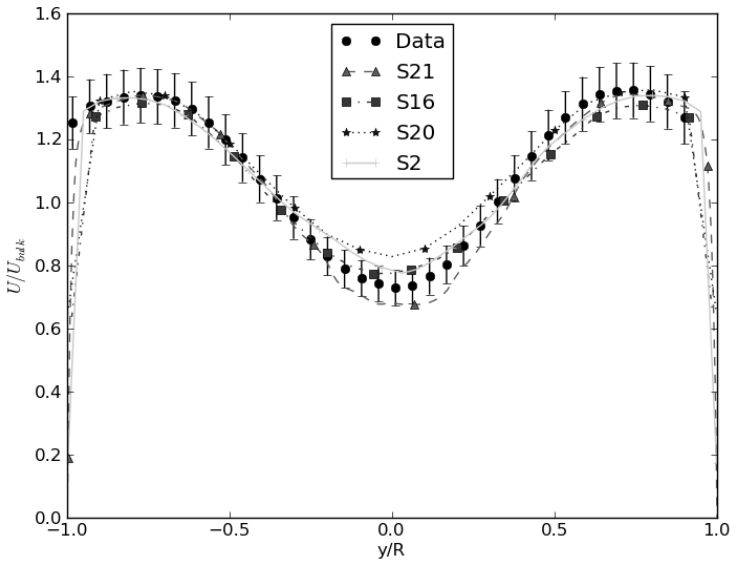

Figure 25. Time-Averaged U at x = 1.6D, z = 0

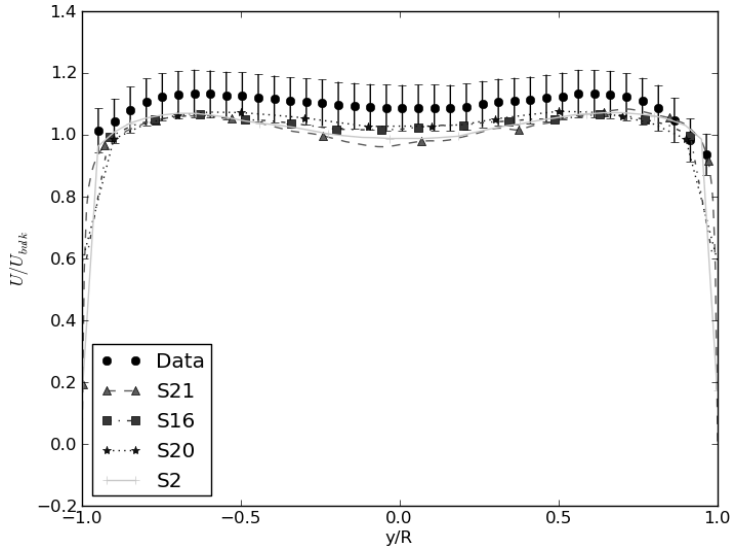

Figure 26. Time-Averaged U at x = 4.6D, z = 0

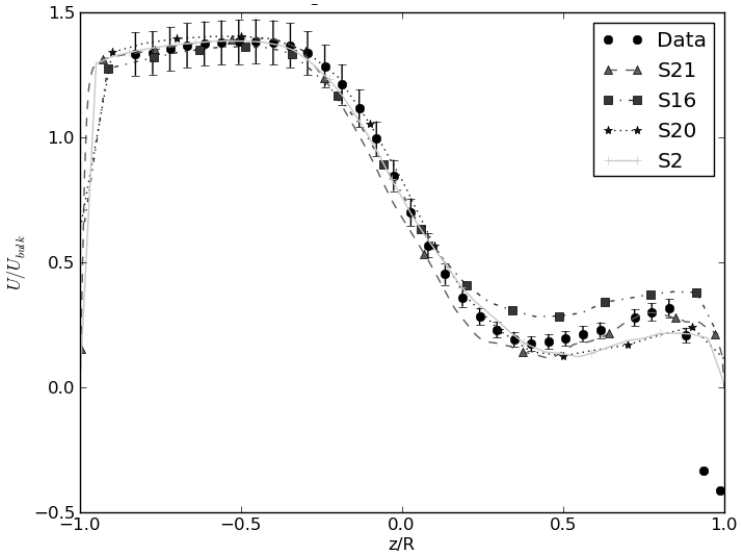

Figure 27. Time Averaged U at x = 1.6, y = 0

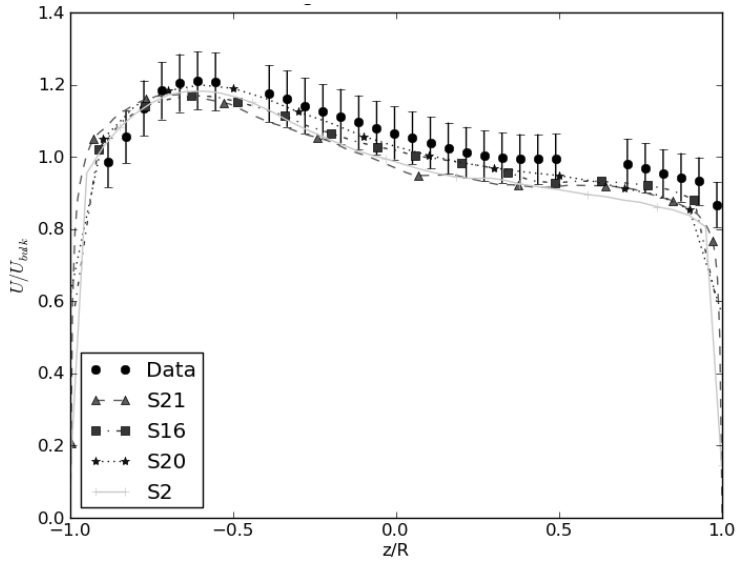

Figure 28. Time Averaged U at x = 4.6D, y = 0

Closer inspection of results reveals that the lower ranking of submission S21 (LES with spectral damping) according to the velocity data comparisons (Table 8) can be attributed to systematically poorer matches to the time-averaged z-component of velocity further downstream of the T-junction (see Fig. 29). Lower ranking of submission S16 in Table 8 is primarily a result of slightly poorer comparison on the RMS-velocity fluctuations.

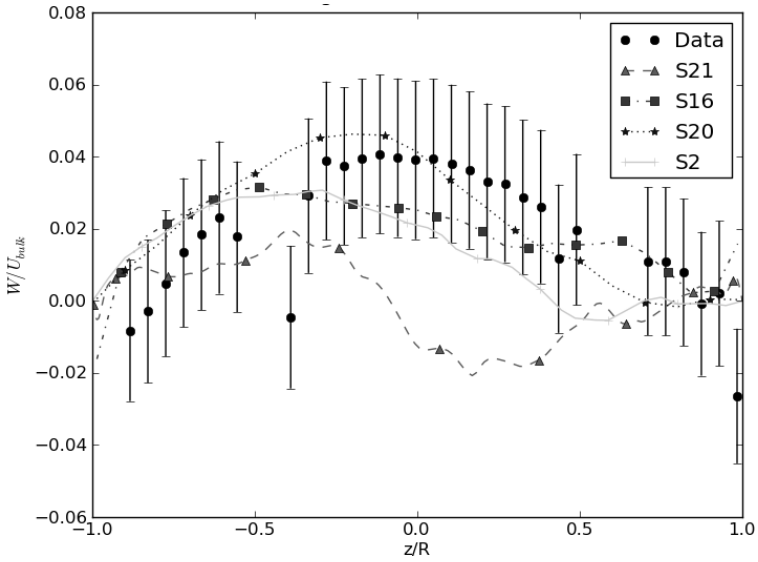

Figure 29. Time Averaged W at x = 4.6D, y = 0

Temperatures are reported in non-dimensional form: T* is the actual temperature minus the cold flow inlet temperature, divided by the difference between hot and cold inlet temperatures. For this benchmark, the hot inflow temperature is 36°C and the cold is 19°C.

Figures 30-33 show comparisons between experimental and calculated values for these same four submissions S21, S16, S20 and S2. RMS fluctuations in T* are provided in Figures 34 to 37. From a simple heat balance calculation, it can be verified that perfect mixing of the streams corresponds to T* ≈ 0.38, and one can recognise an asymptotic trend towards this value from the thermocouple readings along the top of the downstream pipe (Fig. 30), where the turbulent mixing is gradually overcoming any stability imparted to the flow stream due to stratification. The decaying RMS values (Fig. 34) also reflect this behaviour, and the numerical predictions follow the trends very well.

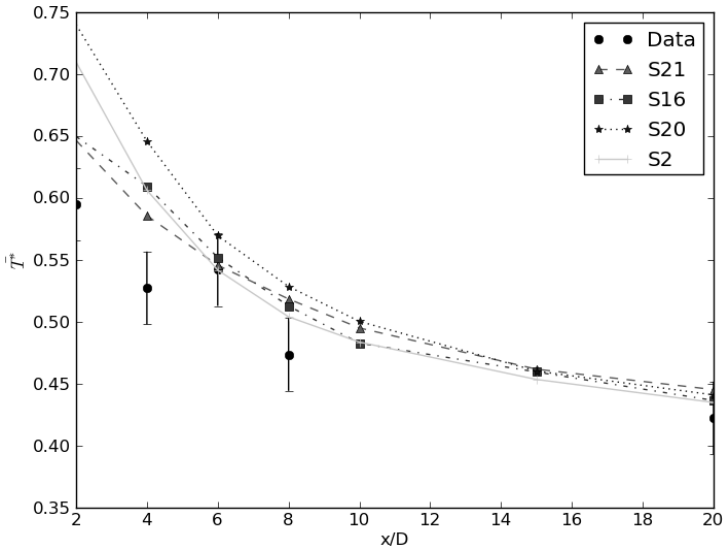

Figure 30. Time-Averaged Temperatures along Pipe at 0° (top)

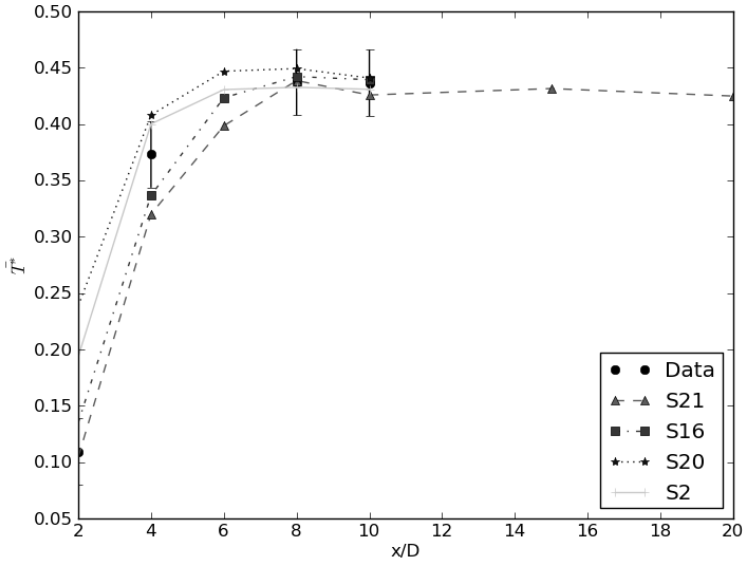

Figure 31. Time-Averaged Temperatures along Pipe at 90°

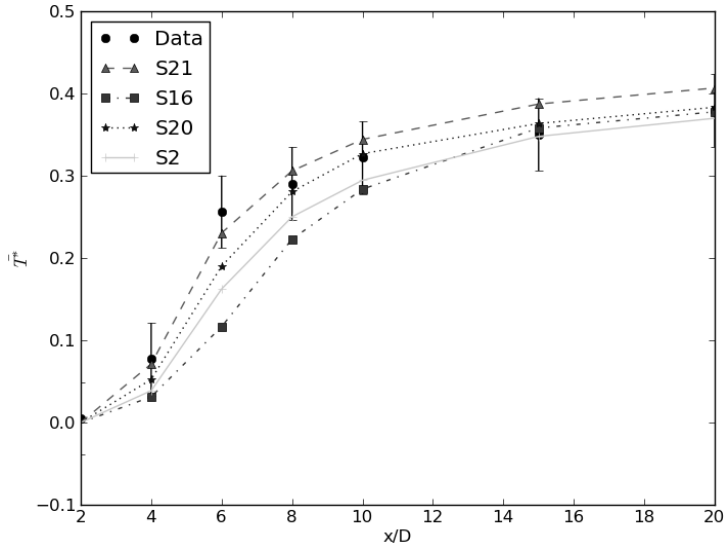

Figure 32. Time-Averaged Temperatures along Pipe at 180° (bottom)

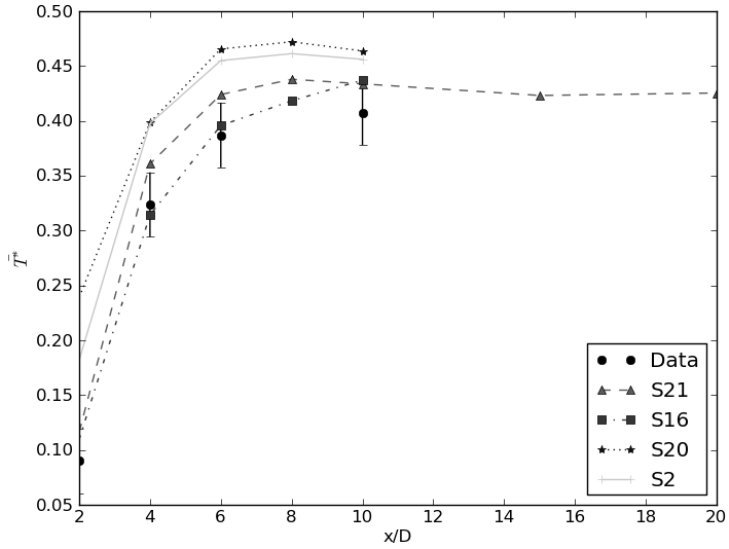

Figure 33. Time-Averaged Temperatures along Pipe at 270^o

Given that the experimental set-up has a vertical symmetry plane down the centre (y = 0), one would expect the temperature readings at 90^o and 270^o to be very similar. A comparison of Figs. 31, 33 for the mean temperatures and Figs. 35, 37 for the RMS values show this to be true within the measurement uncertainty bands, though with a bias to slightly higher mean temperatures at 90^o (that is, on the left side of the pipe looking in the direction of flow). The numerical predictions do not obviously follow this trend, which probably reflects a very small offset from perfect symmetry in the experimental set-up.

Although S2 and S20 show good comparisons against measured data for the thermocouples along the bottom of the pipe (Fig. 32), they have predicted more mixing of the hot stream at other thermocouple stations nearer to the T-junction, thus explaining their lower rating in Table 9. It should also be mentioned that S21, which scores highest in Table 2, and is seen to do well in Fig. 32, does not asymptote to the theoretical fully mixed value T* = 0.38, though the other three submissions do. In Fig. 36, it is seen that S21 overpredicts the magnitude of temperature fluctuations on the bottom of the pipe in the immediate downstream region, S16 underpredicts by about the same margin, while S2 and S20 do well. However, further downstream the predictions tend to merge, and are in good accord with the measured data.

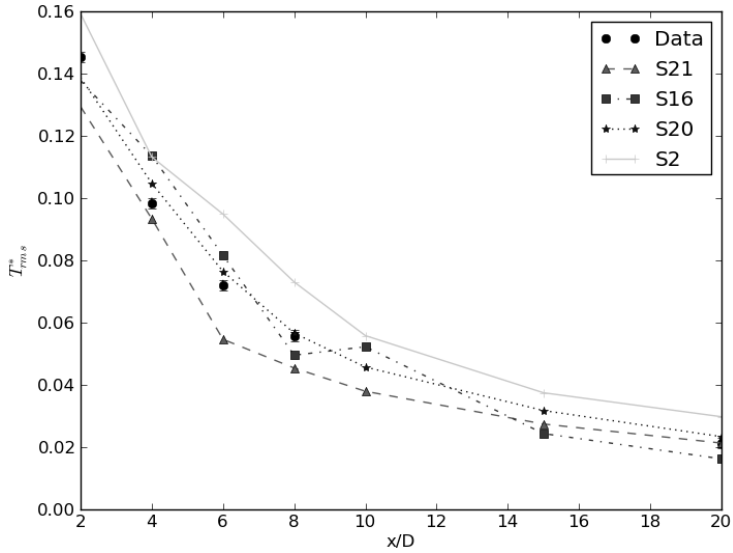

Figure 34. RMS Temperature Fluctuations along pipe at 0° (top)

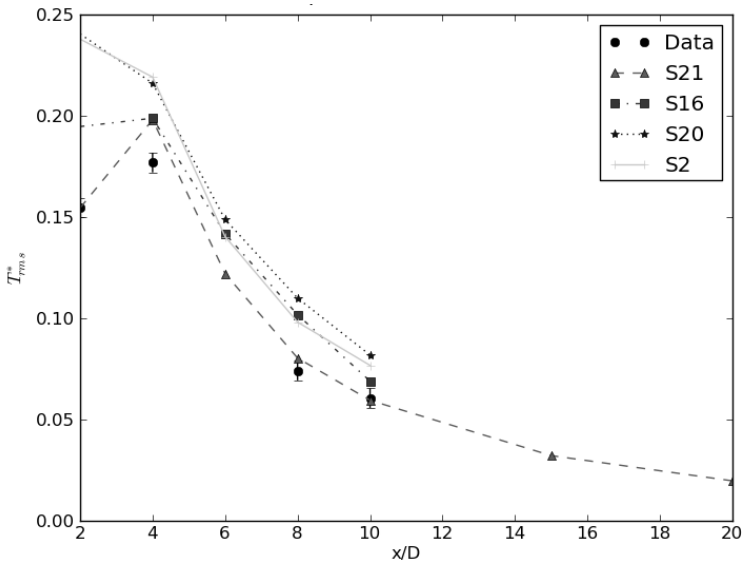

Figure 35. RMS Temperature Fluctuations along pipe at 90°

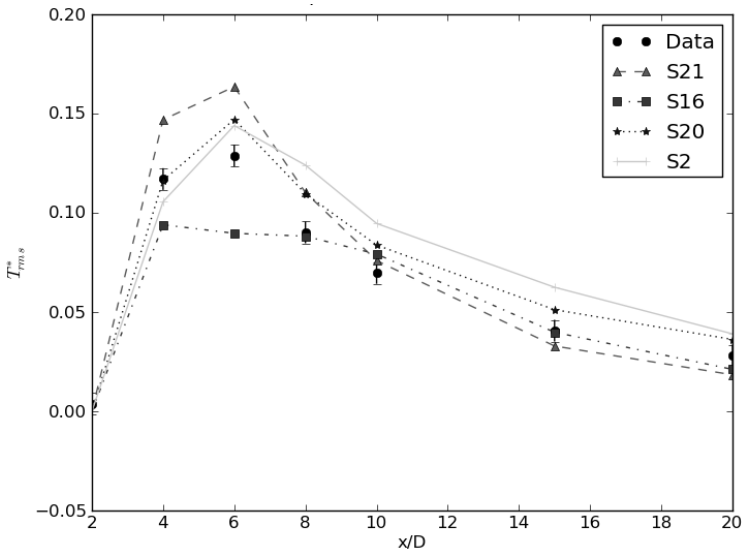

Figure 36. RMS Temperature Fluctuations along pipe at 180^o (bottom)

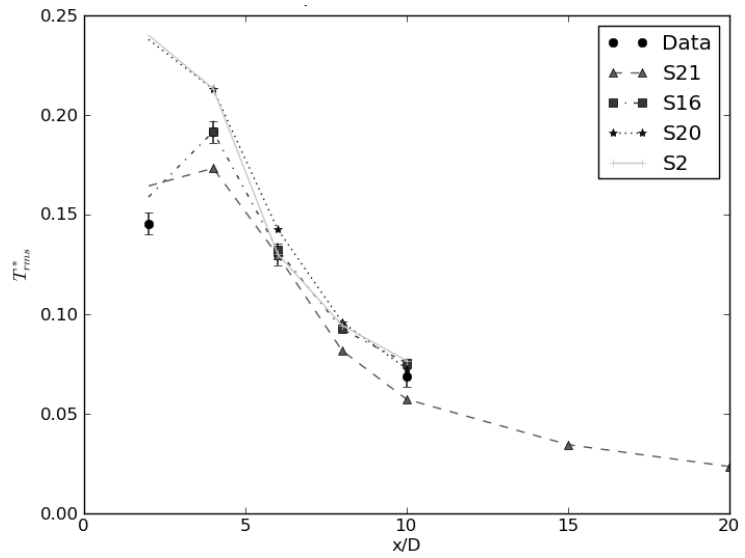

Figure 37. RMS Temperature Fluctuations along pipe at 270^o

Figures 34 to 37 give the RMS temperature fluctuations corresponding to the mean temperatures

5.6 Fourier Analysis

The primary goal of the Fourier analysis was to check the simulations for evidence of periodic low-frequency flow oscillations. A secondary goal was to compare the turbulence spectra predicted by LES with that derived from the measured data. Direct comparisons of calculations against experimental data, or even against other calculations, is not at all straightforward. For a meaningful comparison of amplitudes from the discrete Fourier transforms, all data sets should ideally be of the same time duration, and with the same sampling frequency. Because amplitudes generally drop rapidly with frequency, this analysis does not attempt to re-sample data sets at a set frequency. However, this constraint does not have a significant effect on the primary goal of the analysis.

Comparison of CFD results is much less automated than those presented in previous sections due to lack of time in assembling a good set of tools for spectral analysis. Twenty-nine plot sets were produced and transforms of each set of transient CFD predictions were to the experimental data. A long period of visual inspection followed, where notes were made of data locations (e.g. thermocouple 2D90, v on centreline at x = 1.6D) in which there were spectral peaks in both CFD and experimental data near 3.5 Hz. Co-location of peaks does not imply a match in the height of the peaks. Finally, the number of thermocouples with the match was totalled for each CFD calculation, and the same operation was performed for all available transient PIV information. Table 10 lists all submissions with more than 5 matches to peaks in the PIV spectra near 3.5 Hz.

Table 10. Number of Matches of PIV Peaks

Label	PIV Count	Code	Turbulence	Duration	Total nodes
S4	27	Fluent 6.3.26	LES, Dynamic Smagorinsky	15 s	5.8M
S20	23	FLUENT	LES-Dynamic-Smagorinsky	23 s	70.5M
S8	17	STAR-CCM+/3.06.006	LES-Wale SGS	28 s	13.2M
S18	16	CFX	DES-SST	13 s	2.4M
S5	15	Saturne	LES, Dynamic Smagorinsky	5 s	6.2M
S26	14	FLUENT v12.1	LES - Dynamic Kinetic Energy SGS Model	18 s	7.2 M
S6	14	STAR-CCM+/3.06.006	LES-Wale	10 s	9.3 M
S1	13	Fluent	LES	5 s	4.5M
S17	13	OpenFOAM 1.6	LES, 1eqn. Dynamic eddy	20 s	0.28M
S19	12	FLUENT 12.1	SST-kω	10 s	11M
S27	12	STAR-CCM+	V^2F	5 s	0.62 M
S2	11	Fluent 12	LES, Dynamic Smagorinsky	20 s	34M
S10	9	Fluent 12	LES-Smagorinsky-Lilly	14 s	0.92M
S11	9	CFX	LES-Wale	6.9s	3.4M
S24	9	OpenFOAM 1.6	LES-Dynamic-Smagorinsky	5 s	8 M
S25	9	TransAT	LES-WALE	5.5 s	2.5 M
S16	8	Fluent 12	LES-WALE	5.5 s	7.7M
S21	8	Nec5000	LES, spectral damping	5.9 s	21M
S22	7	Star-CCM+	LES	6.2 s	4.4 M

Because only three thermocouples showed strong peaks at 3.5 Hz, we have emphasized the PIV data for study of flow oscillations. The significant number of peaks seen in the frequency spectra for the U and V velocity components indicates that some reproduction of the physical flow oscillations is present in the CFD results. It is worth noting that a number of submissions do capture one or two of the strong peaks in the temperature spectra. The peak for the thermocouple two hydraulic diameters downstream of the junction at 270° is seen in submissions 6, 10, 17, and 26. The peak for the thermocouple four hydraulic diameters downstream at 90° is seen in submissions 2, 4, 7, 8, 11, 18, 20 and 25. The peak for the thermocouple four hydraulic diameters downstream at 270° is seen in submissions 6, 8, 10, 11, and 18. Submissions 6, 8, 10, 11 and 18 capture two of the three strong spectral peaks in the thermocouple data.

The count of matching peaks is only a partial measure of success in simulating flow oscillations; nearly all submissions in Table 10 had peaks in the spectrum for the y component of velocity (v) along the centreline. Oscillations are present in most of the simulations, but at significantly reduced levels or in a different mode. It would be interesting to see how sensitive the oscillation mode is to relatively minor changes in nodalisation or boundary conditions.

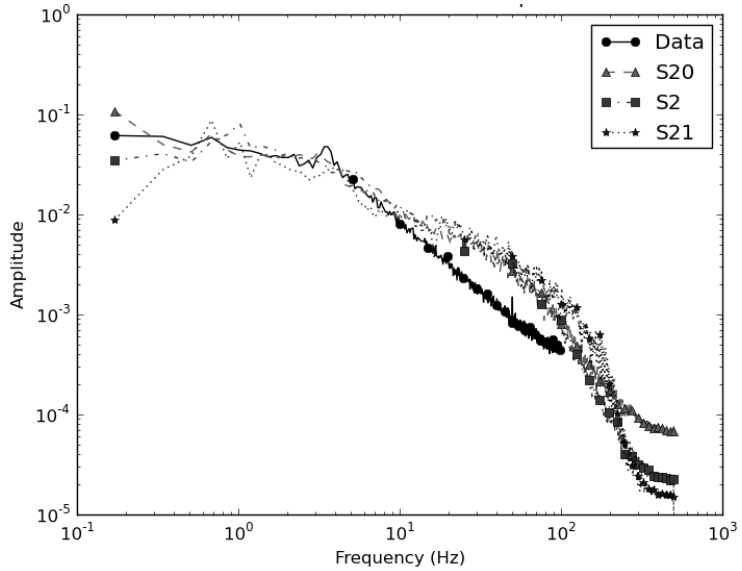

Figure 38. Flatter Spectrum with more Highly Nodalised LES Submissions

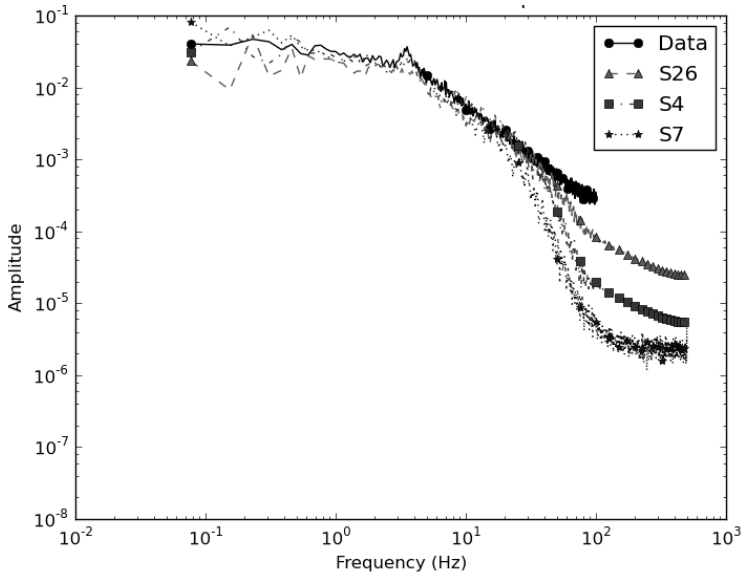

Figure 39. Closer Data Match with Fewer Volumes

Nothing has been said about Fourier spectra of transient temperature results thus far due to the relatively weak peaks seen in the spectra for the measured data. However, there is one phenomenon related to overall shape of the spectra worth noting. At frequencies above about 10 Hz, LES calculations with higher numbers of volumes contain a frequency range with a flatter slope than the data (Fig. 38). Note that S21 uses spectral damping rather than more common sub-grid scale models, but shows the same trends as the other two calculations. For smaller numbers of total volumes, the spectra for the CFD results line up well with data until frequencies at which the turbulence is not being well resolved, and thereafter amplitudes drop rapidly (Fig. 39).

PIV data has not been provided very close to the thermocouples. Figure 40 provides the discrete Fourier transform of u at a nearby location. The results from simulations using 70 million (S20) and 6 million (S4) volumes overlay the experimental data well up to the cut-off of the experimental results. However, discrete Fourier transforms of CFD results one millimetre from the wall show trends similar to those seen in Figs.

38 and 39, though not as pronounced. Distortion of the basic turbulence spectrum near the wall is a possible cause of discrepancies above 10 Hz.

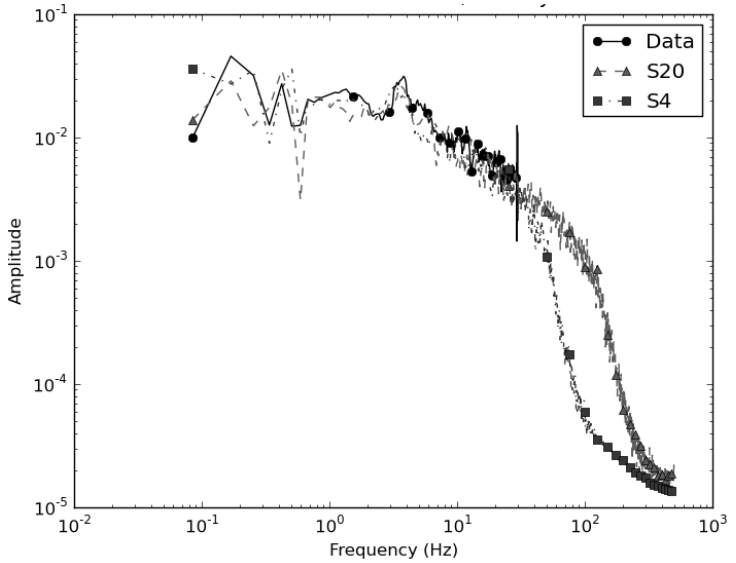

Figure 40. Fourier Transform for u (close to x = 3.6D, y = -35mm, z = 0)

Unfortunately, details on the approaches used for evaluation of the energy conservation equation and modelling of the turbulent thermal diffusivity had not been requested in the benchmark specifications. There could be a mesh-dependency effect in a common approach to modelling energy transport, or there could be a systematic difference in modelling approaches between those using 5-7 million volumes and those using more than 20 million. One argument for a mesh-dependent effect is seen in Fig. 41. The temperature spectrum for a STAR-CCM+ calculation using LES-WALE and approximately 13 million volumes falls between results presented in Figs. 38 and 39.

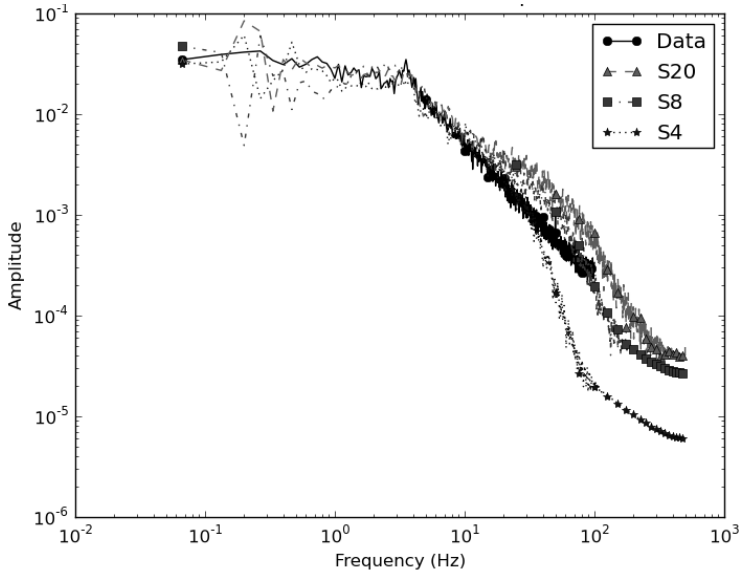

Figure 41. Results for 6, 13, and 70 Million Volumes

5.7 Conclusions from the Synthesis

Results from the Fourier analysis confirmed the observation made for time-averaged behaviour: namely that SAS-SST had some significant problems with this benchmark, and submissions using this turbulence model did not do well enough matching spectral peaks to be included in Table 10. Hopefully, some of the participants using this approach will perform follow-up studies to understand the source of the problems and provide guidelines for future use.

The relationship noted between number of computational volumes and ranking in Tables 8 and 9 did not hold for Table 10. Insufficient information is available to decide whether this is a question of care in nodalisation, or sensitivity of flow oscillation modes to nodalisation or boundary conditions. Perhaps enough participants will publish results of post-benchmark sensitivity studies to improve understanding of simulation behaviour, and thereby aid the creation of best practice guidelines for this class of problem.

Some lessons were learned during synthesis of benchmark results that are worth recording here. It was very difficult for participants to catch minor discrepancies between the files they submitted and the actual file formats specified for the benchmark. However, even minor discrepancies generally halted the automated processing of results, and required a significant amount of time to correct. The script-driving production of plots should have been completed early in the process, and provided to participants before they submitted data files to guarantee compatibility of files with the script. In addition, information submitted on general features of calculations did not always follow the requested list of basic information, and as seen above the basic list is incomplete. Future benchmarks should consider providing a sample report or template to be filled out in addition to the list of required information. Also, more time should be spent composing requests for more detailed descriptions of spatial discretisations used.

6. OVERALL CONCLUSIONS

The number of participants (65 from 22 countries, with 29 submissions ahead of the deadline) to the OECD/NEA-Vattenfall T-Junction Benchmark Exercise has demonstrated the general level of interest in high-cycle thermal fatigue. The subject is topical and pertinent to the plant-life extension initiatives being undertaken in countries with significant commitment to aging Gen II nuclear reactors. State-of-the-art Computational Fluid Dynamics (CFD) codes are needed to predict the important parameters: namely, the amplitudes and dominant frequencies of the temperature fluctuations. High-cycle thermal fatigue has been associated with the mixing of hot and cold streams in a T-junction in several contexts. The geometry is relatively simple and sufficiently generic for there to be wide interest in the problem. Nonetheless, the essential components to understanding the phenomena that could lead to thermal fatigue are represented. Consequently, the idea of organising a T-junction benchmark was attractive.

T-junction mixing experiments had been carried out at a number of facilities in France, Germany, Sweden, Japan and Switzerland, but previously unreleased test data became available from an experiment performed in November 2008 at the Älvkarleby laboratory of Vattenfall Research and Development in Sweden. These data became the basis of the blind CFD benchmarking exercise described in this document. Upstream conditions were well-defined – an essential feature for any CFD benchmarking activity. Downstream of the junction, data were available in the form of mean and fluctuating quantities at strategic locations. Velocities had been measured using Particle Imaging Velocimetry (PIV), and thermocouple measurements around the circumference of the pipe were also available. Participants to the benchmark were given velocity and turbulence data upstream of the junction and the temperatures of the two streams. Without seeing the data in advance (i.e. under *blind* conditions), they were requested to supply time-averaged and instantaneous numerical predictions at specified positions downstream coinciding with the locations of the measurements.

An organizing committee was set up early in 2009, which included the expert from Vattenfall R&D who had carried out the experiment in the previous November: Kristian Angele, who is a co-author of the present document. Detailed specifications were drawn up ahead of a formal announcement of the benchmark exercise and an invitation to attend a kick-off meeting held on May 20, 2009 at the NEA headquarters in Paris. The announcement was sent out to about 750 interested parties. Of these, 65 formally registered interest in the exercise and consequently received the detailed specifications, which also included instructions for standard formatting of the requested data files to facilitate easy processing of the numerical data. A deadline of April 30, 2010 was imposed for participants to present their data files to the organizers. This was followed by an *Open Meeting* on May 12, 2010 on which occasion the downstream data were released. Participants had been warned that if they did present their blind predictions by the deadline, they would not later be able to withdraw them once the test data had been released.

John Mahaffy (formally of Penn State University but now under contract to the US NRC, and also a co-author of this document) agreed to be responsible for the synthesis of the benchmark submissions. Arrangements were made on a PSU website for automatic uploading of participants' data files. Each person submitting data would first apply for a password-protected account on the site. He/she then received an email confirmation from John Mahaffy that their account was active, and full instructions on how to

upload their results files directly to the benchmark drop box. No other participant would have access to the files. The owner could exchange the files for updated ones at any time up to the deadline date, but then no further access was permitted. All participants who had submitted results for synthesis were later (June 2010) given direct access to the test data, which were also uploaded onto the PSU website, and could be reached through the individual user accounts.

Of the 29 participants who submitted results by the deadline, the majority used commercial CFD software (8 used FLUENT, 7 used ANSYS-CFX and 4 used STAR-CCM+), 2 used the open-source software OpenFOAM, while the rest used codes developed in-house. The number of control volumes used varied from 0.28 M to 70.5 M, though most were in the range 1−5 M. The majority (19) chose some variant of Large Eddy Simulation (LES) for turbulence modelling, while others (3) chose Detached Eddy Simulation (DES), while the remainder elected for some form of Reynolds-Averaged Navier Stokes (RANS) model. The time step for advancing the solution ranged from 0.06 ms to 1.0 ms, the average being 0.6 ms. The time for collecting data was set at a minimum of 5 s in the specifications, and 12 participants used this value. One calculation was taken to 28 s, with the average close to 10 s.

There is a mass of data available for analysis, and it is hoped that the participants will explore the possibilities in connection with their own simulations. In the context of an overall assessment, some salient points have been alluded to in Section 5 of this report. Two features stand out immediately for the velocity-based comparisons. For the same selection of turbulence model, total number of discrete volumes is generally a good indicator of quality of results. This suggested that most participants had been careful in their selection of number of meshes within the constraints of available computer resources. Also, for roughly the same number of volumes, the SAS-SST appears to be significantly under-performing LES, independently of the sub-grid scale (SGS) model adopted for the latter. Other results show that SST-kω in particular is performing quite well.

The submissions were ranked according to three separate metrics. Full details are given in Section 5 above. The first was based on the degree of correspondence to the measured velocity data. On this scale, LES approaches occupied the first 9 positions, the SST-kω submission came next, followed by the DES-SST submission. The positions changed somewhat when ranked according to correspondence with the temperature data, but overall LES still occupied the first 9 positions, with SST-kω again in 10^{th} place. Finally, a ranking was made in terms of correspondence of local peaks in the velocity spectra, but only at those measurement positions and for those velocity components for which peaks were clearly discernible. LES again performed well (though the ordering changed again) filling 7 of the top 8 positions of the ranking table. The DES-SST and SST-kω results were also good, and a RANS simulation (with the v2f model) was considered respectable on the basis of the Fourier metric even though it performed the worst of all according to the velocity and temperature metrics.

The Fourier metric also confirmed the observation made for time-averaged behaviour: namely, that SAS-SST had some significant problems with this benchmark, and submissions using this turbulence model did not do well enough matching spectral peaks to even be included in the ranking. Hopefully, some of the participants using this approach will perform follow-up studies to understand the source of the problems and provide guidelines for future use.

It is interesting that the LES simulation with over 70 million meshes, though far outperforming all other submissions on the basis of the velocity metric, slipped significantly down the table for the ranking according to the temperature comparisons, but then reasserted itself in the Fourier rankings. Insufficient information is available to decide whether near-wall nodalisation or wall treatment is responsible for this. Post-benchmark studies could be a valuable source of information here.

Overall, the T-junction benchmark has been very successful. The participation was very high, given that the calculations were extremely demanding in terms of CPU time. The exercise complements the activities in other areas in understanding the origins of thermal fatigue in this geometry, and being able to quantify them. Different codes, different modelling approaches, and different numbers of control volumes have been adopted by the various participants, and there is even useful information forthcoming from those who used the same code.

From the outset, the modus operandi for this exercise was that the numerical analysts were given the challenge of choosing, and then employing, the best tool they had available to supply the information requested. Within the restrictions of the computing power at their disposal, the majority chose an LES turbulence modelling approach, and the results from this benchmark clearly indicate its superiority (when used appropriately) for this application. Generally, the good comparisons to experiment obtained demonstrate the maturity of single-phase CFD models in simulating such types of mixing problems, though from a purely pragmatic viewpoint it is somewhat worrying that LES is also the most computationally demanding of the CFD turbulence models that have so far been developed, and is still a long way from common industrial use.

ACKNOWLEDGEMENTS

The authors of this document are indebted to their colleagues on the benchmark organising committee for their technical support to this initiative, their assistance in finalising the benchmark specifications, and their many helpful tips and guidance. In alphabetical order, thanks are due to Dominique Bestion (CEA) and Ghani Zigh (US NRC). Also, we appreciate the efforts made by the members of the NEA secretariat, A. Amri and J.-C. Jo, who organised meeting facilities at the NEA and OECD headquarters in Paris, wrote Minutes of the meetings, and provided help in structuring the benchmark activity according to NEA standards.

REFERENCES

[1] CSNI Report NEA/CSNI/R(2002)16, OECD Nuclear Energy Agency, Paris, France, 2002.

[2] Mahaffy, J. (ed.) "Best Practice Guidelines for the Use of CFD in Nuclear Reactor Safety Applications", OECD, Nuclear Energy Agency, Technical Report, CSNI/R(2007)5, April 2007

[3] Smith, B.L. (ed.) "Assessment of Computational Fluid Dynamics (CFD) for Nuclear Reactor Safety Problems", OECD Nuclear Energy Agency, Technical Report, NEA/CSNI/R(2007)13, Jan. 2008.

[4] Bestion, D. (ed.) "Extension of CFD Codes to Two-Phase Flow Safety Problems", OECD, Nuclear Energy Agency, Technical Report, NEA/CSNI/R(2010)2, March 2010.

[5] CFD4NRS: Benchmarking of CFD Codes for Application to Nuclear Reactor Safety, Garching, Munich, Germany, 5-7 Sept. 2006 (CD-ROM).

[6] Smith, B. L., Hassan, Y. (eds.) "CFD4NRS: Benchmarking of CFD Codes for Application to Nuclear Reactor Safety", *Special Issue, Nucl. Eng. Des.,* **238**(3), 443-785 (2008).

[7] XCFD4NRS: Experiments and CFD Code Applications to Nuclear Reactor Safety, Grenoble, France, 10-12 Sept. 2008 (CD-ROM).

[8] Smith, B.L., Bestion, D., Hassan, Y. (eds.) "Experiments and CFD Code Applications to Nuclear Reactor Safety (XCFD4NRS)", *Special Issue, Nucl. Eng. Des.,* **240**(9), 2075-2382 (2010).

[9] http://meta.wikimedia.org/wiki/Help:Introduction

[10] IAEA Document, "Validation of Fast Reactor Thermo-Mechanical and Thermal-Hydraulic Codes", IAEA-TECDOC-1318, 31-62, 2002.

[11] Shah, V.N. *et al.* "Assessment of Field Experience Related to Pressurized Water Reactor Primary System Leaks", Proc. ASME Pressure Vessel and Piping Conf., Boston, MA, USA, August 1-5, 1999.

[12] Jungclaus, D. *et al.* "Common IPSN/GRS Safety Assessment of Primary Coolant Unisolable Leak Incidents caused by Stress Cycling", NEA/CSNI Specialist Meeting on Experience with Thermal Fatigue in LWR Piping caused by Mixing and Stratification, OECD/NEA, Paris France, 7-12 June, 1998.

[13] Wakamatsu, M., Nei, H., Hashiguchi, K. "Attenuation of Temperature Fluctuations in Thermal Striping", *J. Nucl. Sci. Tech.*, **32**(8), 752-762 (1995).

[14] Lee, J.I., Saha, P., Kazimi, M.S. "A parametric study of high cycle thermal fatigue caused by thermal striping,", Paper 4104, Proc. ICAPP'04, Pittsburgh, PA, USA, June 13-17, 2004.

[15] Hu, L.W., Kazimi, M.S. "A simplified method for determination of high cycle thermal fluctuations caused by thermal striping", Paper 4081, Proc. ICAPP'04, Pittsburgh, PA, USA, June 13-17, 2004.

[16] Hu, L.W., Kazimi, M.S. "Large Eddy Simulation of Water Coolant Thermal Striping in a Mixing Tee Junction", Proc. 10th Int. Topical Meeting on Nuclear Reactor Thermal Hydraulics (NURETH-10), Seoul, Korea, October 5-9, 2003.

[17] Faidy, C. "Thermal Fatigue in Mixing Tees: A Step by Step Simplified Procedure," Proc. 11th Int. Conf. on Nuclear Engineering (ICONE-11), Tokyo, Japan, 20-23 April, 2003.

[18] Westin, J., *et al.* "Experiments and Unsteady CFD-Calculations of Thermal Mixing in a T-Junction", Proc. Benchmarking of CFD Codes for Application to Nuclear Reactor Safety (CFD4NRS), Garching, Munich, Germany, 5-7 September, 2006 (CD-ROM).

[19] Westin, J. "Thermal Mixing in a T-Junction. Model Tests at Vattenfall Research and Development AB 2006. Boundary Conditions and List of Available Data for CFD-Validations", Vattenfall Internal Document (private communication), 2007.

[20] Odemark, Y. *et al.* "High-Cycle Thermal Fatigue in Mixing Tees: New Large Eddy Simulations Validated against New Data Obtained by PIV in the Vattenfall Experiment", Paper 75962, Proc. 17th Int. Conf. on Nuclear Engineering (ICONE-17), July 12-16, 2009, Brussels, Belgium.

[20] Metzner, K.-J., Wilke, U. "European THERFAT project- thermal fatigue evaluation of piping system tee connections," *Nucl. Eng. Des.,* **235**, 473-484 (2005).

[21] Smith, B.L. "Identification and Prioritization of Generic Nuclear Safety Problems Requiring CFD Analysis", Paper 75482, Proc. 17th Int. Conf. on Nuclear Engineering (ICONE-17), July 12-16, 2009, Brussels, Belgium.

[22] Summary Record of the Kick-Off Meeting of the OECD/NEA—VATTENFALL T-Junction Benchmark Exercise, NEA/SEN/SIN/AMA(2009)6.

[23] Chapuliot, S. et al. "Hydro-thermal-mechanical analysis of thermal fatigue in a mixing tee", *Nucl. Eng. Des.,* **235**, 575-596 (2005).

[24] Westin, J. et al. "High-Cycle Thermal Fatigue in Mixing Tees. Large-Eddy Simulations Compared to a new Validation Experiment", Paper 48731, Proc. 16th Int. Conf. on Nuclear Engineering (ICONE-16), May 11-15, 2008, Orlando, Florida, USA.

[25] Zagarola, M. V., Smits, A. J. "Mean-Flow Scaling of Turbulent Pipe Flow", J. Fluid Mech., 373, 33-79 (1998).

[26] Keane R., Adrian R. "Theory of cross-correlation in PIV", *Appl. Sci. Res.,* **49**, 191–215 (1992).

[27] Incropera, F.P., DeWitt, P. *Fundamentals of Heat and Mass Transfer*, 3rd ed., John Wiley & Sons, New York, 1990.

[28] www.python.org

ANNEX 1: ANNOUCEMENT OF THE BENCHMARK KICK-OFF MEETING

OCDE/NEA Sponsored CFD Benchmark Exercise: Thermal Fatigue in a T-junction
Invitation to Kick-Off meeting
NEA Headquarters, 12 boulevard des Iles, Issy-les-Moulineaux, Paris, France

Background

Failures of structures due to high-cycle thermal fatigue have occurred in several nuclear plants around the world, for different reactor types. Many of these have been associated with mixing zones where hot and cold streams meet, and particularly near T-junctions. An example is the failure event at the Civaux-1 PWR in France in May 1998.

As the hot and cold streams from the main and branch pipes meet, shear instabilities produce turbulent eddies, causing temperature fluctuations on the pipe walls downstream of the junction. The fluctuations induce cyclic strain variations in the pipe material, and may result in fatigue damage and cracking. A typical value for the temperature difference between the hot/cold streams is 160°C.

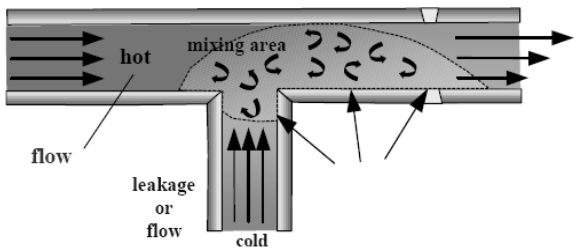

Critical parameters for thermal fatigue analyses are frequencies (ω), temperature differences (ΔT), number of cycles (N), and material properties. Most damaging thermal loads appear to be due to large-scale turbulent fluctuations of low frequency (3-10 Hz). From a thermal hydraulic standpoint, the accurate prediction of such large coherent eddies is a challenging task, requiring CFD and advanced turbulence modelling.

A Blind CFD Benchmark Exercise

In November 2008, a T-junction thermal mixing test was carried out at the Älvkarleby Laboratory of Vattenfall Research and Development (VRD) in Sweden. Data from this test have been reserved specifically for this CFD benchmark exercise, and will be kept secret for its duration.

CFD simulations are invited.

Participants in the exercise will be given details of the test geometry, operating conditions and upstream parameters. Following numerical simulation, participants will supply to the organizers results in the form of temperature, velocity and turbulence profiles at specified locations downstream.

A synthesis of the results, including comparisons against measured data, will be carried out, and reported in the form of a Keynote Lecture at the forthcoming OECD/NEA–IAEA Workshop CFD4NRS-3, which will take place in Washington DC in the fall of 2010. Participants will have the opportunity to present their work in the form of a dedicated Poster Session at this workshop.

Those wishing to participate in the benchmark exercise are encouraged to attend the **Kick-Off Meeting**, to be held at the NEA Headquarters in Paris, France on **Wednesday, May 20, 2009**. Please register your attendance in advance with the NEA Secretariat: JongChull.JO@oecd.org, with copies to Abdallah.AMRI@oecd.org and Brian.Smith@psi.ch.

The Vattenfall T-Junction Experiment

The test section is constructed from Plexiglas, and the junction itself from one solid block into which the main and branch pipes fit. The temperatures of the water in the main and branch pipes were maintained at 15°C and 30°C, respectively, with minimal heat loss.

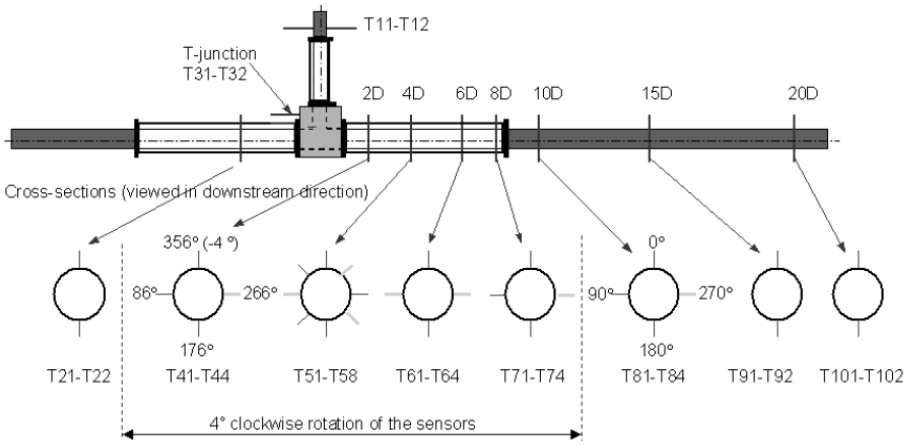

Special care was taken to provide simple and well-defined inlet boundary conditions to remove ambiguities in defining the CFD input data. Temperature fluctuations near pipe walls were measured using thermocouples. These were placed around the inner wall perimeter of the main pipe at seven stations downstream of the junction and at one station upstream. All thermocouples were positioned 1 mm from the wall. Velocity profiles upstream and downstream of the junction were measured using a two-component LDV system. These were positioned at each inlet, and at the outlet. Data are in the form of mean values, rms-values and turbulence statistics.

Preliminary Agenda of Kick-Off Meeting

A detailed agenda is being compiled, but items to be included are:

- Plan of the Benchmark Activity Brian Smith, PSI, Switzerland
- Test Facility and Instrumentation Kristian Angele, VRD, Sweden
- Keynote Speaker Stéphane Chapuliot, CEA, France
- Benchmark Specifications Brian Smith/Kristian Angele
- Synthesis and Reporting Procedure John Mahaffy, NRC, USA
- Open Forum Discussion

Organising Committee

Brian L. Smith, Paul Scherrer Institute, Switzerland
Kristian Angele, Vattenfall R&D, Sweden
John H. Mahaffy, US Nuclear Regulatory Commission, USA
Dominique Bestion, Commissariat à l'Energie Atomique, France
Ghani Zigh, US Nuclear Regulatory Commission, USA
Jong-Chull Jo, OECD Nuclear Energy Agency, France (Secretariat)

Dates & Deadlines

April 30, 2009	Registration for Attendance at Kick-Off Meeting
June 15, 2009	Distribution of Final Benchmark Specifications by Organizers
April 30, 2010	Deadline for Receipt of Simulation Results
May 31, 2010	Latest Date for Open Benchmark Meeting
Sept. 30, 2010	Presentation of Results and Synthesis at CFD4NRS-3 Workshop

ANNEX 2: FINAL BENCHMARK SPECIFICATIONS

OECD/NEA-VATTENFALL T-JUNCTION BENCHMARK SPECIFICATIONS (FINAL VERSION, JULY 2009)

A1. GEOMETRICAL DATA

The complete test rig, which is located at the Vattenfall Research and Development Laboratory at Älvkarleby, Sweden, is illustrated in Fig. A1. Cold water is supplied from a high-level reservoir designed to maintain a constant water level independent of the flow rate. A stagnation chamber of diameter 400 mm is mounted at the beginning of the horizontal pipe, and contains two perforated plates, a tube bundle (inner diameter of the tubes is 10 mm and the length 150 mm), a third perforated plate and finally a contraction with an area ratio of about 8:1. The stagnation chamber is designed to provide a high quality flow without large-scale turbulence or secondary flows. The stagnation chamber is connected to a 10 m long pipe section made from ABS plastic, which is followed by a Plexiglas section extending 1270 mm upstream of the T-junction. The total upstream length of the pipe, with constant diameter D_2=140 mm, is thus more than 80 pipe diameters. The flow rate is measured using an electro-magnetic flow meter (labelled Q2 in Fig. A1).

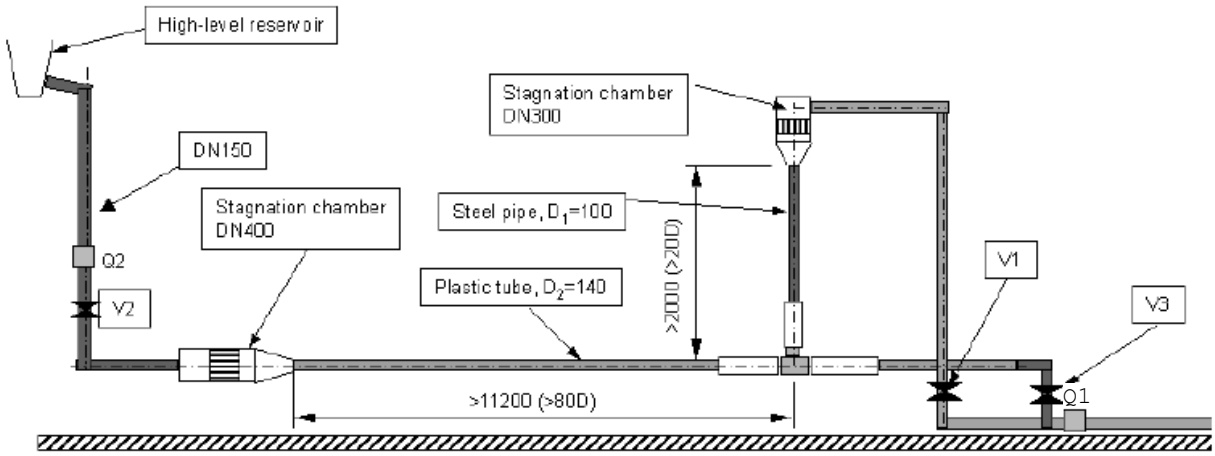

Figure A1: Schematic of Vattenfall T-junction test rig

The hot water is taken from a 70 m^3 reservoir, and a pump is used to feed the model. The rotational speed of pump is automatically controlled to maintain a constant flow rate through flow meter Q1. A stagnation chamber (diameter 300 mm), similar to that on the cold water side, is used here too, though with the water feed being supplied from the side by means of a flow distributor. The stagnation chamber is connected to a steel pipe of inner diameter 100 mm, which gives an area contraction ratio of 9. The total distance with constant diameter (D_1=100 mm) upstream of the T-junction is approximately 20 pipe diameters for the hot

water pipe. Fully developed pipe flow cannot be obtained in this case, though the flow quality is expected to be good due to presence of the stagnation chamber.

A close-up of the test section is given in Fig. A2. The actual tee is made from a solid Plexiglas block through which circular channels have been drilled into which the hot and cold water feed pipes fit, as illustrated in Fig. A3.

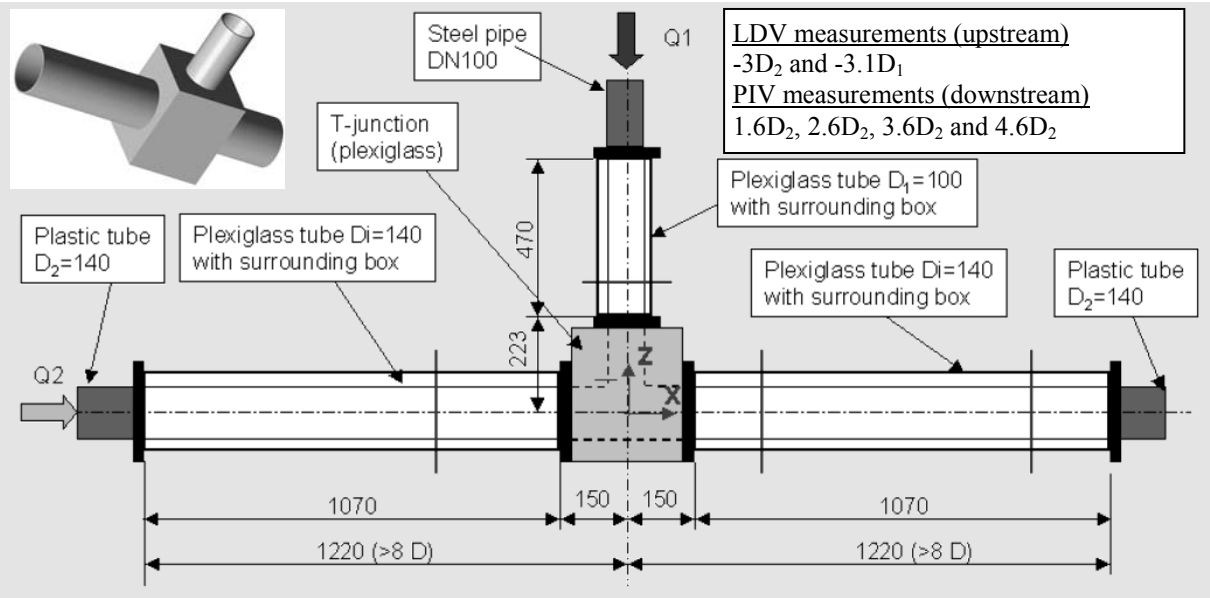

Figure A2: Schematic of T-junction with Plexiglas sections

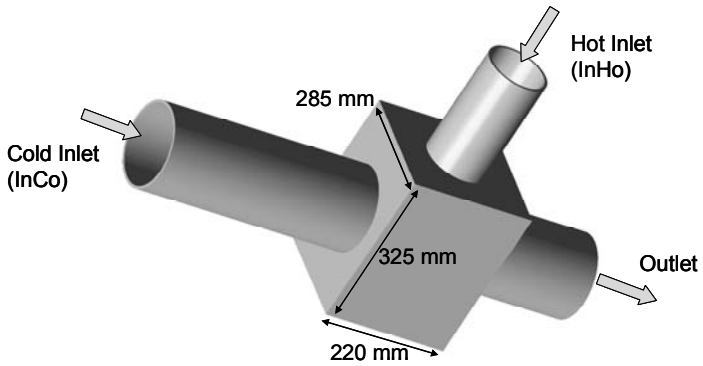

Figure A3: Schematic of the T-junction block showing dimensions

The circular channels within the block are of the same diameter as the attached pipes and are considered hydraulically smooth, though no specific measurement of the roughness has been performed. The tee has been machined with internal “sharp” edges: i.e. the edge at the intersection between the main and branch channels within the block has been only slightly ground. The exact radius of curvature has not been measured, but is certainly smaller than 0.2 mm. Overall dimensions also appear in Table A1.

Table A1: Dimensions of T-junction test section

Component	Material	Dimensions (mm)
Main inlet pipe	Plexiglas	Length: 1070; ID: 140; OD: 150
Branch inlet pipe	Plexiglas	Length: 470; ID: 100; OD: 110
Outlet pipe	Plexiglas	Length: 1070; ID: 140; OD: 150
Tee Block	Plexiglas	Length (x): 220; Width (y): 285, Height (z): 325 Main channel diameter: 140 Branch channel diameter: 100

For the cold (horizontal) inlet pipe, LDA measurements have been taken 3 diameters upstream of the junction. These confirm the fully developed flow conditions expected from the length of the feed line (see Section A3.1). Similar LDA measurements have been taken 3.1 diameters upstream of the junction for the hot inlet. Here, the flow is not fully developed (see Section A3.2).

Close to the T-junction, each of the three pipes (two inlet and one outlet) is surrounded by a rectangular water box; see Fig. A2. This is necessary to avoid distortions of the laser beams at the curved surfaces of the pipes when velocity measurements are made. For the present benchmark experiment, no new upstream velocity measurements have been carried out, since it was considered those taken during the previous test series in 2006 were adequate (see explanation given in Section A3). Downstream, the box was only filled with water – at ambient (15^{o}C) temperature – when velocity measurements (using PIV) were being made, these measurements being carried out under cold operating conditions (i.e. cold water supply to both inlets).

At the time the thermocouple measurements were taken, the box was emptied of water, and contained air at ambient (15^{o}C) temperature. Consequently, heat losses through pipe walls are generally considered negligible. The hot inlet pipe above the test section is made of steel (labelled in Fig. A1), and the pipe is not insulated. However, temperatures taken in the stagnation chamber and just upstream of the junction show differences of 0.1-0.2oC, within the tolerances of the thermocouple measurements. Hence it can be assumed there are no measurable heat losses through the exposed heat pipe. Nonetheless, exact dimensions and material properties of the inlet pipes and water boxes can be supplied by the organizers to specific participants who wish to model them explicitly.

A2. MATERIAL PROPERTIES

The working fluid in this test is deionized tap water between 19°C and 36°C. It is considered that the physical properties are adequately described by the ASME steam tables (1967), with additional information on the thermal expansion coefficient from the book of Incropera and DeWitt (1990). Values are displayed in Table A2 for temperatures of relevance. Note that these data are supplied as a guide only.

Table A2: Physical properties of water

Temperature (°C)	**Density (kg/m^3)**	**Thermal conductivity (W/m K)**	**Dynamic viscosity (N s/m^2)**	**Heat capacity (J/kg K)**	**Molecular Prandtl number (-)**
15	999.2	0.5911	1.138E-3	4186	8.058
20	998.3	0.5996	1.002E-3	4182	6.988
25	997.2	0.6076	0.8904E-3	4179	6.125
30	995.8	0.6151	0.7977E-3	4178	5.419
35	994.1	0.6221	0.7196E-3	4178	4.833
40	992.3	0.6287	0.6533E-3	4178	4.342

Temperature (K)	**Coefficient of volumetric expansion (K^{-1})**
285	114.1E-6
290	174.0E-6
295	227.5E-6
300	276.1E-6
305	320.6E-6
310	361.9E-6
315	400.4E-6

The Plexiglas is of low conductivity, and the temperatures are at or close to ambient everywhere (≈15°C), so it is not anticipated that heat losses from the water in the test section will be important (see remarks above). However, the material properties of the Plexiglas material are as listed in Table A3 for reference, the values being based on the specifications delivered by the supplier.

Table A3: Physical properties of Plexiglas

Density (kg/m^3)	**Thermal conductivity (W/m K)**	**Heat capacity (J/kg K)**	**Coefficient of volumetric expansion (K^{-1})**
1200.0	0.190	1460	240.0E-6

A3. INLET BOUNDARY CONDITIONS

The volumetric flow rates used in the test are given in Table A4, together with the locations where the velocity distributions over the pipe cross-sections were measured (the left and upper red lines in Fig. A2). The temperatures for the cold and hot inlets are also given at these cross-sections. As a consequence of the thorough flow mixing in the upstream stagnation chambers, the temperatures of the inflowing streams were assumed to be uniform at the measuring locations, and only one thermocouple was placed there. The reading taken is that given in the 2nd column of Table A4.

Table A4: Inlet temperatures and flow rates

Inlet/designation	**Temperature (^{o}C)**	**Pipe diameter (mm)**	**Measuring location (mm)#**	**Volumetric flow rate (litres/s)**
Main/InCo	19	140 (D_2)	-420 (-3D_2)	9.0
Branch/InHo	36	100 (D_1)	-310 (-3.1D_1)	6.0

The negative sign indicates upstream of the junction mid-point (i.e. the point where the centrelines of the pipes cross)

The inlet velocity profiles presented in this section are taken from an earlier test (Westin et. al, 2008) in which the volumetric flow ratio between the main and branch streams was 2. In the present test (flow ratio 1.5), the flowrate in the hot inlet was kept the same as before (6 l/s), whereas the one in the cold inlet was 9.0 l/s instead of 12.0 l/s used previously. Since the velocity profile is fully developed in the cold inlet, the results presented below can simply be scaled to fit the present flowrate.

In the earlier test, the velocity measurements were taken at upstream locations using a two-component LDA system, which gave one component of velocity in the main flow direction (i.e. parallel to the axis of the pipe) and one component transverse to this. The coordinate systems adopted in the measuring planes of the two upstream pipes are shown in Fig. A4.

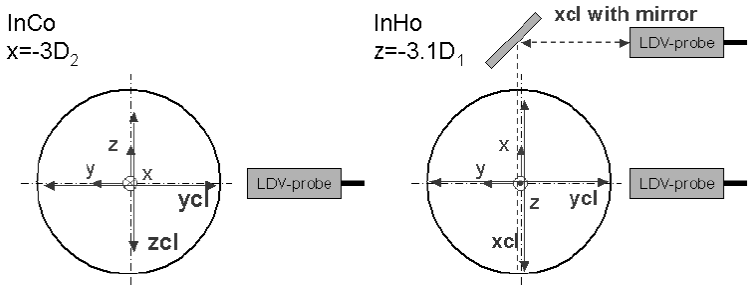

Figure A4: Overview of the upstream LDV measurement orientations

Velocity profiles and turbulence statistics are available in the two perpendicular directions defined in Fig. A4 for the main (InCo) and branch (InHo) pipes, respectively. It should be noted that special means to obtain accurate near-wall measurements have not been undertaken. This should be kept in mind when measurement data close to the pipe walls are used, since the accuracy of these data can be expected to be lower than for those away from the wall.

A3.1 Main Pipe: InCo

The measuring plane is -3D_2 upstream of the centre of the T-junction. Profiles are drawn in the left column of Fig. A5. Note that the streamwise mean velocity component (U) is scaled with the bulk velocity; U_{bulk}, while the other velocity components are scaled with the mean centreline velocity, U_{cl}, where U_{cl} = 1.17 U_{bulk}. The two cross-stream profiles zcl and ycl for the streamwise component are in good agreement, which is to be expected given that the flow should be axisymmetric. The higher moments, skewness and flatness, also show typical values for fully-developed turbulent flow. The definitions of these quantities are listed here:

Mean $U = \bar{u} = \frac{1}{n}\sum_{i=1}^{n} u_i$ RMS $U_{rms} = \left(\overline{(u-\bar{u})^2}\right)^{1/2}$

Skewness $S = \left(\overline{(u-\bar{u})^3}\right)/U_{rms}^3$ Flatness $F = \left(\overline{(u-\bar{u})^4}\right)/U_{rms}^4$

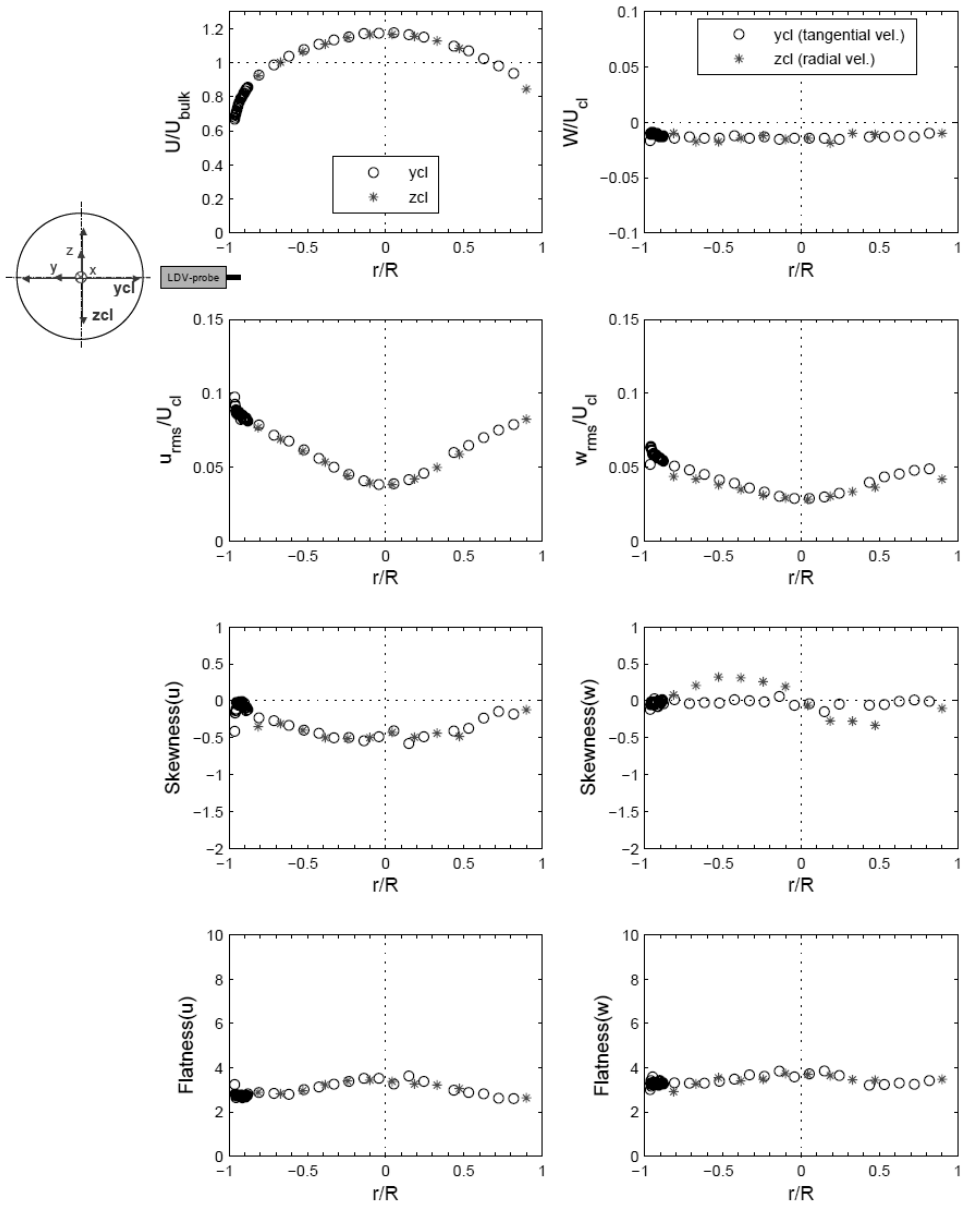

Figure A5: Velocity measurements in the cold inlet pipe at x = -3D_2, measured along zcl and ycl. The left column shows data for the axial velocity component (u), and the right column shows corresponding data for the transverse components.

The plots in the right column of Fig. A5 refer to the transverse velocity components. Note that these are scaled with respect to the mean centreline velocity U_{cl} and not the bulk velocity. For convenience, all these data have been reproduced in tabular form at the end of this document.

The Reynolds shear stresses are given in Fig. A6. The correlation between the streamwise and the tangential (azimuthal) velocity component (profile ycl) should be zero for pure axisymmetric flow, and the values in the Figure are close to zero, except for some scatter near the wall. The correlation between the radial and the streamwise velocity fluctuations (profile zcl) is more interesting. For fully turbulent pipe flow, the Reynolds stress can be exactly derived (e.g. Tennekes and Lumley, 1972), and takes the following form:

$$\overline{uw} = u_\tau^2 \left(\frac{r}{R} + \upsilon \frac{\partial U}{\partial r} \right)$$

$$u_\tau = \text{friction velocity} = \sqrt{\tau_w / \rho}$$

The second term within the brackets is small, except close to the pipe wall, so the uw-profile should be linear in the central part of the pipe. A linear fit has been applied to the data in Fig. A6, and the friction velocity (u_τ), scaled with respect to the centreline velocity U_{cl}, derived accordingly. The inverse gives the ratio $U_{cl}/u_\tau = U_{cl}^+ = 25.8$. The ratio is dependent on Reynolds number. Zagarola and Smits (1998) report $U_{cl}^+ \approx 25.5$ for Re = 98 000, very close the values found here.

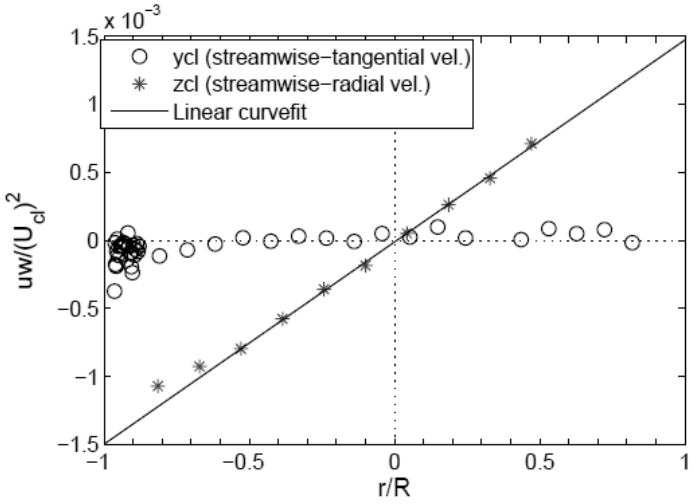

Figure A6: Reynolds shear stress (uw) in the cold inlet pipe at x = -3D_2. The straight line is a fit to the central part of the data (-0.5 < r/R < 0.5).

Figure A7 shows the measured streamwise mean velocity, plotted in wall coordinates, using a logarithmic scale for the distance from the wall. Note that $y^+ = 0$ corresponds to the inner pipe wall in this plot. The friction velocity obtained from the Reynolds stress profile in Fig. A6 has been used ($u_\tau = 0.026$ m/s), which gives a viscous length scale $l^* = \mu/\rho u_\tau \approx 40$ μm. However, the slope of the log-region is very sensitive to the estimated wall position, which results in an uncertainty. In Fig. A7, the velocity profile is plotted according to the original coordinates obtained from the measurements, but also with the coordinates shifted by –0.7 mm in the y-direction. It should also be noted that with a length scale of the order of 40 μm the measurement volume and the spatial resolution for the LDV measurements is around $\Delta y^+ = 30$, which means that the points in the inner region are influenced by a gradient bias affecting the slope of the curve.

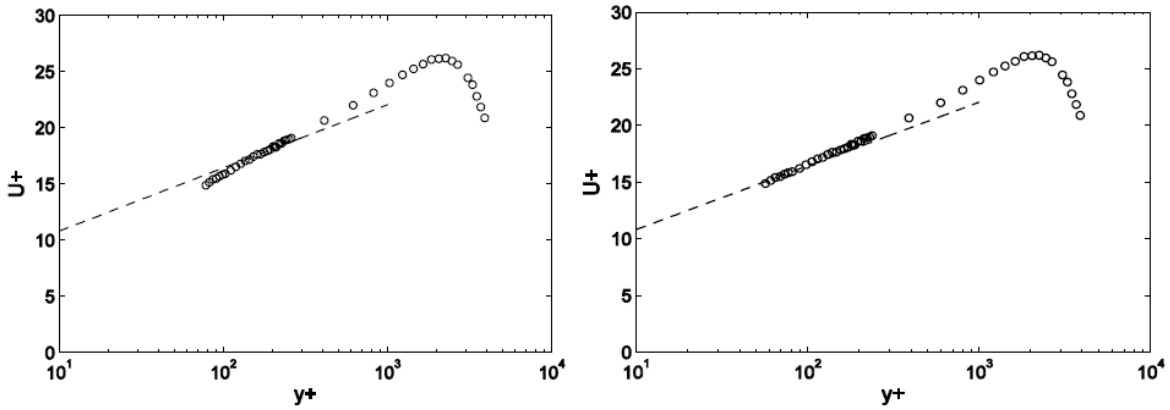

Figure A7: Streamwise mean velocity in the cold inlet pipe plotted in wall-coordinates. In the left plot, the original coordinates are used, while in the right plot the profile is shifted $\Delta y = -0.7$ mm. The dashed line is $U^+ = 1/0.41 \ln(y^+) + 5.2$.

A3.2 Branch Pipe: InHo

As mentioned earlier, the inlet velocity profiles had been measured earlier (Westin et al., 2008) when measurements were carried out with a main/branch flow ratio of 2. In the present measurements, the flowrate in the hot inlet has been kept the same, so the same velocity profiles can be applied for the present case (flow ration 1.5).

Figures A8, A9 show the axial and transverse velocity data for the hot water inlet pipe, measured at a cross-section $-3.1D_1$ upstream of the centre of the tee. Recalling that this inlet pipe is considerably shorter than the cold inlet pipe (only 20 diameters compared with 80 diameters for the cold inlet), fully developed turbulent pipe flow cannot be expected. This fact is clear already from the mean streamwise (x-direction) velocity profile shown in Fig. A8. This has a more "top hat" shape than that shown for the cold inlet in Fig. A5. The centreline velocity in the hot inlet pipe is $U_{cl} = 1.11\ U_{bulk} \approx 0.86$ m/s. Note again how the velocities have been scaled for these Figures: the mean streamwise (axial) velocity is scaled with respect to the mean bulk velocity, U_{bulk}, while all others are scaled with respect to the centreline velocity, U_{cl}.

All profiles indicate a flow with developing boundary layers on the pipe wall, while the central region of the pipe shows characteristics similar to a mainly undisturbed free stream with a turbulence level of approximately 1.5% with respect to the centreline velocity, the values signifying a generally low level of turbulence. The higher moments (skewness, S, and flatness, F) exhibit some scatter, but it is still possible to detect local peaks in both quantities close to the edge of the growing boundary layer. Flatness is a good indicator of the intermittency in the flow. In the free stream, just outside the boundary layer, one can expect that the signal would be rather undisturbed, except at instances when strong disturbances emanate from the boundary layer. The large flatness values (7–8) indicate the location of the outer edge of the boundary layer to be at $r/R \approx 0.5$.

It was preferred to perform these measurements under isothermal conditions, since the changes in the refractive index of the water due the temperature difference ΔT caused troublesome distortions of the laser beams. However, a check was made that the flow at isothermal conditions would be similar to that in which $\Delta T \approx 10$-20°C, as used for the temperature measurements with thermocouples. Both sets of data are included in Fig. A8, and show good correspondence. Note that some profiles (along xcl) were obtained using a mirror.

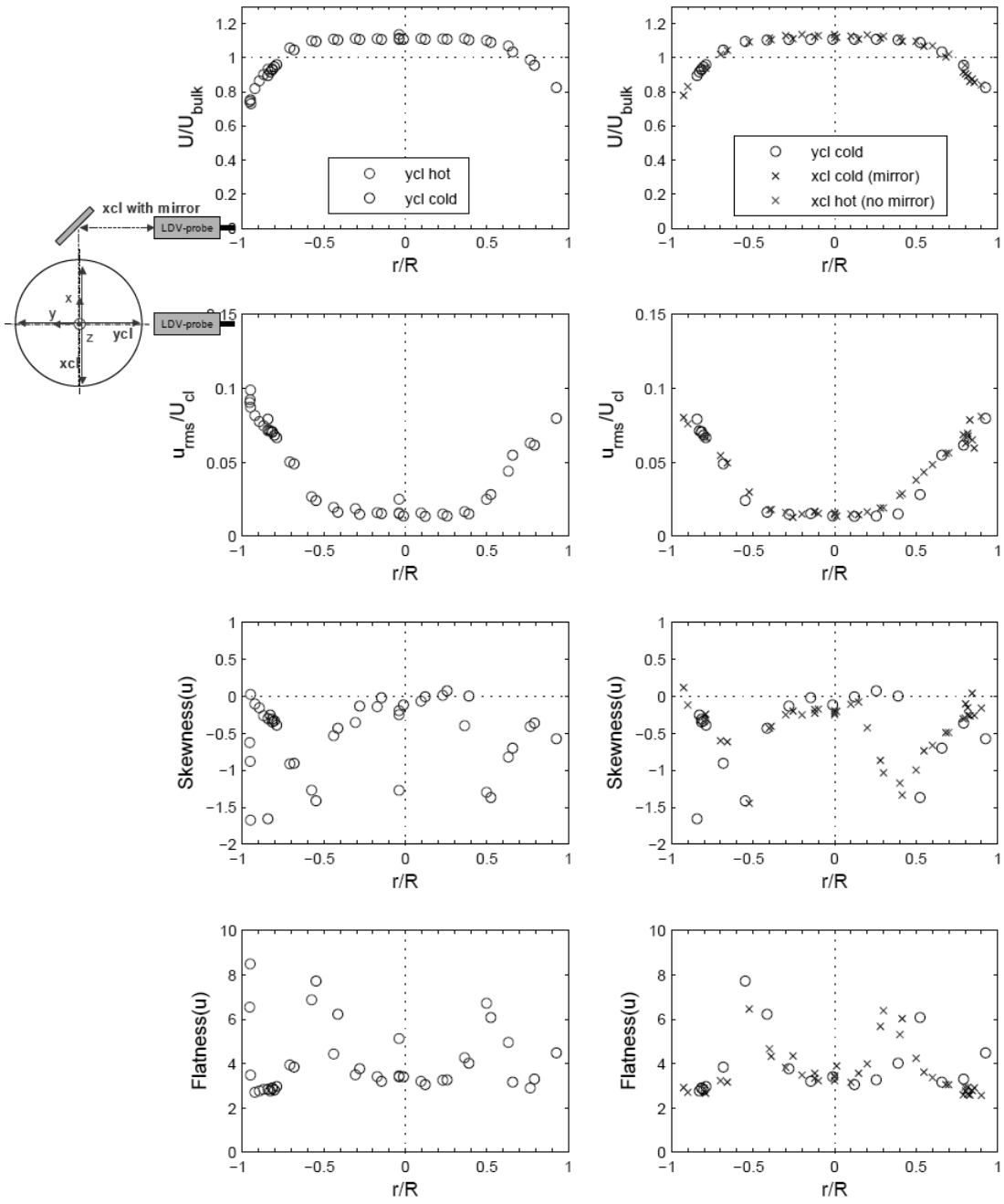

Figure A8: Streamwise (axial) velocity component for the hot inlet at z = -3.1D_1: left column, ycl with hot and cold water; right column, ycl with cold water, xcl with hot and cold water.

Figure A9 gives the measured profiles of the velocity components in the xcl and ycl directions (see inset to Fig. A8 for coordinate orientation) at the same upstream cross-section (z = -3.1D_1). Reynolds stress data are also included.

The accuracy of the electromagnetic flowmeters used for the inlet flow rates is ±0.5%. The inlet temperatures are measured using Pt100 sensors, with an accuracy of between ±0.1°C and ±0.2°C. The uncertainty in the upstream LDV measurements is estimated to be between 6% and 8% for the different measured quantities.

For convenience, all upstream LDV data are also given in tabular form at the end of the document.

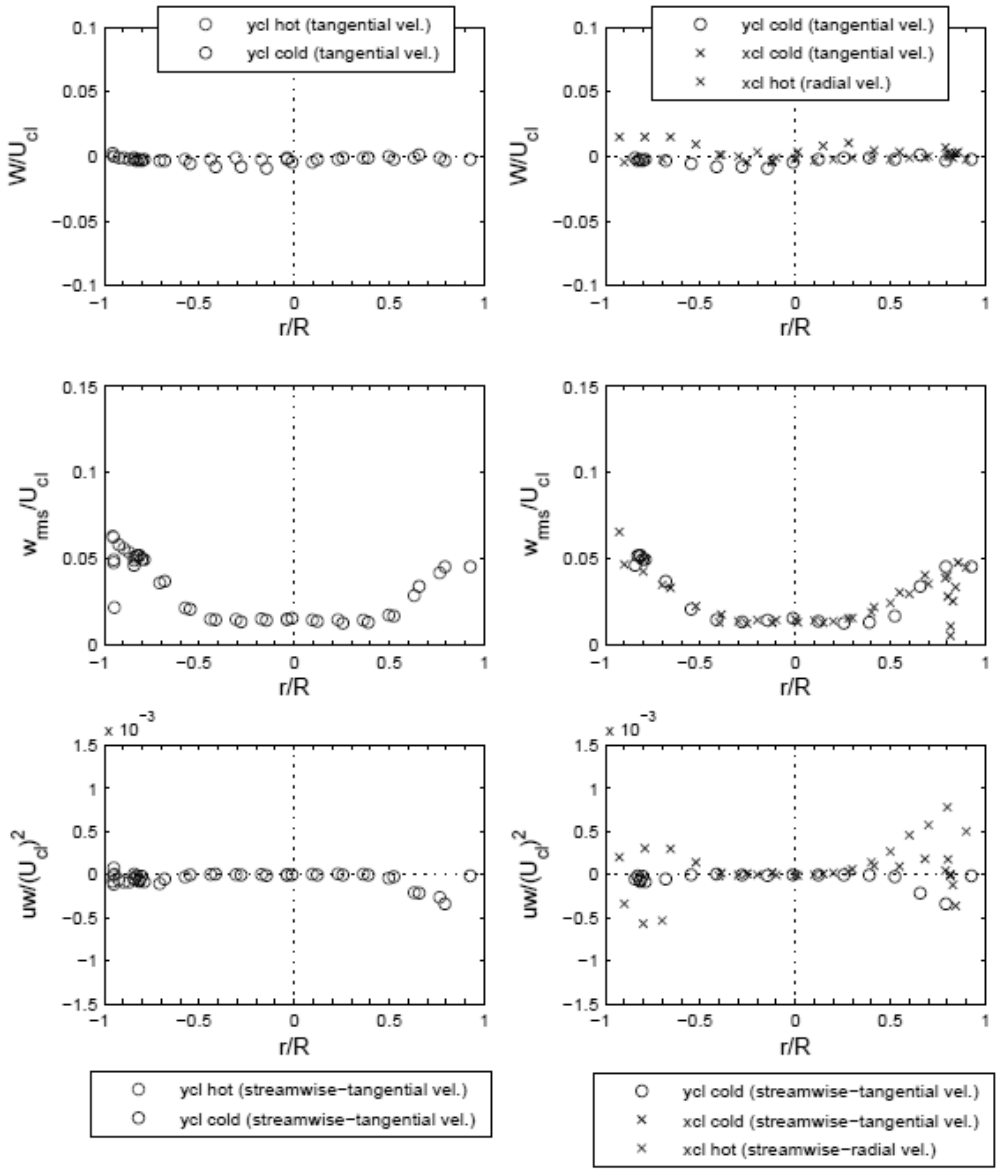

Figure A9: Scaled transverse (radial/tangential) velocity components, and Reynolds shear stresses (uw) for the hot inlet, measured at z = -3.1D_1: left column, ycl with hot and cold water; right column, ycl with cold water, and xcl with hot and cold water.

A4. DOWNSTREAM NUMERICAL DATA REQUESTED

A4.1 Introduction

Very basic quantities are requested from this benchmark, to permit flexibility in the choice of summary results, and uniform processing to obtain those results. It is assumed that most analyses will probably involve a scale-resolving turbulence modeling approach. However, the selected state information should be useful for most other approaches.

A4.2 Coordinate System Used for Reporting

The same Cartesian coordinate system developed for earlier tests in this facility will be used, as given in the previous Sections of this document, and described by Westin (2007). The origin is at the intersection of the centerlines for the main and branch pipes, with the x-axis along the main pipe's centerline, with positive direction downstream of the origin. The z-axis is along the centerline of the branch pipe, and the y axis spans the main pipe perpendicular to both main and branch centerlines. In the following discussion, use of the standard notation of u, v and w for the x, y and z components of velocity, the coordinate directions forming a right-handed set.

A4.3 Location of Instrumentation

The inside diameter of the main pipe is 140 mm (D_2). Thermocouples of 0.13mm diameter (frequency response 30 Hz) are placed approximately 1 mm (with an estimated uncertainty of about a couple of hundred microns, primarily in the positive direction) from the inner pipe wall at x = $2D_2$, $4D_2$, $6D_2$, $8D_2$, $10D_2$, $15D_2$ and $20D_2$. Taking 0° to be the top of the main pipe (y=0, z=70mm), thermocouple locations around the circumference of the pipe are given in Table A5. Angles in the Table increase in a counter-clockwise direction if the viewing perspective is from the tee junction (coordinate origin) towards the thermocouples (looking in the positive x-direction).

PIV data are available roughly spanning 1 to 5 hydraulic diameters downstream of the tee junction in the x-y and x-z planes intersecting the pipe's centerline.

Table A5. Thermocouple Locations

Location on x axis	**Angular Positions (Degrees)**
2 D_2	0, 90, 180, 270
4 D_2	0, 90, 180, 270
6 D_2	0, 90, 180, 270
8 D_2	0, 90, 180, 270
10 D_2	0, 90, 180, 270
15 D_2	0, 180
20 D_2	0, 180

A4.4 Transient Data to be Reported

Prior to the period of reported data, it is the participant's responsibility to run the simulation for a long enough time interval for time-averaged velocities to become steady. Past simulations of this facility have accomplished this in two to four seconds, though these times should be used as a guide only. After this initial period, all transient data are to be reported at every 0.001 seconds for at least the last 5 seconds of

the transient calculation, and for no more than 20 seconds. If time step sizes other than the 0.001s required for the analysis are used in the calculation, participants shall report their method for data conversion.

A non-dimensional temperature T^* shall be reported at each thermocouple location. T^* is the actual temperature minus the cold flow inlet temperature, divided by the difference between hot and cold inlet temperatures: that is,

$$T^* = \frac{T - T_{cold}}{T_{hot} - T_{cold}}$$

This is the same definition used in the paper by Frank et al. (2008). For the present benchmark case, the values T_{hot} = 36°C and T_{cold} = 19°C are to be used.

Velocities shall be reported at x = 1.6D_2, 2.6D_2, 3.6D_2, and 4.6D_2 along two lines perp-endicular to the flow: horizontal (-70mm<y<70mm, z=0), and vertical (-70mm<z<70mm, y=0). To characterize the velocity field, we are asking for all three resolved components of the velocities at each reported point, and the turbulent kinetic energy (k_{SGS}) from your subgrid turbulence model (if available). Results should be reported at no less than 20 and no more than 50 points along each line segment.

In addition to the basic data, we request a characterization of your CFD methodology and mesh in an accompanying document (typically 1-2 pages). As a minimum, please provide the time step size (or range) used in the transient, range of y^+ (wall normal coordinate), total number of nodes/meshes used for the calculation, and, in each of the coordinate directions:

- an average number of cells (N_x, N_y, N_z);
- minimum cell length (Δx_{min}, Δy_{min}, Δz_{min});
- maximum cell length (Δx_{max}, Δy_{max}, Δz_{max}).

Also, summarize other mesh configurations that you used to estimate errors associated with spatial discretization, where applicable.

A4.4.1 Transient Data File Formats

All files shall be written in ASCII text format with space-delimited fields. Values of temperatures, velocity components and turbulent kinetic energies shall be written with 8 significant digits (e.g. 1.2345678 or 1.2345678E-2). Values for time or location may be written with fewer significant digits, if appropriate.

Files containing non-dimensional **temperatures** start with a line specifying thermocouple locations for corresponding values in subsequent lines. Each entry in the line is a composite providing the axial and angular location, with an integer followed by "D" followed by another integer. A portion of the first line might be:

2D0 2D90 2D180 2D270 4D0 4D45 4D90 4D135 4D180 4D225 …

Subsequent lines start with the time, and the remainder of the line contains scaled temperatures at that time, located at positions provided in the first line of the file.

Files with **velocity components** or **turbulent kinetic energy** begin with a line listing the y or z positions at which the values are located. Values are in millimetres, and in the range -70 to 70. With a very coarse sampling of results, an example of this line would be: -69.0 -60.0 -40.0 -20.0 0.0 20.0 40.0 60.0 69.0

Subsequent lines start with the time, and the remainder of the numbers in the line are CFD results interpolated to the positions provided in the first line of the file.

A4.4.2 Transient Data File Names

To enable automated processing of results, all data files must follow the same naming convention. All temperature results shall be provided in a single file named "temperatures.txt". Results for velocity components and turbulent kinetic energy are divided into files by data type, axial location, and direction of line in space (horizontal or vertical).

The specific file names and contents are:

u1.6Dh.txt x component of velocity 1.6 diameters downstream of the tee junction for z=0 and -70mm<y<70mm (horizontal line);

u1.6Dv.txt x component of velocity 1.6 diameters downstream of the tee junction for y=0 and -70mm<z<70mm (vertical line);

v1.6Dh.txt y component of velocity 1.6 diameters downstream of the tee junction for z=0 and -70mm<y<70mm (horizontal line);

v1.6Dv.txt y component of velocity 1.6 diameters downstream of the tee junction for y=0 and -70mm<z<70mm (vertical line);

w1.6Dh.txt z component of velocity 1.6 diameters downstream of the tee junction for z=0 and -70mm<y<70mm (horizontal line);

w1.6Dv.txt z component of velocity 1.6 diameters downstream of the tee junction for y=0 and -70mm<z<70mm (vertical line);

k1.6Dh.txt subgrid turbulent kinetic energy 1.6 diameters downstream of the tee junction for z=0 and -70mm<y<70mm (horizontal line);

k1.6Dv.txt subgrid turbulent kinetic energy 1.6 diameters downstream of the tee junction for y=0 and -70mm<z<70mm (vertical line).

This set of eight files is repeated three more times with the "1.6" in the title and description replaced by "2.6", "3.6", and "4.6" to capture results at these three other locations downstream of the tee junction.

A4.5 Time-Averaged Data to be Reported

In addition to transient data, we ask participants to provide:

- time-averaged values for all three velocity components;
- RMS-values of the fluctuating portions of all three velocity components, as well as of the Reynolds shear stresses; and
- Time-average of the subgrid turbulent kinetic energy, if available.

This information shall be reported at x=1.6D, 2.6D, 3.6D, and 4.6D, along two lines perpendicular to the flow: horizontal (-70mm<y<70mm, z=0), and vertical (-70mm<z<70mm, y=0). As with transient data, results should be reported at no less than 20 and no more than 50 points along each line segment.

A4.5.1 Time-Averaged Data File Formats

As before, all files shall be written in ASCII text format with space-delimited fields. Time-averaged values shall be written with 8 significant digits (e.g. 1.2345678 or 1.2345678E-2). Values for times and locations may be written with fewer significant digits, if appropriate.

Files for time-averaged data start with a line listing the beginning and ending time of the window used for averaging. The next line contains y or z positions at which the values are located (same information as the first line of a corresponding transient file). Values are in millimetres, and in the range -70 to 70. The third line contains time-averaged values for the x component of velocity at the locations provided in the second line. The fourth line contains time-averaged values for the y component of velocity, and the fifth line contains time-averaged values for the z component of velocity. Lines six through eight contain RMS-values of the x, y, and z components of the velocity fluctuations in the respective coordinate directions. If the information is available, a ninth line contains the time-averaged values of the subgrid turbulent kinetic energy.

A4.5.2 Time-Averaged Data File Names

To enable automated processing of results, all data files must follow the same naming convention. Files are generated by axial location and direction of line in space used to sample data (horizontal or vertical). The specific file names and contents are:

avg1.6Dh.txt time-averaged data 1.6 diameters downstream of the tee junction for z=0 and -70mm<y<70mm (horizontal line);
avg1.6Dv.txt time-averaged data 1.6 diameters downstream of the tee junction for y=0 and -70mm<z<70mm (vertical line);
avg2.6Dh.txt time-averaged data 2.6 diameters downstream of the tee junction for z=0 and -70mm<y<70mm (horizontal line);
avg2.6Dv.txt time-averaged data 2.6 diameters downstream of the tee junction for y=0 and -70mm<z<70mm (vertical line);
avg3.6Dh.txt time-averaged data 3.6 diameters downstream of the tee junction for z=0 and -70mm<y<70mm (horizontal line);
avg3.6Dv.txt time-averaged data 3.6 diameters downstream of the tee junction for y=0 and -70mm<z<70mm (vertical line);
avg4.6Dh.txt time-averaged data 4.6 diameters downstream of the tee junction for z=0 and -70mm<y<70mm (horizontal line);
avg4.6Dv.txt time-averaged data 4.6 diameters downstream of the tee junction for y=0 and -70mm<z<70mm (vertical line).

A4.6 Transmission of Results

Start by creating a text file named “Information.txt”. The first line of the file contains a comma-delimited list of the authors of the study. The second line contains the name of your organization, and the third line contains the name of the CFD program that you used. The fourth line contains an acronym, or brief phrase, describing your choice of turbulence model. For example:
B. Smith, G. Zigh
OECD/NEA
ANSYS-CFX
SAS-SST
Use GNU tar or a zip utility to create a compressed archive containing Information.txt, temperatures.txt, the 32 files for transient velocity components and turbulent kinetic energies, and the 8 files containing

time-averaged information. If your modelling approach does not include a subgrid turbulence model, or the subgrid turbulent kinetic energy cannot be obtained (directly or through post-processing), then do not include the 8 files associated with transient subgrid turbulent kinetic energy. The scripts used to post-process the CFD results will automatically note and adjust for absence of these subgrid-scale data.

The file shall have a name that begins with "TeeResults", followed by a hyphen, followed by the initials of the first-listed participant, followed by another hyphen, followed by initials for the participating organization. The suffix for the file name will be either tgz or zip. Examples are:
"TeeResults-JHM-USNRC.tgz" or "TeeResults-BS-PSI.zip".

A5. CONCLUDING REMARKS

A5.1 Organizing Committee

Brian L. Smith, PSI, Switzerland Kristian Angele, Vattenfall R&D, Sweden
John H. Mahaffy, US NRC, USA
Dominique Bestion, CEA, France
Ghani Zigh, US NRC, USA
Jong-Chull Jo, OECD/NEA, France (Secretariat)

A5.2 Schedule

May 20, 2009		Kick-Off Meeting
June 15, 2009	(latest)	Distribution of Draft Version of Benchmark Specifications
June 30, 2009		Deadline for comment/queries from participants concerning Benchmark Specifications
July 15, 2009 (earliest)		Distribution of Final Version of Benchmark Specifications
April 30, 2010		Deadline for Receipt of Simulation Results
June 30, 2010 (latest)		Open Benchmark Meeting (Release of Test Data)
Sept. 30, 2010 (latest)		Presentation of Results and Synthesis at CFD4NRS-3 Workshop

To ensure that there are no errors, ambiguities, etc. in the specifications, the latest date of June 15, 2009 is set for the initial distribution of the draft benchmark specifications, some 3 weeks after the kick-off meeting. Participants are requested to communicate any queries/comments within 15 days. Final specifications will then be issued, earliest July 15, 2009. The participants then have more than 9 months to perform the simulations and submit their results to the organizers.

This benchmark activity is an integral part of the CFD4NRS-3 Workshop, and the scheduling is part due to the timing of this event (in the fall of 2010). However, it is intended to release the data ahead of this time. An *Open Benchmark Meeting* will be organized in June 2010, at which time the measured data downstream of the junction will be released for the first time.

The synthesis of the blind benchmark results will be undertaken by J. H. Mahaffy, US NRC, and he will present his findings in an *Invited Lecture* at the CFD4NRS-3 Workshop, which will take place in the Washington DC area: provisional date 14-16 September 2010. The Workshop will be under joint OECD/NEA and IAEA sponsorship, as with previous workshops in the series. A paper will also be prepared to accompany the Invited Lecture, and will be part of the official conference proceedings (to be issued early in 2011).

It is hoped that many participants will take the opportunity to display their results at this Workshop, and a special Poster Session is being organized for this purpose. It will not be necessary to produce an

accompanying paper in support of the poster. However, if more than the blind benchmark simulation has been performed, for example a comparison of several turbulence modelling approaches, a full paper can be submitted to the Workshop organizers in the usual way for consideration for inclusion in the technical programme. The number of such papers will be limited, however.

A5.3 Submittal Procedures

In order to be able to efficiently handle and compare calculated and measured data, all participants are requested to adhere STRICTLY to the formatting requested in Section A4. Datasets not conforming to the specified norms will be returned to the participant for correction.

The deadline for submission of code predictions is April 30, 2010. Earlier submissions will be very welcome, and will considerably ease the burden on the organizers. Later submissions will be accepted or refused at the discretion of the organizing committee. Only one submission per participant will be processed.

A special webpage will be created on an appropriate website to which participants will be able to upload their results. Details will be distributed once the webpage is functional. Individual usernames and passwords will be allocated, and all data sets will be regarded as confidential. Access to the data will only be available to the owner and to J. H. Mahaffy. After uploading, participants are advised to download their datasets and compare with the originals to ensure that perfect transmission has been accomplished. Each participant will have the opportunity to exchange the dataset submitted for a newer version, but only up to the time of the Open Benchmark Meeting, at which time no further user access to the website will be possible.

After the test data are released at the Open Benchmark Meeting (June 2010, precise date to be announced), no more submissions will be accepted. **Additionally, participants will thereafter not be permitted to withdraw their submissions.**

Participants are free to repeat their calculations once they have the test data, and display the details at the special Poster Session at the CFD4NRS-3 Workshop, as desired. However, only the "blind" code predictions will be considered for the synthesis.

REFERENCES

ASME Steam Tables, American Society of Mechanical Engineers, New York, (1967).

Frank, Th., Adlakha, M., Lifante, C., Prasser, H.-M., Menter, F. "Simulation of Turbulent and Thermal Mixing in T-Junctions Using URANS and Scale-Resolving Turbulence Models in ANSYS CFX," Proc. XCFD4NRS, Grenoble, France, Sept. 10-12, 2008.

Incropera, F. P., DeWitt, P. *Fundamentals of Heat and Mass Transfer*, 3rd ed., John Wiley & Sons, New York, 1990.

Tennekes H., Lumley, J. L. *A First Course in Turbulence*, MIT Press, 1972.

Westin, J. "Thermal Mixing in a T-Junction. Model Tests at Vattenfall Research and Development AB 2006. Boundary Conditions and List of Available Data for CFD Validation," Vattenfall Memo U 07-26 (2007).

Westin, J., et al. (2008) High-cycle thermal fatigue in mixing Tees. Large-Eddy Simulations compared to a new validation experiment, ICONE16-48731, 16th International Conference on Nuclear Engineering, Orlando, Florida, USA, May 11-15, 2008.

Zagarola, M. V., Smits, A. J. "Mean-Flow Scaling of Turbulent Pipe Flow", J. Fluid Mech., **373**, 33-79 (1998).

UPSTREAM DIGITAL DATA

Main Pipe: InCo (Figure A5)

r/R-zcl	U/Ubulk-ycl	urms/Ucl	Skew(u)	Flat(u)	W/Ucl	wrms/ucl	Skew(w)	Flat(w)
-8.14E-01	9.23E-01	7.67E-02	-3.48E-01	2.89E+00	-9.89E-03	4.35E-02	8.10E-02	2.92E+00
-6.71E-01	1.00E+00	6.87E-02	-3.09E-01	2.83E+00	-1.76E-02	4.16E-02	2.09E-01	3.27E+00
-5.29E-01	1.07E+00	6.09E-02	-3.98E-01	2.96E+00	-1.76E-02	3.78E-02	3.24E-01	3.55E+00
-3.86E-01	1.11E+00	5.33E-02	-5.01E-01	3.24E+00	-1.43E-02	3.47E-02	3.10E-01	3.40E+00
-2.43E-01	1.15E+00	4.42E-02	-5.10E-01	3.40E+00	-1.21E-02	3.10E-02	2.59E-01	3.48E+00
-1.00E-01	1.16E+00	3.91E-02	-4.98E-01	3.44E+00	-1.54E-02	2.90E-02	1.92E-01	3.74E+00
4.29E-02	1.17E+00	3.81E-02	-4.26E-01	3.38E+00	-1.43E-02	2.80E-02	-5.90E-02	3.70E+00
1.86E-01	1.16E+00	4.19E-02	-4.92E-01	3.26E+00	-1.87E-02	3.02E-02	-2.71E-01	3.64E+00
3.29E-01	1.13E+00	4.97E-02	-4.38E-01	3.21E+00	-9.89E-03	3.33E-02	-2.77E-01	3.46E+00
4.71E-01	1.08E+00	5.86E-02	-4.80E-01	3.06E+00	-1.10E-02	3.62E-02	-3.32E-01	3.44E+00
9.00E-01	8.45E-01	8.23E-02	-1.21E-01	2.64E+00	-9.89E-03	4.18E-02	-1.02E-01	3.48E+00

r/R-ycl	U/Ubulk-ycl	urms/Ucl	Skew(u)	Flat(u)	W/Ucl	wrms/ucl	Skew(w)	Flat(w)
8.19E-01	9.37E-01	7.88E-02	-1.78E-01	2.61E+00	-9.89E-03	4.88E-02	-7.00E-03	3.42E+00
7.23E-01	9.81E-01	7.49E-02	-1.44E-01	2.62E+00	-1.32E-02	4.78E-02	1.20E-02	3.25E+00
6.27E-01	1.02E+00	6.99E-02	-2.32E-01	2.83E+00	-1.21E-02	4.54E-02	-7.00E-03	3.31E+00
5.31E-01	1.07E+00	6.46E-02	-3.72E-01	2.88E+00	-1.32E-02	4.33E-02	-4.90E-02	3.25E+00
4.36E-01	1.10E+00	5.98E-02	-4.07E-01	2.99E+00	-1.32E-02	3.96E-02	-5.80E-02	3.22E+00
2.44E-01	1.15E+00	4.58E-02	-4.84E-01	3.39E+00	-1.54E-02	3.23E-02	-4.40E-02	3.65E+00
1.49E-01	1.16E+00	4.14E-02	-5.78E-01	3.63E+00	-1.43E-02	2.97E-02	-1.46E-01	3.86E+00
5.29E-02	1.18E+00	3.87E-02	-4.05E-01	3.27E+00	-1.43E-02	2.87E-02	-3.80E-02	3.72E+00
-4.29E-02	1.17E+00	3.81E-02	-4.84E-01	3.53E+00	-1.43E-02	2.87E-02	-6.00E-02	3.59E+00
-1.39E-01	1.17E+00	4.07E-02	-5.40E-01	3.52E+00	-1.54E-02	3.02E-02	6.10E-02	3.85E+00
-2.34E-01	1.15E+00	4.51E-02	-4.96E-01	3.39E+00	-1.32E-02	3.31E-02	-1.40E-02	3.61E+00
-3.30E-01	1.13E+00	4.99E-02	-4.99E-01	3.26E+00	-1.43E-02	3.58E-02	2.00E-03	3.68E+00
-4.26E-01	1.11E+00	5.58E-02	-4.38E-01	3.14E+00	-1.21E-02	3.90E-02	1.50E-02	3.49E+00
-5.21E-01	1.08E+00	6.16E-02	-3.96E-01	3.01E+00	-1.43E-02	4.12E-02	-2.90E-02	3.39E+00
-6.17E-01	1.04E+00	6.76E-02	-3.31E-01	2.80E+00	-1.43E-02	4.49E-02	-2.40E-02	3.31E+00
-7.13E-01	9.87E-01	7.15E-02	-2.67E-01	2.85E+00	-1.32E-02	4.80E-02	-3.50E-02	3.30E+00
-8.09E-01	9.27E-01	7.85E-02	-2.29E-01	2.88E+00	-1.43E-02	5.07E-02	1.60E-02	3.32E+00
-9.04E-01	8.19E-01	8.34E-02	-8.20E-02	2.76E+00	-1.21E-02	5.56E-02	-2.20E-02	3.28E+00
-8.79E-01	8.56E-01	8.11E-02	-1.17E-01	2.83E+00	-1.21E-02	5.40E-02	-3.90E-02	3.26E+00
-8.83E-01	8.51E-01	8.16E-02	-1.19E-01	2.75E+00	-1.32E-02	5.46E-02	4.00E-03	3.33E+00
-8.87E-01	8.49E-01	8.18E-02	-9.10E-02	2.73E+00	-1.21E-02	5.45E-02	1.80E-02	3.26E+00
-8.91E-01	8.46E-01	8.33E-02	-1.32E-01	2.70E+00	-1.32E-02	5.46E-02	-3.00E-03	3.26E+00
-8.95E-01	8.35E-01	8.23E-02	-9.70E-02	2.67E+00	-1.21E-02	5.51E-02	-3.10E-02	3.30E+00
-8.99E-01	8.35E-01	8.35E-02	-9.70E-02	2.74E+00	-1.21E-02	5.55E-02	9.00E-03	3.37E+00
-9.02E-01	8.21E-01	8.37E-02	-2.80E-02	2.74E+00	-1.21E-02	5.63E-02	-2.60E-02	3.43E+00
-9.06E-01	8.23E-01	8.32E-02	-6.20E-02	2.76E+00	-1.32E-02	5.64E-02	-5.30E-02	3.25E+00
-9.10E-01	8.12E-01	8.24E-02	-5.60E-02	2.75E+00	-1.21E-02	5.58E-02	8.00E-03	3.21E+00
-9.14E-01	8.05E-01	8.52E-02	-4.50E-02	2.65E+00	-1.10E-02	5.69E-02	-7.70E-02	3.27E+00
-9.18E-01	8.00E-01	8.40E-02	-9.00E-03	2.72E+00	-1.10E-02	5.70E-02	-7.80E-02	3.31E+00
-9.22E-01	7.92E-01	8.53E-02	-4.70E-02	2.78E+00	-9.89E-03	5.66E-02	-2.10E-02	3.31E+00

-9.25E-01	7.91E-01	8.22E-02	-1.10E-02	2.75E+00	-1.10E-02	5.81E-02	-2.90E-02	3.25E+00
-9.29E-01	7.82E-01	8.53E-02	-3.40E-02	2.69E+00	-9.89E-03	5.78E-02	-2.80E-02	3.35E+00
-9.33E-01	7.71E-01	8.59E-02	-4.50E-02	2.76E+00	-9.89E-03	5.76E-02	-1.50E-02	3.31E+00
-9.37E-01	7.65E-01	8.73E-02	-1.30E-02	2.74E+00	-1.10E-02	5.85E-02	2.90E-02	3.28E+00
-9.41E-01	7.54E-01	8.73E-02	-5.70E-02	2.75E+00	-9.89E-03	5.92E-02	-5.80E-02	3.25E+00
-9.44E-01	7.42E-01	8.54E-02	-3.80E-02	2.78E+00	-9.89E-03	5.91E-02	-1.40E-02	3.34E+00
-9.48E-01	7.27E-01	8.70E-02	-3.70E-02	2.77E+00	-8.79E-03	5.86E-02	-4.80E-02	3.59E+00
-9.52E-01	7.14E-01	8.63E-02	-2.00E-02	2.79E+00	-8.79E-03	6.09E-02	-3.10E-02	3.33E+00
-9.54E-01	7.10E-01	8.73E-02	-1.30E-01	2.73E+00	-1.10E-02	6.18E-02	-3.70E-02	3.24E+00
-9.56E-01	7.04E-01	8.87E-02	-1.10E-01	2.65E+00	-9.89E-03	6.19E-02	-1.60E-02	3.24E+00
-9.58E-01	6.95E-01	8.80E-02	-1.33E-01	2.78E+00	-1.10E-02	6.31E-02	-1.10E-02	3.17E+00
-9.60E-01	6.91E-01	9.13E-02	-1.62E-01	2.80E+00	-1.10E-02	6.40E-02	-4.00E-02	3.42E+00
-9.62E-01	6.79E-01	9.25E-02	-1.64E-01	2.82E+00	-9.89E-03	6.33E-02	-5.20E-02	3.31E+00
-9.64E-01	6.68E-01	9.74E-02	-4.11E-01	3.25E+00	-1.65E-02	5.18E-02	-1.14E-01	3.01E+00

Main Pipe: InCo (Figure A6)

r/R-ycl	uw/Ucl2 (ycl)	r/R-zcl	uw/Ucl2 (zcl)	r/R-curve	uw-curve
8.19E-01	-1.70E-05	-8.14E-01	-1.07E-03	########	-1.50E-03
7.23E-01	7.83E-05	-6.71E-01	-9.26E-04	-9.00E-01	-1.35E-03
6.27E-01	4.90E-05	-5.29E-01	-7.96E-04	-8.00E-01	-1.20E-03
5.31E-01	8.61E-05	-3.86E-01	-5.77E-04	-7.00E-01	-1.05E-03
4.36E-01	6.04E-06	-2.43E-01	-3.59E-04	-6.00E-01	-9.03E-04
2.44E-01	1.78E-05	-1.00E-01	-1.85E-04	-5.00E-01	-7.54E-04
1.49E-01	9.78E-05	4.29E-02	5.13E-05	-4.00E-01	-6.06E-04
5.29E-02	2.46E-05	1.86E-01	2.63E-04	-3.00E-01	-4.57E-04
-4.29E-02	5.10E-05	3.29E-01	4.57E-04	-2.00E-01	-3.09E-04
-1.39E-01	-8.09E-06	4.71E-01	7.12E-04	-1.00E-01	-1.60E-04
-2.34E-01	1.63E-05	9.00E-01	NaN	0.00E+00	-1.19E-05
-3.30E-01	3.10E-05			1.00E-01	1.37E-04
-4.26E-01	-5.55E-06			2.00E-01	2.85E-04
-5.21E-01	1.91E-05			3.00E-01	4.34E-04
-6.17E-01	-2.66E-05			4.00E-01	5.82E-04
-7.13E-01	-6.96E-05			5.00E-01	7.31E-04
-8.09E-01	-1.15E-04			6.00E-01	8.79E-04
-9.04E-01	-8.77E-05			7.00E-01	1.03E-03
-8.79E-01	-4.43E-05			8.00E-01	1.18E-03
-8.83E-01	-8.19E-05			9.00E-01	1.32E-03
-8.87E-01	-2.38E-05			1.00E+00	1.47E-03
-8.91E-01	-6.82E-05				
-8.95E-01	-1.09E-04				
-8.99E-01	-3.45E-05				
-9.02E-01	-2.37E-04				
-9.06E-01	-1.93E-04				
-9.10E-01	-9.13E-05				
-9.14E-01	-4.49E-05				
-9.18E-01	5.43E-05				
-9.22E-01	-1.45E-04				
-9.25E-01	-2.99E-05				
-9.29E-01	-2.06E-05				
-9.33E-01	-1.57E-05				

-9.37E-01	-3.63E-05
-9.41E-01	-4.20E-05
-9.44E-01	-1.13E-04
-9.48E-01	-4.53E-05
-9.52E-01	-1.08E-04
-9.54E-01	8.82E-06
-9.56E-01	-7.96E-05
-9.58E-01	-1.91E-04
-9.60E-01	-1.76E-04
-9.62E-01	-1.65E-05
-9.64E-01	-3.73E-04

Main Pipe: InCo (Figure A7)

y+ (dy=0)	U+ (dy=0)	y+ (dy=-0.70)	U+ (dy=-0.7)
3.91E+03	2.09E+01	3.89E+03	2.09E+01
3.70E+03	2.19E+01	3.68E+03	2.19E+01
3.50E+03	2.28E+01	3.48E+03	2.28E+01
3.29E+03	2.38E+01	3.27E+03	2.38E+01
3.09E+03	2.45E+01	3.06E+03	2.45E+01
2.67E+03	2.56E+01	2.65E+03	2.56E+01
2.47E+03	2.59E+01	2.45E+03	2.59E+01
2.26E+03	2.62E+01	2.24E+03	2.62E+01
2.06E+03	2.61E+01	2.04E+03	2.61E+01
1.85E+03	2.61E+01	1.83E+03	2.61E+01
1.65E+03	2.57E+01	1.62E+03	2.57E+01
1.44E+03	2.53E+01	1.42E+03	2.53E+01
1.23E+03	2.47E+01	1.21E+03	2.47E+01
1.03E+03	2.40E+01	1.01E+03	2.40E+01
8.23E+02	2.31E+01	8.01E+02	2.31E+01
6.17E+02	2.20E+01	5.96E+02	2.20E+01
4.11E+02	2.07E+01	3.90E+02	2.07E+01
2.06E+02	1.83E+01	1.84E+02	1.83E+01
2.59E+02	1.91E+01	2.38E+02	1.91E+01
2.51E+02	1.90E+01	2.29E+02	1.90E+01
2.43E+02	1.89E+01	2.21E+02	1.89E+01
2.35E+02	1.89E+01	2.13E+02	1.89E+01
2.26E+02	1.86E+01	2.05E+02	1.86E+01
2.18E+02	1.86E+01	1.97E+02	1.86E+01
2.10E+02	1.83E+01	1.88E+02	1.83E+01
2.02E+02	1.83E+01	1.80E+02	1.83E+01
1.93E+02	1.81E+01	1.72E+02	1.81E+01
1.85E+02	1.79E+01	1.64E+02	1.79E+01
1.77E+02	1.78E+01	1.55E+02	1.78E+01
1.69E+02	1.77E+01	1.47E+02	1.77E+01
1.60E+02	1.76E+01	1.39E+02	1.76E+01
1.52E+02	1.74E+01	1.31E+02	1.74E+01
1.44E+02	1.72E+01	1.23E+02	1.72E+01
1.36E+02	1.71E+01	1.14E+02	1.71E+01
1.28E+02	1.68E+01	1.06E+02	1.68E+01
1.19E+02	1.65E+01	9.78E+01	1.65E+01
1.11E+02	1.62E+01	8.96E+01	1.62E+01

1.03E+02	1.59E+01	8.14E+01	1.59E+01
9.87E+01	1.58E+01	7.72E+01	1.58E+01
9.46E+01	1.57E+01	7.31E+01	1.57E+01
9.05E+01	1.55E+01	6.90E+01	1.55E+01
8.64E+01	1.54E+01	6.49E+01	1.54E+01
8.23E+01	1.51E+01	6.08E+01	1.51E+01
7.82E+01	1.49E+01	5.67E+01	1.49E+01

Branch Pipe: InHo (Figure A8)

Ycl-hot

r/R	U/Ubulk	urms/Ucl	skew(u)	flat(u)
-3.87E-02	1.14E+00	1.53E-02	-2.48E-01	3.45E+00
-3.87E-02	1.11E+00	1.57E-02	-1.92E-01	3.40E+00
7.65E-01	9.87E-01	6.30E-02	-4.07E-01	2.89E+00
6.31E-01	1.07E+00	4.40E-02	-8.21E-01	4.95E+00
4.97E-01	1.10E+00	2.50E-02	-1.30E+00	6.72E+00
3.63E-01	1.11E+00	1.66E-02	-3.97E-01	4.26E+00
2.29E-01	1.11E+00	1.50E-02	1.30E-02	3.25E+00
9.53E-02	1.11E+00	1.57E-02	-6.40E-02	3.20E+00
-3.87E-02	1.11E+00	2.51E-02	-1.27E+00	5.12E+00
-1.73E-01	1.11E+00	1.60E-02	-1.40E-01	3.41E+00
-3.07E-01	1.11E+00	1.86E-02	-3.51E-01	3.50E+00
-4.41E-01	1.11E+00	1.95E-02	-5.32E-01	4.43E+00
-5.75E-01	1.10E+00	2.67E-02	-1.27E+00	6.87E+00
-7.09E-01	1.06E+00	5.03E-02	-9.12E-01	3.94E+00
-8.43E-01	9.33E-01	7.13E-02	-2.96E-01	2.85E+00
-8.43E-01	9.33E-01	7.21E-02	-3.02E-01	2.84E+00
-8.70E-01	9.01E-01	7.48E-02	-2.61E-01	2.84E+00
-8.96E-01	8.64E-01	7.76E-02	-1.54E-01	2.76E+00
-9.23E-01	8.19E-01	8.16E-02	-1.01E-01	2.71E+00
-9.50E-01	7.54E-01	8.73E-02	2.60E-02	3.48E+00
-9.47E-01	7.29E-01	1.51E-01	-2.81E+00	1.33E+01
-9.50E-01	7.51E-01	9.90E-02	-1.67E+00	1.34E+01
-9.53E-01	7.51E-01	9.24E-02	-8.79E-01	8.49E+00
-9.55E-01	7.41E-01	9.05E-02	-6.24E-01	6.55E+00

Ycl-cold

r/R	U/Ubulk	urms/Ucl	skew(u)	flat(u)
9.26E-01	8.24E-01	7.98E-02	-5.74E-01	4.48E+00
7.92E-01	9.55E-01	6.16E-02	-3.61E-01	3.31E+00
6.58E-01	1.03E+00	5.48E-02	-6.99E-01	3.17E+00
5.24E-01	1.09E+00	2.82E-02	-1.37E+00	6.08E+00
3.90E-01	1.10E+00	1.51E-02	5.00E-03	4.02E+00
2.56E-01	1.11E+00	1.36E-02	7.50E-02	3.27E+00
1.22E-01	1.11E+00	1.34E-02	-4.00E-03	3.05E+00
-1.24E-02	1.11E+00	1.36E-02	-1.15E-01	3.41E+00
-1.46E-01	1.11E+00	1.54E-02	-1.80E-02	3.20E+00
-2.80E-01	1.11E+00	1.49E-02	-1.31E-01	3.77E+00
-4.14E-01	1.10E+00	1.62E-02	-4.32E-01	6.22E+00
-5.48E-01	1.09E+00	2.42E-02	-1.41E+00	7.72E+00
-6.82E-01	1.04E+00	4.90E-02	-9.06E-01	3.85E+00
-8.16E-01	9.29E-01	7.08E-02	-3.08E-01	2.91E+00
-7.90E-01	9.59E-01	6.67E-02	-3.89E-01	2.96E+00
-8.03E-01	9.46E-01	6.83E-02	-3.30E-01	2.81E+00
-8.16E-01	9.33E-01	7.04E-02	-3.45E-01	2.88E+00
-8.30E-01	9.17E-01	7.13E-02	-2.52E-01	2.77E+00
-8.43E-01	8.95E-01	7.92E-02	-1.66E+00	1.71E+01

Xcl-hot

r/R	U/Ubulk	urms/Ucl	skew(u)	flat(u)
0.00E+00	1.14E+00	1.53E-02	-2.48E-01	3.45E+00
9.00E-01	8.41E-01	8.10E-02	-1.59E-01	2.56E+00
8.00E-01	9.56E-01	6.76E-02	-2.95E-01	2.93E+00
7.00E-01	1.02E+00	5.64E-02	-4.88E-01	3.04E+00
6.00E-01	1.07E+00	4.84E-02	-6.63E-01	3.37E+00
5.00E-01	1.10E+00	3.80E-02	-9.95E-01	4.24E+00
4.00E-01	1.12E+00	2.76E-02	########	5.31E+00
3.00E-01	1.13E+00	1.92E-02	########	6.39E+00
2.00E-01	1.13E+00	1.64E-02	-4.25E-01	3.99E+00
1.00E-01	1.13E+00	1.50E-02	-1.05E-01	3.16E+00
0.00E+00	1.13E+00	1.47E-02	-2.21E-01	3.23E+00
-1.00E-01	1.13E+00	1.54E-02	-1.72E-01	3.22E+00
-2.00E-01	1.14E+00	1.50E-02	-2.50E-01	3.48E+00
-3.00E-01	1.13E+00	1.60E-02	-2.48E-01	3.82E+00
-4.00E-01	1.12E+00	1.79E-02	-4.30E-01	4.66E+00
-7.00E-01	1.02E+00	5.46E-02	-6.00E-01	3.23E+00
-8.00E-01	9.40E-01	6.68E-02	-3.38E-01	2.90E+00
-9.00E-01	8.31E-01	7.60E-02	-1.16E-01	2.71E+00
0.00E+00	1.11E+00	1.57E-02	-1.92E-01	3.40E+00

Xcl-cold

r/R	U/Ubulk	urms/Ucl	skew(u)	flat(u)
-9.26E-01	7.78E-01	8.03E-02	1.19E-01	2.92E+00
-7.92E-01	9.38E-01	6.72E-02	-2.38E-01	2.67E+00
-6.58E-01	1.04E+00	4.96E-02	-6.15E-01	3.16E+00
-5.24E-01	1.09E+00	2.98E-02	########	6.46E+00
-3.90E-01	1.11E+00	1.82E-02	-4.04E-01	4.32E+00
-2.56E-01	1.11E+00	1.28E-02	-1.98E-01	4.34E+00
-1.22E-01	1.12E+00	1.63E-02	-2.25E-01	3.56E+00
-1.22E-01	1.12E+00	1.68E-02	-1.78E-01	3.34E+00
1.24E-02	1.12E+00	1.35E-02	-2.04E-01	3.89E+00
1.46E-01	1.11E+00	1.46E-02	-7.60E-02	3.56E+00
2.80E-01	1.11E+00	1.91E-02	-8.65E-01	5.68E+00
4.14E-01	1.10E+00	2.88E-02	########	6.02E+00
5.48E-01	1.07E+00	4.34E-02	-7.38E-01	3.61E+00
6.82E-01	1.00E+00	5.61E-02	-4.90E-01	3.05E+00
8.16E-01	8.94E-01	6.96E-02	-2.55E-01	2.94E+00
7.90E-01	9.15E-01	6.87E-02	-3.05E-01	2.59E+00
8.03E-01	9.05E-01	6.28E-02	-1.02E-01	2.77E+00
8.16E-01	8.92E-01	6.76E-02	-1.52E-01	2.62E+00
8.30E-01	8.62E-01	7.86E-02	-2.64E-01	2.58E+00
8.43E-01	8.76E-01	6.52E-02	4.30E-02	2.78E+00
8.57E-01	8.55E-01	5.97E-02	-2.57E-01	2.90E+00

Branch Pipe: InHo (Figure A9)

Ycl-hot

r/R	W/Ucl	wrms/Ucl	uw/Ucl^2
-3.87E-02	-2.31E-03	1.49E-02	-1.04E-05
-3.87E-02	-1.16E-03	1.45E-02	-1.87E-06
7.65E-01	-1.16E-03	4.17E-02	-2.66E-04
6.31E-01	-1.16E-03	2.86E-02	-2.11E-04
4.97E-01	0.00E+00	1.71E-02	-4.41E-05
3.63E-01	-1.16E-03	1.42E-02	2.41E-06
2.29E-01	-2.31E-03	1.45E-02	7.22E-06
9.53E-02	-4.62E-03	1.43E-02	1.20E-06
-3.87E-02	-2.31E-03	1.46E-02	5.35E-07
-1.73E-01	-2.31E-03	1.50E-02	-1.07E-06
-3.07E-01	-1.16E-03	1.47E-02	-2.54E-06
-4.41E-01	-2.31E-03	1.48E-02	1.07E-06
-5.75E-01	-2.31E-03	2.13E-02	-2.97E-05
-7.09E-01	-3.47E-03	3.58E-02	-1.06E-04
-8.43E-01	-2.31E-03	5.08E-02	-4.41E-05
-8.43E-01	-2.31E-03	4.89E-02	4.28E-06
-8.70E-01	-2.31E-03	5.35E-02	-9.05E-05
-8.96E-01	-1.16E-03	5.57E-02	-9.13E-05
-9.23E-01	-1.16E-03	5.79E-02	-6.27E-05
-9.50E-01	0.00E+00	4.75E-02	-1.16E-04
-9.47E-01	0.00E+00	2.15E-02	1.74E-06
-9.50E-01	0.00E+00	4.92E-02	7.60E-05
-9.53E-01	0.00E+00	6.23E-02	-8.95E-06
-9.55E-01	2.31E-03	6.29E-02	-8.21E-05

Ycl-cold

r/R	W/Ucl	wrms/Ucl	uw/Ucl^2
9.26E-01	-2.31E-03	4.52E-02	-1.54E-05
7.92E-01	-3.47E-03	4.52E-02	-3.41E-04
6.58E-01	1.16E-03	3.39E-02	-2.16E-04
5.24E-01	-2.31E-03	1.65E-02	-2.76E-05
3.90E-01	-1.16E-03	1.29E-02	-6.50E-06
2.56E-01	-1.16E-03	1.25E-02	-7.23E-06
1.22E-01	-2.31E-03	1.35E-02	-6.63E-06
-1.24E-02	-4.62E-03	1.54E-02	-4.64E-06
-1.46E-01	-9.25E-03	1.41E-02	-1.33E-05
-2.80E-01	-8.09E-03	1.32E-02	-6.74E-06
-4.14E-01	-8.09E-03	1.45E-02	5.04E-06
-5.48E-01	-5.78E-03	2.06E-02	-4.20E-06
-6.82E-01	-3.47E-03	3.68E-02	-5.27E-05
-8.16E-01	-2.31E-03	5.19E-02	-8.20E-05
-7.90E-01	-2.31E-03	4.94E-02	-8.55E-05
-8.03E-01	-3.47E-03	4.95E-02	-2.17E-05
-8.16E-01	-2.31E-03	5.14E-02	-5.90E-05
-8.30E-01	-3.47E-03	5.17E-02	-1.75E-05
-8.43E-01	-1.16E-03	4.60E-02	-5.26E-05

Xcl-hot

r/R	W/Ucl	wrms/Ucl	uw/Ucl^2
0.00E+00	1.49E-02	1.49E-02	-1.04E-05
9.00E-01	4.47E-02	4.47E-02	5.01E-04
8.00E-01	4.00E-02	4.00E-02	7.79E-04
7.00E-01	3.51E-02	3.51E-02	5.73E-04
6.00E-01	2.94E-02	2.94E-02	4.56E-04
5.00E-01	2.40E-02	2.40E-02	2.65E-04
4.00E-01	1.87E-02	1.87E-02	1.42E-04
3.00E-01	1.55E-02	1.55E-02	5.97E-05
2.00E-01	1.35E-02	1.35E-02	1.86E-05
1.00E-01	1.39E-02	1.39E-02	-4.68E-06
0.00E+00	1.46E-02	1.46E-02	1.34E-07
-1.00E-01	1.43E-02	1.43E-02	-6.42E-06
-2.00E-01	1.43E-02	1.43E-02	-1.20E-06
-3.00E-01	1.35E-02	1.35E-02	-6.68E-06
-4.00E-01	1.28E-02	1.28E-02	-1.78E-05
-7.00E-01	3.47E-02	3.47E-02	-5.35E-04
-8.00E-01	4.24E-02	4.24E-02	-5.71E-04
-9.00E-01	4.66E-02	4.66E-02	-3.40E-04
0.00E+00	1.45E-02	1.45E-02	-1.87E-06

Xcl-cold

r/R	W/Ucl	wrms/Ucl	uw/Ucl^2
-9.26E-01	1.50E-02	6.53E-02	2.00E-04
-7.92E-01	1.50E-02	4.91E-02	3.04E-04
-6.58E-01	1.50E-02	3.31E-02	2.98E-04
-5.24E-01	9.25E-03	2.23E-02	1.39E-04
-3.90E-01	1.16E-03	1.75E-02	1.52E-05
-2.56E-01	-4.62E-03	1.23E-02	8.43E-06
-1.22E-01	-3.47E-03	1.29E-02	2.31E-05
-1.22E-01	-4.62E-03	1.27E-02	1.74E-05
1.24E-02	3.47E-03	1.28E-02	-1.11E-05
1.46E-01	8.09E-03	1.28E-02	7.46E-06
2.80E-01	1.04E-02	1.54E-02	3.24E-05
4.14E-01	4.62E-03	2.17E-02	9.86E-05
5.48E-01	3.47E-03	3.03E-02	9.27E-05
6.82E-01	-1.16E-03	4.03E-02	1.82E-04
8.16E-01	0.00E+00	5.20E-03	1.32E-06
7.90E-01	6.94E-03	3.86E-02	4.49E-05
8.03E-01	2.31E-03	2.80E-02	1.75E-04
8.16E-01	1.16E-03	1.06E-02	-1.68E-05
8.30E-01	-1.16E-03	2.52E-02	-1.22E-04
8.43E-01	2.31E-03	3.34E-02	-3.66E-04